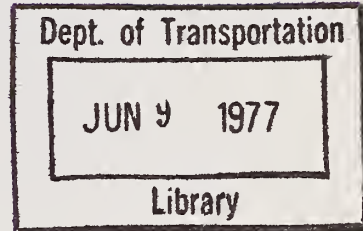


TE
662
.A3
no.
FHWA-
RD-
76-
164

No. FHWA-RD-76-164

HIGHWAY-VEHICLE-OBJECT SIMULATION MODEL--1976

Vol. 3. Engineering Manual--Analysis



February 1976
Final Report

Document is available to the public through
the National Technical Information Service,
Springfield, Virginia 22161

Prepared for
FEDERAL HIGHWAY ADMINISTRATION
Offices of Research & Development
Washington, D. C. 20590

NOTICE

This document is disseminated under the sponsorship of the Department of Transportation in the interest of information exchange. The United States Government assumes no liability for its contents or use thereof.

The contents of this report reflect the views of Calspan Corporation, which is responsible for the facts and the accuracy of the data presented herein. The contents do not necessarily reflect the official views or policy of the Department of Transportation. This report does not constitute a standard, specification, or regulation.

FHWA DISTRIBUTION NOTICE

Limited copies of this report are being distributed by memorandum to individual researchers involved in computer simulations of highway vehicles and impacts with roadside obstacles.

A limited number of additional copies of this report is available from the Protective Systems Group of the Structures and Applied Mechanics Division, Office of Research.

Copies may also be obtained from the National Technical Information Service (NTIS), Department of Commerce, 5285 Port Royal Road, Springfield, Virginia 22161. A small charge is imposed for copies provided by NTIS.

TE
662
A3
no.
FHWA
RP
76-164

Technical Report Documentation Page

1. Report No. FHWA-RD-76-164 ,	2. Government Accession No.	3. Recipient's Catalog No.	
4. Title and Subtitle Highway-Vehicle-Object Simulation Model - 1976 , Engineering Manual - Analysis		5. Report Date December 1975	
6. Performing Organization Code		7. Author(s) David J. Segal	
8. Performing Organization Report No. ZR-5461-V-8		9. Performing Organization Name and Address Calspan Corporation P. O. Box 235 Buffalo, New York 14221	
10. Work Unit No. (TRAIS) FCP 31H2232		11. Contract or Grant No. DOT-FH-11-8265	
12. Sponsoring Agency Name and Address U.S. Department of Transportation Federal Highway Administration Contracts and Procurement Division Washington, D.C. 20590		13. Type of Report and Period Covered 1 Report February 1974 - December 1975	
15. Supplementary Notes FHWA Contract Manager: Morton S. Oskard		14. Sponsoring Agency Code S0609	
16. Abstract A series of reports have been written to document revised and updated versions of the simulation of highway-vehicle-object interactions in a single vehicle highway environment. The programs documented were developed under FHWA sponsorship to provide the highway safety community with an analytical means of evaluating the effects of highway/roadside environment on safety.			
This manual is addressed to the engineer who wishes to become familiar with the mathematical model which is the basis for the HVOSM computer simulation. It contains a detailed description of the governing equations and logic for the three documented versions of the HVOSM.			
This manual is one of four volumes.			
Contractors Report No. ZR-5461-V		<u>Short Title</u>	
-6 -7 -8 -4-R		HVOSM - 1976 Users Manual HVOSM - 1976 Programmers Manual HVOSM - 1976 Engineering Manual - Analysis HVOSM - 1976 Engineering Manual - Validation	
17. Key Words HVOSM, Vehicle Dynamics Computer Simulation		18. Distribution Statement No restrictions. This report is available to the public through the National Technical Information Service, Springfield, Virginia, 22161.	
19. Security Classif. (of this report) Unclassified	20. Security Classif. (of this page) Unclassified	21. No. of Pages 188	22. Price

FOREWORD

This report is one of four manuals prepared under Contract Number DOT-FH-11-8265 for the Federal Highway Administration, U.S. Department of Transportation for the purpose of summarizing and upgrading documentation of the Highway-Vehicle-Object Simulation Model (HVOSM). The HVOSM had been previously developed for the Federal Highway Administration (FHWA) by the Calspan Corporation (formerly Cornell Aeronautical Laboratory) under Contract Number CPR-11-3988 during the period from 1966 to 1971 and extended under this contract. Contained in this report is a complete summary of the mathematical analysis which is the basis for the simulation model.

Complete documentation of the HVOSM is contained in the following manuals:

- Highway-Vehicle-Object Simulation Model
Volume 1 - Users Manual
- Highway-Vehicle-Object Simulation Model
Volume 2 - Programmers Manual
- Highway-Vehicle-Object Simulation Model
Volume 3 - Engineering Manual - Analysis
- Highway-Vehicle-Object Simulation Model - Volume 4 -
Engineering Manual - Validation

This report has been reviewed and is approved by:



Edwin A. Kidd, Head
Transportation Safety Department

TABLE OF CONTENTS

	<u>Page No.</u>
FOREWORD	ii
LIST OF FIGURES	vi
LIST OF TABLES	viii
1. INTRODUCTION	1
2. SYMOLOGY AND NOTATION	6
2.1 Symbology	6
2.2 Notation	6
3. HVOSM MATHEMATICAL MODEL ANALYSIS	16
3.1 Derivations of Equations of Motion	16
3.1.1 Sprung Mass	17
3.1.2 Unsprung Masses	24
3.1.3 Steering System	30
3.1.4 Wheel Spin	32
3.1.5 Summary of Equations of Motion for Sprung and Unsprung Masses	35
3.1.5.1 Independent Front Suspension - Beam Axle Rear Suspension Equations of Motion	35
3.1.5.2 Independent Front and Rear Suspension Equations of Motion	38
3.1.5.3 Beam Axle Front and Rear Suspension Equations of Motion	41
3.2 Vehicle Position and Orientation	44
3.2.1 Sprung Mass	44
3.2.2 Unsprung Masses	49
3.2.2.1 Independent Front/Solid Axle Rear Suspension	49
3.2.2.2 Independent Front and Rear Suspension	51
3.2.3 Beam Axle Front and Rear Suspension	52

TABLE OF CONTENTS (Contd.)

	<u>Page No.</u>	
3.3	Vehicle to Ground Orientation	53
3.4	Tire Contact With the Ground	60
3.4.1	Ground Contact Point	60
3.4.2	Flat Terrain Ground Characteristics	62
3.4.3	Variable Terrain Ground Characteristics	63
3.4.4	Curb Impacts	71
3.4.5	Road Roughness	77
3.5	Suspension Forces	81
3.5.1	Front Suspension	82
3.5.2	Rear Suspension	85
3.6	Braking and Tractive Torques	88
3.6.1	HVOSM-RD2 Version	88
3.6.2	HVOSM-VD2 Version	89
3.6.2.1	Braking Torque	89
3.6.2.2	Tractive Torque	102
3.7	Tire Forces	103
3.7.1	HVOSM-RD2 Version	103
3.7.2	HVOSM-VD2 Version	116
3.7.3	Components of Tire Forces	126
3.8	Impact Forces	128
3.8.1	Vehicle to Barrier Interface	129
3.8.2	Area Calculation	140
3.8.3	Simulation of Deformable Barrier Load-Deflection Characteristics	148
3.8.4	Resultant Forces and Moments	155
3.9	Preview-Predictor Driver Model	156
3.9.1	Path-Following Mode	160

TABLE OF CONTENTS (Contd.)

	<u>Page No.</u>
3.9.1.1 Specification of the Desired Path	160
3.9.1.2 Determination of Predicted Path	160
3.9.1.3 Error Determination	162
3.9.1.4 Importance Weighting Function	165
3.9.1.5 Filter Structure	166
3.9.2 Skid Control Mode	168
3.9.3 Speed Control Mode	170
3.9.4 Driver-Vehicle Interface	172
3.9.4.1 Braking	172
3.9.4.2 Engine Torque	172
3.10 Aerodynamic and Rolling Resistances (HVOSM Vehicle Dynamics Version)	173
3.11 Resultant Forces and Moments	175
4. REFERENCES	180

LIST OF FIGURES

<u>Figure No.</u>	<u>Title</u>	<u>Page No.</u>
3.1	Analytical Representation of Vehicle	18
3.2	Thin Rod Approximation of Rear Axle Inertial Properties	21
3.3	Rear Axle Representation	28
3.4	Steering System Resistance vs. Steer Angle	31
3.5	Inertial Coupling of Drive Wheels	32
3.6	Terrain Table Grid	64
3.7	General Form of Simulated Suspension Load- Deflection Characteristics	84
3.8	Generation of Wheel Torques	90
3.9	Control Inputs for Speed Control	91
3.10	Type 1 Brake - Drum Type with Leading and Trailing Shoes, Uniform or Stepped Cylinder	94
3.11	Type 2 Brake - Drum Type with Two Leading Shoes, Two Cylinders	95
3.12	Type 3 Brake - Bendix Duo Servo	96
3.13	Type 4 Brake - Caliper Disc	97
3.14	Adjustment of $(TQ)_{Bi}$, $(TQ)_{Bi + 1}$	98
3.15	Effects of Inertial Coupling of Drive Wheels	100
3.16	Inputs to Define Engine Properties	102
3.17	Logic to Permit a Standing Start	104
3.18	Vector Summation of Forces with Components Along the Line of Action of the Radial Tire Force	105

LIST OF FIGURES (Contd.)

<u>Figure No.</u>	<u>Title</u>	<u>Page No.</u>
3.19	Simulated Variation of Small-Angle Cornering and Camber Stiffness with Loading Normal to Tire-Terrain Contact Patch	107
3.20	Assumed Variation of Camber Force with Camber Angle	109
3.21	Nondimensional Tire Side-Force Curve	111
3.22	Friction Circle Concept	112
3.23	Friction Ellipse Concept	118
3.24	Normalized Tractive Force vs. SLIP Model	121
3.25	Intersection Area	140
3.26	Centroid of Intersection Area	143
3.27	General Form of Barrier Load-Deflection Characteristics	150
3.28	Assumed Form of Load-Deflection for Recurrent Loading	151
3.29	General Subroutine for Nonlinear Load-Deflection	153
3.30	Driver Model Outline	157
3.31	Error Calculation	162
3.32	Neuro-Muscular Filter Characteristics	166
3.33	Vehicle Slip Angle	169

LIST OF TABLES

<u>Table No.</u>	<u>Title</u>	<u>Page No.</u>
3-1	Definition of Elements of Matrix Equation (276)	135
3-2	Definition of Elements of Matrix Equation (276)	138

1.

INTRODUCTION

In 1966 Calspan Corporation (formerly Cornell Aeronautical Laboratory, Inc.) began development of a general mathematical model and computer simulation of the dynamic responses of an automobile in accident situations under Contract CPR-11-3988 with the Bureau of Public Roads.

The mathematical model of vehicle dynamics developed in the first year of that effort included the general three-dimensional motion resulting from vehicle control inputs, traversal of irregular terrain, or from collisions with simple roadside barriers. The model was subsequently named the Highway-Vehicle-Object Simulation Model (HVOSM). Later, the model was further developed and a comprehensive validation program was carried out including a series of repeatable full-scale tests with an instrumented vehicle in order to objectively assess the degree of validity of the vehicle model. Extensive measurements of the vehicle parameters required for input to the HVOSM were made under a subcontract with the Ford Motor Company as a part of the validation procedure. This effort was reported in Reference 5 and the model as described therein has been referred to as the V-3 version of the HVOSM.

Modifications were subsequently made to the simulation in order to study the effects of terrain (specifically, railroad grade crossings) on vehicle controllability. The impact routines were removed and extended terrain definition capabilities were added along with a more realistic model of suspension properties. This program version (Reference 10) has been informally referred to as the V-4 version of the HVOSM and has since been used extensively for study of roadway and roadside geometrics.

Further developments of HVOSM aimed at providing a simulation model more suitable for the study of the complex dynamics resulting from accident avoidance evasive maneuvers were reported in Reference 11. This version, informally called the V-7 version of the HVOSM, includes a detailed model of the braking and engine-driveline systems and an empirically based definition of the relationships between longitudinal and lateral tire forces through the inclusion of rotational degrees of freedom of the four vehicle wheels.

During development of the HVOSM, documentation efforts primarily fulfilled the objectives of maintaining communication within the program development structure, ensuring quality control of the development and providing a historical reference. It was, however, recognized early in the development of the HVOSM, that this state-of-the-art advance in the modeling of a vehicle and its environment could be put to best use through its widespread distribution to organizations interested in its application to highway safety. As a result, distribution of the HVOSM was begun before its development was complete and before instructional documentation could be provided.

Recognizing the need to bring documentation of the several HVOSM versions together and to provide the highway safety community with an effective description of the programs and their use, the Federal Highway Administration (FHWA) awarded Calspan Corporation contract number DOT-FH-11-8265 for the purpose of providing such documentation for the then existing versions of the HVOSM.

Three versions of the HVOSM were covered by this documentation. They were, the HVOSM-SMI1 (Sprung Mass Impact) version (formerly known as the V-3 version), the HVOSM-RD1 (Roadside Design) version (formerly known as the V-4 version) and the HVOSM-VD1 (Vehicle Dynamics) version (formerly known as the V-7 version). Under the first phase of that effort, only those versions as developed by Calspan were covered by the documentation.

The second phase of contract number DOT-FH-11-8265 called for extension of the capabilities of the HVOSM by adding new features, including some additional modifications made by other research organizations, and providing additional ease of use features.

Accordingly, Calspan has:

- Generalized the basic vehicle model to include the capability for simulating an independent front and rear suspension vehicle and a vehicle with solid front and rear axles.
- Generalized the tire model to allow specification of up to four different tires on a vehicle and revised the friction ellipse tire model.
- Combined the sprung mass impact version with the roadside design version resulting in only two program versions at the end of the second phase.
- Incorporated the Preview-Predictor Driver Model described in Reference 15 into the vehicle dynamics model.
- Incorporated impact forces due to localized structural hard points into the sprung mass impact algorithm. This modification was originally developed by the Texas Transportation Institute (TTI) and was added as reported in Reference 13.

- Extended the curb impact algorithm to allow up to six planes to describe a curb. This modification was also developed by TTI and was reported in Reference 16.
- Developed a road roughness algorithm to allow determination of the effects of road roughness on vehicle performance.
- Revised input and output format to provide an easy to use, more flexible data interface.
- Developed a Pre-Processing Program to calculate a number of program inputs including vehicle and terrain data or to supply input cards from a stored library of vehicle data.

The documentation provided now covers the two program versions: the HVOSM-RD2 Version (Roadside Design) and the HVOSM-VD2 Version (Vehicle Dynamics). It is intended to be a base to which further developments and modifications to the HVOSM can be added, thus providing a uniform reporting format and centralized source of information for the many HVOSM users. It consists of four volumes, each describing a separate aspect of the HVOSM. Two volumes are directed toward the engineer/analyst containing the analysis (derivation of governing equations, assumptions, and development of controlling logic) and experimental validation. Another volume is directed toward the general program user and contains analysis/program symbology, descriptions of the models and solution procedures, descriptions of input requirements and program output, and a number of program application examples. The remaining volume of documentation is intended for use by those interested in the detailed computer programs. This volume contains descriptions of the computer code including a discussion of subroutine functions, annotated flowcharts and program listings. Also included are a list of program changes, a description of program stops and messages, and computer system requirements necessary to run the programs.

The HVOSM analysis is covered in this report. Section 2 contains a list of symbols and their definitions and the notation used in the analysis. The analytical derivations of the HVOSM mathematical model are presented in Section 3, and references are listed in Section 4.

2. SYMBOLIC AND NOTATION

2.1 Symbology

The HVOSM symbology is presented in this section. The listing of symbols is ordered with respect to analytical symbol and includes a corresponding program symbol, a brief definition and an equation number referencing the calculation of the variable. Input variables are indicated by an I in the equation number column.

2.2 Notation

The time derivative of a variable is indicated by a dot over the symbol for the variable (i.e., $\alpha = \frac{d\alpha}{dt}$, $\ddot{\alpha} = \frac{d^2\alpha}{dt^2}$).

The following subscript notation is employed:

0 = initial value of a variable at zero time.

t = value of a variable at the end of the current time increment.

t-1 = value of a variable at the end of the previous time increment.

F = front.

R = rear, or rear axle.

i = wheel identification -- 1, 2, 3, 4 = RF,
LF, RR, LR, respectively.

j = identification of vehicle end. j = F, R
for front end and rear end, respectively.

s = sprung mass.

u = unsprung mass.

ANALYTICAL SYMBOL	PROGRAM SYMBOL	DEFINITION	UNITS	ANALYTICAL SYMBOL	PROGRAM SYMBOL	DEFINITION	UNITS
a	A	I Distance along vehicle fixed x axis from the sprung mass center of gravity to the center line of the front wheels	in.	(AR) _j	ARBRF ARBRR	I Drive axle ratio (propeller shaft speed/wheel speed). Default of 1.0	
a _i , b _i , c _i		155 Directional components of a line perpendicular to both the normal to the wheel plane and the radial tire force, F _{Ri}		A _D , A ₁ , A ₂	AD,A1,A2	I Constant coefficients for tire side force due to slip angle	
APD APDMAX	APD APDMAX	345 Accelerator pedal deflection and maximum accelerator pedal deflection	in	A ₃ , A ₄	A3,A4	I Constant coefficients for tire side force due to camber angle	in.
a _{x_i} , b _{x_i} , c _{x_i}	AS(4) BS(4) CS(4)	258 Directional components of a line perpendicular to both a normal to the tire-terrain contact plane and the line of intersection of the wheel and ground planes		b	B	I Distance along the vehicle fixed x axis from the sprung mass center of gravity to the centerline of the rear wheels (entered positive)	
a _{x_i} , b _{x_i} , c _{x_i}	AX(4) BX(4) CX(4)	99 Direction components of a line perpendicular to both a normal to the tire-terrain contact plane and the vehicle fixed y axis		[B]	BMTX(3,3)	134 Transformation matrix from wheel fixed to space fixed coordinate systems	psi/lb ²
a _{y_i} , b _{y_i} , c _{y_i}	AY(4) BY(4) CY(4)	104 Direction component of a line perpendicular to both a normal to the tire-terrain contact plane and the vehicle fixed x axis		B _{FP1} B _{FP2}	BFP1 BFP2	I First and second order coefficients for relationship between brake pedal force and brake system pressure	psi/lb ²
[A]	AMTX(3,3)	53 Transformation matrix from vehicle fixed to space fixed coordinate systems		[B] _n	BNMTX(3,3)	60 Transformation matrix from orientation of vehicle axes at indexing to space fixed axes (Euler angles=ψ _n ', θ _n ', φ _n ')	1b/rad
(A _{INT}) _i	AINTI	287 Intersection area of cutting plane i with the sprung mass	in ²	C _{CO} C _F , C _R	CF CR	I Small angle camber stiffness	1b-sec/in
[A] _j	AJMTX(3,3)	134 Transformation matrix from wheel fixed to vehicle fixed coordinate systems		C' _F , C' _R	CFP CRP	I Front and rear viscous damping coefficient for a single wheel, effective at the wheel for the front and at the spring at the rear	1b
AMU	AMU	I Tire-terrain friction coefficient at zero speed and nominal tire loading		[C] _i	CMTX(3,4)	I Front and rear coulomb damping for a single wheel, effective at the wheel for the front and at spring for the rear	
AMUG	AMUG(5)	I Tire-terrain friction coefficient factor for 5 terrain tables		CONS	CONS	I Coefficient matrix for simultaneous solution of the ground contact point	
(AP) _F	APF(21)	I Anti-pitch coefficients for front suspension positive for anti-pitch for forward braking	lb/lb-ft	[C] _n	CNMTX(3,3)	I Ratio of conserved energy to total energy absorbed by the sprung mass	
(AP) _R	APR(21)	I Anti-pitch coefficients for rear suspension, effective at the wheels; positive for anti-pitch effect for forward braking	lb/lb-ft	C _{RRM1}	RRMC(4)	I Transformation matrix from vehicle fixed axes to most recently indexed axes (Euler angles=ψ _e ', θ _e ', φ _e ')	1b-in/lb
				C _{So} (CT.)	TCT(12)	I Rolling resistance moment coefficient	
						I Small angle cornering stiffness	1b/rad
						I Closed throttle engine torque	1b-ft

ANALYTICAL SYMBOL	PROGRAM SYMBOL	ON-BOARD	DEFINITION	UNITS	ANALYTICAL SYMBOL	PROGRAM SYMBOL	ON-BOARD	DEFINITION	UNITS
C_{Ti}	CT(4)	I	Circumferential tire force stiffness	lb	F_{NSTi}	FNSTI(3)	300	Structural hard point force	lb
$C'v$	CPSP	I	Coulomb resistance torque in the steering system effective at the wheels	lb-in	F_{R_i}	FR(4)	114	Radial tire force in the plane of the wheel	lb
C_1, C_2, C_3	CONE CTWO CTHREE	I	Coefficients in relationship approximating aerodynamic and rolling resistance		F'_{Ri}	FRCP(4)	212	Tire force perpendicular to the tire-terrain contact plane	lb
$[D]$	DMTX(10,11)	46	Mass matrix of coupled second order differential equations. Column 11 contains the forcing functions		(FRICT)	FRICT	306	Friction force acting between the vehicle sprung mass and barrier	lb
Dax	DELTAX	342	Desired vehicle acceleration	in/sec ²	F_{Rxui}	FRXU(4)	253	Components of F'_{Ri} along the sprung mass axes for wheel i	lb
DELB	DELB	I	Beginning, end, and incremental	in	F_{Ryu}	FRYU(4)	144	Summation of the components of radial spring mode forces over tire i, with respect to space	lb
DELE	DELE	I	wheel deflection for entered	in	F_{Rzu}	FRZU(4)	145		
DDEL	DDEL	I	front wheel camber table		$\Sigma F_{Rx'i}$	SFRX(4)	146		
DIST	DIST	I	Desired speed differential nulling distance	in	$\Sigma F_{Ry'i}$	SFRY(4)			
DRWHJ	DRWHJ	I	Incremental tire deflection for calculation of the equivalent tire force-deflection characteristic in the radial mode	in	$\Sigma F_{Rz'i}$	SFRZ(4)			
D_{1i}, D_{2i}, D_{3i}	D1(4) D2(4) D3(4)	87	Direction components of a line perpendicular to the normals of both the wheel plane and the tire-terrain contact plane		F_{Si}	FS(4)	227	Tire side force in the plane of the tire-terrain contact patch perpendicular to the line of intersection of the wheel plane and ground plane	lb
e_i	EI	320	Error between predicted and desired path at the i th viewing position	in	F'_{Si}		228	Resultant side force corresponding to small angle properties for slip and camber angles	lb
EN	EN		Number of points at which e_i is determined		(F_{Si}) _{max}		229	Maximum achievable side force as limited by the available friction	lb
FAPi	APITCH	188	Anti-pitch force at wheel i	lb	ΣF_{xs}	SFXS	357	Sprung mass impact force or combination of rolling resistance and aerodynamic drag acting along the vehicle x axis	lb
FARI		187	Force at wheel i due to auxiliary roll stiffness	lb	F_{sxui}	FSXU(4)	256	Components of tire side force, F_{Si} along the sprung mass axes	lb
FB	FB		Resistance force normal to the contact surface of a deformable barrier	lb	F_{syui}	FSYU(4)			
FBRK	FBRK	346	Brake pedal force	lb	F_{szui}	FSZU(4)			
F_{C_i}	FC(4)	225	Circumferential tire force	lb	F_{xui}	FXU(4)	259	Total tire force components along the vehicle axes	lb
F_{Cxui}	FCXU(4)	254	Components of the circumferential tire force along the x,y, and z axes	lb	F_{yui}	FYU(4)	260		
F_{Cyui}	FCYU(4)			F_{zui}	FZU(4)	261			
F_{Czui}	FCZU(4)			ΣF_{xu}	SFXU	353	Resultant forces acting on the vehicle through the unsprung masses in the x and y directions	lb	
F_j	FJP(35)	144	Table of equivalent radial spring forces as a function of deflection	lb	ΣF_{yu}	SFYU	354		
F_{JFi}	FJF(4)	179	Jacking force at wheel i	lb	ΣF_{ys}	SFYS	357	Sprung mass impact force acting along the vehicle y axis	lb
$(F_n)_t$	FN	298	Vehicle force produced by deformation of the vehicle structure normal to the contacted surface	lb	ΣF_{zs}	SFZS	357	Sprung mass impact force acting along the vehicle z axis	lb
				ΣF_{zi}	SFZI	356	Resultant force transmitted through the suspensions in the z direction	lb	
				F_{1fi}	F1FI(2)	174	Front and rear suspension coulomb damping forces for a wheel, effective at the wheel for the front and at the spring for the rear	lb	
				F_{1ri}	F1RI(2)	184			

ANALYTICAL SYMBOL	PROGRAM SYMBOL	EDN NO.	DEFINITION	UNITS	ANALYTICAL SYMBOL	PROGRAM SYMBOL	EDN NO.	DEFINITION	UNITS
F _{2Fi} F _{2Ri}	F2FI(2) F2RI(2)	175 185	Front and rear suspension spring and bumper forces for a wheel, effective at the wheel for the front and at the spring for the rear	lb	I _R	XIR	I	Rear unsprung mass moment of inertia about a line through its center of gravity and parallel to the vehicle x axis	lb-sec ² -in
g	G	I	Acceleration due to gravity	in/sec ²	I _{wj}	FIWJ(4)	I	Rotational inertia of an individual wheel at the front or rear	lb-sec ² -in
GEAR ₁ GEAR ₂ GEAR ₃ GEAR ₄	GEAR1 GEAR2 GEAR3 GEAR4	I	Transmission gear ratios	—	I _{x,y,z}	XIX XYI XIZ	I	Spring mass moments of inertia about the vehicle axes	lb-sec ² -in
G _{1j}	GN(1,J)	I	Lever arm lengths in brake types 1,2 and 3	in	I _{xz}	XIXZ	I	Spring mass roll-yaw product of inertia	lb-sec ² -in
G _{2j}	GN(2,J)	I	Brake actuation constant, assumed to be equal for both shoes of brake types 1 and 2	(I'x)t	(I'z)t	+7	Effective inertial term due to time varying positions of the unspring masses	lb-sec ² -in	
G _{3j}	GN(3,J)	I	Effective lining-to-drum or lining to-disk friction coefficient at design temperature for all shoes or disks in types 1,2 and 4 and for the primary shoe of type 3	(I'xz)t	(I'yz)t	47	Effective inertial term due to time varying positions of the unspring masses	lb-sec ² -in	
G _{4j}	GN(4,J)	I	Cylinder area for actuation of leading shoe of brake type 1, or for each shoe in types 2 and 3. Also used for total cylinder area per side of disk in type 4	in ²	I _y	XIPS	47	Effective inertia term due to time varying positions of the unspring masses	lb-sec ² -in
G _{5j}	GN(5,J)	I	Cylinder area for actuation of trailing shoe of brake Type 1	in ²	K _d	FKD	I	Moment of inertia of the steering system effective at the front wheels (includes both wheels)	sec ² /in
G _{6j} -G _{11j}	GN(6,J)- GN(11,J)	I	Brake dimensions for type 3.	in	K _F , K _R	AKF AKR	I	Performance parameter characterizing understeer/oversteer properties of the vehicle	lb/in
G _{12j}	GN(12,J)	I	Effective lining to drum friction coefficient for secondary shoe of brake type 3		K _{FC} , K _{RC}	AKFC AKRC	I	Front and rear suspension load deflection rate in the quasi-linear range about the design position effective at the front wheels and the rear springs	lb/in
G _{13j}	GN(13,J)	I	Mean lining radius for brake type 4	in	K _{FC} , K _{RC}	AKFCP AKRCP	I	Coefficients for the compression bumpers of the front and rear suspension effective at the front wheels and rear springs	lb/in
G _{14j}	GN(14,J)	I	Coefficient of heat transfer for convective losses		K _{FE} , K _{RE}	AKFF AKRE	I	Coefficients for the cubic terms of the suspension compression bumpers	lb/in
G _{15j}	GN(15,J)	I	Specific heat of brake assembly	BTU/lb°F					
G _{16j}	GN(16,J)	I	Effective weight of brake assembly for heat absorption	lb					
h _j	HI(4)		Tire rolling radius	in					
I _{Dj}	FIDJ(2)	I	Driveline inertia for front or rear (Note that a value of zero is entered at the non-driving end of the vehicle)	lb-sec ² -in					

ANALYTICAL SYMBOL	PROGRAM SYMBOL	EQN NO	DEFINITION	UNITS	ANALYTICAL SYMBOL	PROGRAM SYMBOL	EQN NO	DEFINITION	UNITS
K_{FE}, K_{RE}	AKFEP AKREP	I	Coefficients for the cubic terms of the suspension extension bumpers		P_1, P_2	PONE PTWO	I	"Break" pressures for brake system proportioning valve	psig
K_p	FKP	928	Driver steer control gain		$(RATIO)_i$				
K_{RS}	AKRS	I	Rear axle roll-steer coefficient, positive for roll understeer						
K_{S1}, K_{S2}	FKS1 FKS2	I	Drivers estimate of vehicle braking and accelerating gains		R_{BB}	RBB	280	Constant for barrier bottom plane	in
K_{STi}	AKST(3)	I	Structural hard point spring rates	lb/in	R_{Bi}	RBI	269	Constant for barrier face plane	in
K_T	AKT	I	Radial tire rate in the quasi-linear range	lb/in	R_{BT}	RBT	281	Constant for barrier top plane	in
K_V	AKV	I	Load-deflection characteristic of the vehicle structure	lb/in ³	R_{B1}	RB1	273	Constant for the plane perpendicular to the barrier face plane and containing the axis of rotation	in
$K_{SS}, K_{S1}, K_{S2}, K_{S3}$	AKDS AKDS1 AKDS2 AKDS3	I	Coefficients of the cubic representation of rear wheel steer as a function of deflection for independent rear suspension		$NZ5$	NZ5	I	Flag to indicate whether the variable increment terrain table is supplied, =0,no,#0, yes	
K_γ	AKPS	I	Load-deflection rate for the linear steering stop, effective at the wheels	lb-in/rad	$\Sigma N_{\phi F}$	SNPF	367	Roll moment acting on the front axle	lb-in
K_1	AK1	I	Slope of P_R vs P_F for values of P_F between P_1 and P_2		$\Sigma N_{\phi R}$	SNPR	360	Roll moment acting on the rear axle	lb-in
K_2	AK2	I	Slope of P_R vs P_F for values of P_F greater than P_2		$\Sigma N_{\phi S}$	SNPS	368	Roll moment on the sprung mass resulting from sprung mass impact forces	lb-in
$(LF)_i$	FLF	I	Fade coefficient for brake at wheel i		$\Sigma N_{\phi S}$	SNTS	309	Pitch moment on the sprung mass resulting from sprung mass impact forces	lb-in
M_S	XMS	I	Sprung mass	lbsec ² /in	$\Sigma N_{y S}$	SNPSS	310	Yaw moment on the sprung mass resulting from sprung mass impact forces	lb-in
M_{UF}, M_{UR}	XMUF XMUF	I	Front (both sides) and rear unsprung masses. Note $M_1=M_2=M_{UF}/2$, $M_3=M_{UR}$	lbsec ² /in	$\Sigma N_{y U}$	SNPU	357	Moments acting on the sprung mass produced by forces acting on the unsprung masses	lb-in
M_1, M_2	XMUF/2	I	Right and left front unsprung masses	lbsec ² /in	$\Sigma N_{z U}$	SNTU	358		
M_3	XMUR	I	Rear unsprung mass	lbsec ² /in	$\Sigma N_{z U}$	SNPSU	359		
NBX	NBX(5)	I	Number of x' boundaries supplied for 5 terrain tables		P,Q,R	P,Q,R	+6	Scalar components of the sprung mass angular velocity along the vehicle x,y and z axes	rad/sec
NBY	NBY(5)	I	Number of y' boundaries supplied for 5 terrain tables		P_C	PC	I	Hydraulic pressure in brake system master cylinder	psig
NDEL	NDEL	I	Number of entries in the front wheel camber table		P_j	PP(2)	197	Hydraulic pressure in brake cylinders at front or rear brakes	psig
NX	NX(5)	I	Number of x' grid points in 5 terrain tables		(PS)			Prop shaft speed	rpm
NY	NY(5)	I	Number of y' grid points in 5 terrain tables						
NZTAB	NZTAB	I	Number of terrain tables entered						

ANALYTICAL SYMBOL	PROGRAM SYMBOL	DEFINITION	UNITS	ANALYTICAL SYMBOL	PROGRAM SYMBOL	DEFINITION	UNITS
(PT) R_F, R_R	XPS RF, RR	I Pneumatic trail of front tires I Auxiliary roll stiffness of the front and rear suspensions	in lb/in/rad	(TQ) _E (TQ) _F (TQ) _R	TQE TQF(50) TQR(50)	210 Engine torque Front and rear torque tables for a single wheel and effective at the wheel (positive for traction, negative for braking)	1b-ft 1b-ft
(RPME)	RPME	211 Engine speed	rpm	(TR)	TTTR	I Transmission ratio (speed ratio of engine to prop shaft)	
(RPS) _i	RPSI(4)	44 Rotational velocity of wheel i , positive for forward motion of the vehicle	rad/sec	T_{R_1}, T_{R_2}	TESTR1 TESTR2	I Lower and upper skid thresholds	
R_{RMi}	RRM(4)	352 Rolling resistance moment acting on wheel i	lb-in	T_S	TS	I Distance between spring mounts for a solid rear axle	in
R_W RWHJB RWHJE	RW RWHJB RWHJE	I Undeflected tire radius I Beginning and ending radii for calculation of the radial tire force-deflection characteristic used in the radial tire mode	in in	T_{SF}	TSF	I Distance between spring mounts for a solid front axle	in
SET	SET	I Ratio of permanent deflection to maximum deflection of deformable barrier		(TS)	TTTS	I Throttle setting expressed as the decimal portion of wide open throttle	
S_i	SI(4)	173 Total suspension force for a wheel, acting at the front wheels and rear springs 183	lb	T_{S1}, T_{S2}	TESTS1 TESTS2	I Driver threshold/indifference levels for positive and negative speed errors	in/sec
(SLIP) _i	SLIP(I)	241 The amount by which the rotational speed of wheel i is less than that of free rotation expressed as a decimal portion of the speed of free rotation		(TYPE)	NBTYPE	I Brake type indicator	
(SLIP) _{f1}	SLIPP	198 The value of (SLIP) _i , at a given wheel center speed U_{Gi} for which the value of μ_{x_i} is a maximum		T_{1y}	T1PSI	36 Coulomb friction torque in steering system effective at the wheel	1b-in
SP_n	ST(5,2)	I Coefficients for straight line segments defining the desired path		T_{2y}	T2PSI	36 Resistance torque produced by the front wheel steer stops, effective at the wheel	1b-in
$(S_x)_1, (S_x)_2,$ $(S_x)_3$	S11 S21 S31	284 Characteristic lengths of intersection area between the sprung mass and barrier 285 286	in	U, V, W	U,V,W	48 Scalar components of linear velocity of the sprung mass along the sprung mass x, y and z axes	in/sec
t	T	Time	sec	U^*, V^*, W^*	DXCP DYCP DZCP	64 Scalar components of linear velocity of the sprung mass along the space fixed x^*, y^* and z^* axes	in/sec
T_b	TESTB	I Braking indifference level	in/sec	u_i, v_i, w_i	UI(4) VI(4) WI(4)	90-98 Scalar components of the tire contact points linear velocity along the vehicle axes	in/sec
T_B, T_E TINCR	TB, TE TINCR	I Beginning, ending and incremental times for entry of control tables (TQ) _F , (TQ) _R and ψ_F	sec	U_{Gi}	UG(4)	103 Wheel center forward velocity in direction parallel to the tire-terrain contact plane	in/sec
T_F, T_R	TF, TR	I Front and rear track	in	U_{Gwi}	UGW(4)	195 Ground contact point velocity along the circumferential direction of the wheel	in/sec
T_I	TI(4)	125 Circumferential tire force resulting from applied torque	lb	u^*, v^*, w^*	UNP(17) VNP(17) WNP(17)	282 Components of the velocity of the three or four points that define the intersection area of the barrier and vehicle along the space-fixed axes	in/sec
T_I, T_L	TIL TL	I Driver steering model lag and lead times	sec				
(TQ) _{Bi}	TQB(4)	204 Brake torque at wheel i	1b-ft				
(TQ) _{Dj}	TQD(4)	211 Drive line torque at prop shaft at vehicle end j	1b-ft				

ANALYTICAL SYMBOL	PROGRAM SYMBOL	NO	DEFINITION	UNITS	ANALYTICAL SYMBOL	PROGRAM SYMBOL	NO	DEFINITION	UNITS
u'_r v'_r w'_r	URP VRP WRP	303	Components of the velocity of the point of application of the sprung mass impact force along the space-fixed axes	in/sec	x_n y_n z_n	XNN(17) YNN(17) ZNN(17)	276	Coordinates of intercept points between the barrier and sprung mass in the vehicle axes	in
U'_{STi} V'_{STi} W'_{STi}	UPT(4) VPT(4) WPT(4)	299	Components of the velocity of the deformed structural hard points along the space fixed axes	in/sec	x'_{Pi} y'_{Pi}	X Y	318	Coordinates of the location on the desired path at which the i th error is determined	in
U_T	UT	313	Total vehicle velocity	in/sec	x_{Ri} y_{Ri} z_{Ri}	XRI YRI ZRI	294	Coordinates of the centroid of the intersection area on cutting plane i , projected on to the actual vehicle barrier interface of the previous time increment	in
v_{Gi}	VG(4)	106	Contact point lateral velocity in the direction parallel to the tire-terrain contact plane	in/sec	$(\sum x_R)_t$ $(\sum y_R)_t$ $(\sum z_R)_t$	SXR SYR SZR	295 296 297	Coordinates of the point of application of the sprung mass impact force	in
VGR_{12} VGR_{21} VGR_{23} VGR_{32} VGR_{34} VGR_{43}	VGR12 VGR21 VGR23 VGR32 VGR34 (VTAN)	I	Vehicle speed at which transmission upshifts and downshifts occur	mph	x_{STi} y_{STi} z_{STi}	XSTI(3) YSTI(3) ZSTI(3)	301	Coordinates of the deformed structural hard points in the vehicle axes	in
WE_i	WEIGHT(I)	328	Driver steering error weighting function		x_{STi_0} y_{STi_0} z_{STi_0}	XSTIO(3) YSTIO(3) ZSTIO(3)	I	Coordinates of the underformed structural hard points in the vehicle axes	in
WI_i	XIMPOR(I)	I	Driver steering error importance weighting function		x_{VF}	XVF	I	Distance from the sprung mass c.g. to the vehicle front along the x axis	in
(WOT)	TWOT		Wide open throttle torque	lb-ft	x_{VR}	XVR	I	Distance from the sprung mass c.g. to the vehicle rear along the x axis	in
x_B, x_E XINCR	XB(5) XE(5) XINCR(5)	I	Beginning, ending and incremental x' for terrain tables	in	x'_{VP_i} y'_{VP_i}	XVP YVP	312 313	Driver prediction of vehicle location at the i th sample increment in the future	in
x_{BB}, y_{BB} z_{BB}	XBB YBB ZBB	279	Coordinates of the intersection of the z' axis with the barrier bottom plane in the vehicle axes	in	x_1, y_1, z_1 x_2, y_2, z_2	X1,Y1,Z1 X2,Y2,Z2	I	Coordinates of accelerometer positions with respect to the vehicle axes for which acceleration components are output	in
x_{BDRY}	XBDRY(4,5)	I	x' intercept for angled boundaries within terrain tables	in	$\{y\}$	VAR		System dependent variable, integral of $\{y\}$	
x_{Bi} y_{Bi} z_{Bi}	XBI YBI ZBI	267	Coordinates of the intersection of the y' axis with cutting plane i , in the vehicle axes	in	$\{\dot{y}\}$	DER	47	First derivatives with respect to time of the system dependent variables	
x_{BT} y_{BT} z_{BT}	XBT YBT ZBT	278	Coordinates of the intersection with the barrier top plane in the vehicle axes	in					
$x'_{C_p}, y'_{C_p}, z'_{C_p}$	XCP YCP ZCP	65 66 67	Coordinates of the origin of the vehicle axes (sprung mass center of gravity) with respect to the space fixed axes	in	y_B, y_E YINCR	YB(5) YE(5) YINCR(5)	I	Beginning, ending and incremental y' for terrain tables	in
x'_{cpn} y'_{cpn} z'_{cpn}	XCPNP(3) YCPNP(3) ZCPNP(3)	214	Coordinates of the vehicle corner n in the vehicle axes	in	y'_{BDRY}	YBDRY(4,5)	I	Lateral position of y' terrain boundaries with respect to space	in
x'_{cpn} y'_{cpn} z'_{cpn}	XCPNP(3) YCPNP(3) ZCPNP(3)	214	Coordinates of the vehicle corner n in the space-fixed axes	in	y'_{B}	YBP	I	Lateral position of the barrier face plane with respect to space	in
$x'_{G_p}, y'_{G_p}, z'_{G_p}$	XGPP(4) YGPP(4) ZGPP(4)	150 151	Coordinates of the ground contact points with respect to the space-fixed axes	in	y'_{C1}, y'_{C2} y'_{C3}, y'_{C4} y'_{C5}, y'_{C6}	YC1P YC2P YC3P YC4P YC5P YC6P	I	Lateral positions of slope changes defining a curb	in
x'_{i}, y'_{i}, z'_{i}	XP(4) YP(4) ZP(4)	68-82	Coordinates of the wheel centers with respect to the space fixed axes	in	y_v	YV	I	Distance from the sprung mass c.g. to the vehicle side	in
					z'_{BB}	ZBBP	I	Elevation of the bottom barrier plane in space	in

ANALYTICAL SYMBOL	PROGRAM SYMBOL	EDN NO.	DEFINITION	UNITS	ANALYTICAL SYMBOL	PROGRAM SYMBOL	EDN NO.	DEFINITION	UNITS
Z'_{BT}	ZBTP	I	Elevation of the top barrier plane in space	in	$\alpha_{ci}, \beta_{ci}, \gamma_{ci}$		255	Direction angles of a line perpendicular to the normals of both the wheel plane and tire-terrain contact plane with respect to space	rad
Z'_{C2}, Z'_{C3}	ZC2P	I	Elevation of curb at slope C_2	in					
Z'_{C4}, Z'_{C5}	ZC3P	I	Change lateral positions	in	$\alpha_{Gz_i}, \beta_{Gz_i}, \gamma_{Gz_i}$		84	Direction angles of a normal to the tire-terrain contact plane at wheel i with respect to space	rad
Z'_{C6}	ZC4P ZCSP ZCGP				$\alpha_x, \beta_x, \gamma_x$		116	Direction angles of the resultant radial force on wheel i with respect to the vehicle axes	rad
Z_F	ZF	I	Static distance along z axis between the sprung mass center of gravity and the center of gravity of the front unsprung masses	in	$\alpha_x, \beta_x, \gamma_x$		143	Direction angles of a line from wheel center i to the ground contact point of tire radial spring j with respect to the vehicle axes	rad
\bar{Z}'_G	ZGP(21,21,5)	I	Input elevations of the terrain table grid points	in	$\alpha_x, \beta_x, \gamma_x$		148	Direction angles of the resultant radial force on wheel i with respect to the space axes	rad
Z'_{Gi}	ZPGI(4)	126	Ground elevation with respect to the space axes of the point beneath the wheel centers	in	$\alpha_{hi}, \beta_{hi}, \gamma_{hi}$		257	Direction angles of a line perpendicular to both a normal to the tire-terrain contact plane and the wheel axis with respect to space	rad
Z'_{G1}			A vector through the ground contact point normal to the actual or equivalent ground contact plane		$\alpha_s, \beta_s, \gamma_s$				
Z_R	ZR	I	Static distance along the z axis between the sprung mass center of gravity and the rear axle roll center	in	$\alpha_x, \beta_x, \gamma_x$		102	Direction angles of the x axis with respect to space	rad
Z_{VB}	ZBV	I	Distance from the sprung mass c.g. to the plane defining the bottom of the vehicle along the z axis	in	$\alpha_y, \beta_y, \gamma_y$		100	Direction angles of the y axis with respect to space	rad
Z_{VT}	ZVT	I	Distance from the sprung mass c.g. to the plane defining the top of the vehicle, along the z axis	in	$\alpha_{y4}, \beta_{y4}, \gamma_{y4}$		85	Direction angles of a normal to the wheel i with respect to space	rad
α, β, γ $B^* B^* B^*$		266	Direction angles of a normal to the barrier face plane in the vehicle axes		$\alpha_{y4}, \beta_{y4}, \gamma_{y4}$		88	Direction angles of kingpin axis of wheel i	rad
α, β, γ $BT^* BT^* BT^*$		277	Direction angles of a normal to the barrier top plane in the vehicle axes		β_i	BETP(4)	219	Slip angle at wheel i	rad
α, β, γ $B1^* B1^* B1^*$		273	Direction angles of a normal to the plane perpendicular to the barrier face plane and containing the axis of rotation		β_i	BETBR(4)	223	Equivalent slip angle produced by camber of wheel i	rad
					γ_1	GAM1		Non dimensional slip angle variable for wheel i	
					$(T_2)_t$	GAM2	47	Inertial expressions	
					$(T_3)_t$	GAM3			

ANALYTICAL SYMBOL	PROGRAM SYMBOL	DEFINITION	UNITS	ANALYTICAL SYMBOL	PROGRAM SYMBOL	DEFINITION	UNITS
$(\tau_4)_t$	GAM4			ϵ_F, ϵ_R	EPSF	Friction lag in front and rear suspensions	in/sec
$(\tau_5)_t$	GAM5			ϵ_n	EPSR	Permanent set of the barrier for secondary impacts	in
$(\tau_6)_t$	GAM6			ϵ_V	EPSL		
$(\tau_7)_t$	GAM7			ϵ_W	EPSV	Friction lag in the vehicle-barrier friction force	in/sec
$(\tau_8)_t$	GAM8			ϵ_{WS}	EPSPS	Friction lag in steering system	deg/sec
$(\tau_9)_t$	GAM9			ζ_B	ZETAB	Threshold value of wheel rotational velocity below which logic is applied to limit brake torques	rad/sec
δ_1	DELBB	Barrier deflection	in	ζ_i		Suspension displacement of the relative to the vehicle from the position of static equilibrium	in
	DEL1	Right front suspension deflection for independent front suspension or front axle roll center deflection relative to the vehicle from position of static equilibrium	in	$(\zeta_0)_n, (\zeta_1)_n$	CDO	Coefficients for unloading force deflection characteristic of the barrier	
δ_2	DEL2	Left front suspension deflection relative to the vehicle from static equilibrium position	in	$(\zeta_2)_n$	CD1		
δ_3	DEL3	Right rear suspension deflection for independent rear suspension or rear axle roll center deflection relative to the vehicle from static equilibrium position	in	θ_c	THESKD	Vehicle slip angle	rad
	DEL4	Left rear suspension deflection relative to the vehicle from static equilibrium position	in	θ_{ci}	THGI(4)	Pitch angle of terrain under wheel i relative to the space axes	rad
ΔG	DELG	I Distance between road roughness input points	in	θ'_n	THETN	Value of θ at t=0 or at the nth indexing of the axes	rad
Δi	DELTA(4)	I Distance between the wheel center and ground contact point	in	$\dot{\theta}_t$	THETT	integrated value of $\dot{\theta}$ from t=0 or the nth indexing of the axes	
Δt	DT	I Numerical integration step interval	sec	$\theta_{xi, gi}$			
Δt_B	DELTB	I Time increment for use during barrier impacts	sec	λ_B	TLAMB	Angle between the x axis and the tire-terrain contact plane at wheel i	rad
Δt	DELTC	I Numerical integration step size for curb impact option	sec	λ_F, λ_R	XLAMF	Coefficient for inertial coupling terms in relationships for driving end of vehicle	
Δt_n	DTR	Integration step size for use with wheel spin equations of motion	sec	λ_T	XLAMR	Ratio of conserved to absorbed energy in the front and rear suspension bumpers or multiple of K_F, K_R for use in simulating suspension bumpers	
ΔT_{HF1}	DTHF1	I Front and rear half-track changes with suspension deflection	in	$\lambda_{zi}, \lambda_{zi}$	XLM1(4)	I Multiple of K_T for use in non-linear range of tire deflection	
ΔT_{HR1}	DTHR2			λ_{gi}	XLM2(4)	Constants for simultaneous solution of the ground contact point	
ΔT_{HR3}	DTHR3			μ_B	XLM3(4)		
ΔT_{HR4}	DTHR4				AMUB	I Effective coefficient of friction between the vehicle sprung mass and barrier	
$\Delta y'_B$	DELYBP	I Incremental deflection of the barrier position	in	μ_C	AMUC	Tire-curb friction factor	
$\Delta y_{f,j}$	DPSILF	I Ideal steer angle change	rad				
\bar{e}_B	EPSB	I Acceptable error in the force balance between the vehicle structure and barrier	lbs				

ANALYTICAL SYMBOL	PROGRAM SYMBOL	EDN NO.	DEFINITION	UNITS	ANALYTICAL SYMBOL	PROGRAM SYMBOL	EDN NO.	DEFINITION	UNITS
μ_{gl}	XMUIG(4)	I	Nominal coefficient of friction between tire i and ground		ϕ_f	PHIF		Angular displacement of front axle relative to the vehicle about a line parallel to the x-axis through the front roll center	rad
μ_i	XMU(4)	I	Peak value of friction coefficient for side forces for prevailing conditions of speed and load at wheel i		ϕ_{gi}	PHGI(4)	125	Camber angle of terrain under wheel i	rad
μ_{mi}	XMUM(4)	I	Nominal test surface friction coefficient on which tire properties were measured		ϕ_i	PHII(4)		Camber angles of four wheels relative to vehicle	rad
μ_{xi}	XMUX(4)	240	Effective friction coefficient between tire and terrain at wheel i in the direction along the tire circumference		ϕ_n	PHIN		Value of ϕ at t=0 or at the nth indexing of the axes	rad
μ_{xp_i}	XMUXP(4)	I	Peak circumferential friction coefficient for tire i		ϕ_r	PHIR		Angular displacement of rear axle relative to the vehicle about a line parallel to the x-axis through the rear roll center	rad
μ_{xs_i}	XMUXS(4)	I	Sliding circumferential friction coefficient for tire i		$\dot{\phi}_r$	PHIT	58	Integrated value of $\dot{\phi}$ from t=0 or the nth axis indexing	rad
π	PI		3.14159...		ϕ_{ygi}		105	Angle between y axis and tire-terrain contact plane	rad
ρ	RHO	I	Distance between rear axle center of gravity and roll center, positive for roll center above c.g.	in	ψ_{bdry}	PSBDRY(4,5)	I	Angle of interpolation boundaries in terrain tables, measured from the x'axis	rad
ρ_f	RHOF	I	Distance between front axle center of gravity and roll center, positive for roll center above c.g.	in	ψ_f	PSIF(50)	I	Table of front wheel steer angle vs time	rad
$\rho_s i$	RHOS(I)	198	Ratio of circumferential to peak side force friction coefficients for prevailing conditions of speed and load		ψ_i	PSII(4)		Steer angles of wheels relative to vehicle (positive-clockwise as viewed from above)	rad
$(\rho_s i)_{max}$	RHOMAX	198	Maximum value of $\rho_s i$ at the existing forward velocity of wheel i		ψ'_i	PSIIP(4)	89	Steer angles of wheels in tire-terrain contact plane	rad
σ_R	SIGR	I	Coefficients for the polynomial form of barrier load deflection characteristic		ψ_n	PSIN		Value of ψ at t=0 or the nth indexing of the axes	rad
σ_T	SIGT	I	Maximum radial tire deflection for quasi-linear load-deflection characteristic	in	ψ'_t	PSIT	99	Integrated value of ψ from t=0 or the nth axis indexing	rad
τ_A	TAUA	I	Ambient temperature	°F	Ω_F	OMEGR	I	Maximum suspension deflections from the equilibrium position for linear load-deflection characteristic of the springs	in
τ_i	TAU(4)	I	Temperature of brake assembly	°F	Ω_{FC}	OMEGR	I	Front and rear suspension deflections at which the compression bumpers are contacted, measured at the front wheels and the rear springs	in
τ_{i_0}	TAUO(4)	I	Initial temperature of brake assembly	°F	Ω_{RC}	OMEGR	I	Front and rear suspension deflections at which the extension bumpers are contacted, measured at the front wheels and rear springs	in
θ, θ, ψ	PHIT THETT PSIT		Euler angles of sprung mass axes relative to inertial axes	rad	Ω_{FE}	OMEGR	I	Front and rear suspension deflections at which the extension bumpers are contacted, measured at the front wheels and rear springs	in
ϕ_c	PHIC(50)	I	Table of front and rear wheel camber as a function of deflection	deg	Ω_{RE}	OMEGR	I	Front and rear suspension deflections at which the extension bumpers are contacted, measured at the front wheels and rear springs	in
ϕ_{cr}	PHIRC(50)								
ϕ_{ci}	PHICI(4)	86	Camber angles of wheels relative to the normal to tire-terrain contact plane	rad	Ω_T	OMEGR	I	Multiple of A_2 at which the assumed parabolic variations of small angle cornering and camber stiffnesses with tire loading are abandoned	rad
α_c, α_{cp}	PHIC1, PHIC2	I	Curb slope angles	rad	Ω	OMGPS	I	Front wheel steering angle at which the linear steering stops are engaged	rad
α_{cs}, α_{cp}	PHIC3, PHIC4								
α_{cs}, α_{cp}	PHIC5, PHIC6								

3. HVOSM MATHEMATICAL MODEL ANALYSIS

3.1 Derivation of Equations of Motion

The derivation of the equations that govern the general, unsteady motion of the vehicle is based on Euler's equations of motion written with respect to a moving axis system in order to avoid the appearance of the derivatives of the moments and products of inertia of the vehicle sprung mass in the equations. These equations take the general form (see for example, Reference 1):

$$\begin{aligned} m(\dot{u} + wQ - vR) &= F_x \\ m(\dot{v} + uR - wP) &= F_y \\ m(\dot{w} + vP - uQ) &= F_z \\ \dot{L}_x + QL_z - RL_y &= N_x \\ \dot{L}_y + RL_x - PL_z &= N_y \\ \dot{L}_z + PL_y - QL_x &= N_z \end{aligned} \quad (1)$$

where (u, v, w) , (P, Q, R) , (L_x, L_y, L_z) , (F_x, F_y, F_z) , and (N_x, N_y, N_z) are the scalar components along the vehicle axes of the linear velocity, the angular velocity, the angular momentum, the external forces, and the external moments, respectively.

Applying the assumption that symmetry exists in the xy and yz planes, i.e., the xy and yz products of inertia are zero, ($I_{xy} = I_{yz} = 0$) the angular equations become:

$$I_x \dot{P} - I_{xz} \dot{R} - QR(I_y - I_z) - QPI_{xz} = N_x \quad (2)$$

$$I_y \dot{Q} - (R^2 - P^2)I_{xz} - RP(I_z - I_x) = N_y \quad (3)$$

$$-I_{xz} \dot{P} + I_z \dot{R} - PQ(I_x - I_y) + QRI_{xz} = N_z \quad (4)$$

3.1.1

Sprung Mass

In the following derivations, inertial forces produced by accelerations of the unsprung masses are treated as external forces acting on the sprung mass. That is, the Euler equations of motion for the sprung mass are modified to include inertial effects of the unsprung masses.

For the case of sprung mass accelerations in the X direction, each of the unsprung masses is assumed to act as a point mass. With this assumption, the equating of inertial and applied forces in the X direction is

$$M_s(\ddot{u} - vR + wQ) = \sum F_{xu} + \sum F_{xs} - (\sum M)g \sin \theta - \sum F_{ixi} \quad (5)$$

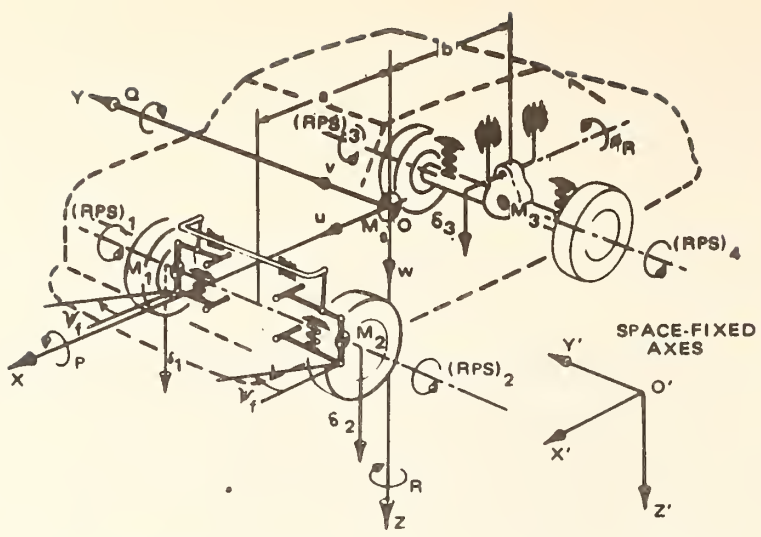
where $\sum F_{ixi}$ are the unsprung mass inertial forces in the X direction.

The scalar component in the X direction of the acceleration of a particle in a moving frame of reference (e.g., see Reference 1) is

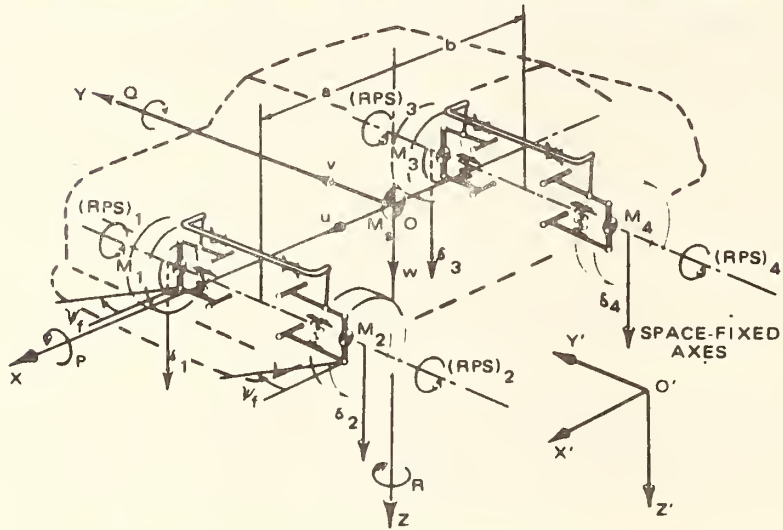
$$\begin{aligned} a_x &= \dot{u} - vR + wQ + \ddot{x} + 2Q\dot{z} - 2R\dot{y} \\ &\quad - x(Q^2 + R^2) + y(PQ - R) + z(PR + Q) \end{aligned} \quad (6)$$

In the vehicle representations depicted in Figure 3.1, constraints on the suspension system preclude motions of the unsprung masses, relative to the sprung mass, in the x direction. Therefore, in the present application of Equation (6), $\ddot{x} = 0$. Also, dynamic effects of motion of independently suspended unsprung masses, relative to the sprung mass, in the y direction are assumed to be negligible. Application of (6) to the cases of the independently suspended unsprung mass centers of gravity yields the following expression for inertial forces:

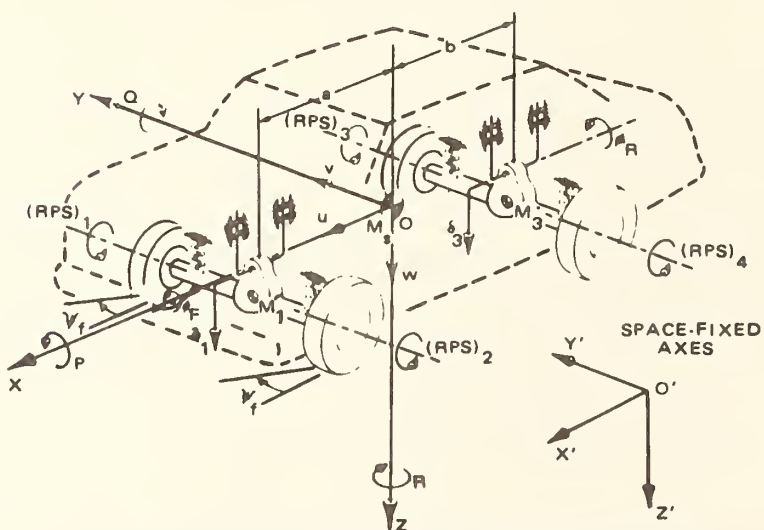
$$F_{ixi} = M_i a_{xi} = M_i [\dot{u} - vR + wQ + 2Q\dot{z}_i - x(Q^2 + R^2) + y(PQ - R) + z(PR + Q)] \quad (7)$$



(a) INDEPENDENT FRONT - SOLID AXLE REAR SUSPENSION



(b) INDEPENDENT FRONT AND REAR SUSPENSION



(c) SOLID AXLE FRONT AND REAR SUSPENSIONS

Figure 3.1 ANALYTICAL REPRESENTATION OF VEHICLES

where

$$\begin{array}{lll}
 x_1 = a & y_1 = T_F/2 & z_1 = z_F + \delta_1 \\
 x_2 = a & y_2 = -T_F/2 & z_2 = z_F + \delta_2 \\
 x_3 = -b & y_3 = T_R/2 & z_3 = z_R + \delta_3 \\
 x_4 = -b & y_4 = -T_R/2 & z_4 = z_R + \delta_4
 \end{array}$$

and $M_i = M_{UF}/2$ for $i = 1, 2$ or $M_i = M_{UR}/2$ for $i = 3, 4$.

Similar application of (6) to the beam axle centers of gravity yield:

$$F_{Ix_i} = M_i a_{x_i} = M_i [\ddot{x} - vR + wQ + 2Q\dot{z}_i + 2R\dot{y}_i - x(Q^2 + R^2) + y(PQ - R\dot{Q}) + z(PR + Q\dot{R})] \quad (8)$$

where

$$\begin{array}{lll}
 x_1 = a & y_1 = -\rho_F \dot{\phi}_F & z_1 = z_F + \delta_1 + \rho_F \\
 x_3 = -b & y_3 = -\rho \dot{\phi}_R & z_3 = z_R + \delta_3 + \rho \\
 \dot{y}_1 = -\rho_F \dot{\phi}_F & \dot{z}_1 = \dot{\delta}_1 + \rho_F \dot{\phi}_F & \\
 \dot{y}_3 = -\rho \dot{\phi}_R & \dot{z}_3 = \dot{\delta}_3 + \rho \dot{\phi}_R &
 \end{array}$$

and $M_i = M_{UF}$ for $i = 1$ and $M_i = M_{UR}$ for $i = 3$.

Substitution of (7) and/or (8) into (5) yields the equation of motion for acceleration of the sprung mass in the x direction as shown in the first row of the $\|D\|$ and $\|E\|$ matrices in Section 3.1.5.

The equation of motion for acceleration of the sprung mass in the y direction is:

$$M_s(\ddot{y} + uR - wP) = \sum F_{yu} + \sum F_{ys} + (\sum M)g \cos \theta \sin \phi - \sum F_{Iy_i} \quad (9)$$

The scalar component in the y direction of the acceleration of a particle in a moving frame of reference can be expressed as:

$$a_y = \dot{v} + uR - wP + \ddot{y} + 2R\dot{x} - 2P\dot{z} + x(PQ + \dot{R}) - y(P^2 + R^2) + z(QR - \dot{P}) \quad (10)$$

Independently suspended unsprung masses are assumed to act as point masses, and for purposes of dynamic interactions are also assumed to be constrained to motion parallel to the Z axis. For this case, the unsprung mass inertial forces acting on the sprung mass are:

$$F_{Iy_i} = M_i a_{y_i} = M_i [\dot{v} + uR - wP - 2P\dot{z}_i + x_i(PQ + \dot{R}) - y_i(P^2 + R^2) + z_i(QR - \dot{P})] \quad (11)$$

where

$$\begin{array}{lll} x_1 = a & y_1 = T_F/2 & z_1 = Z_F + \delta_1 \\ x_2 = a & y_2 = -T_F/2 & z_2 = Z_F + \delta_2 \\ x_3 = -b & y_3 = T_R/2 & z_3 = Z_R + \delta_3 \\ x_4 = -b & y_4 = -T_R/2 & z_4 = Z_R + \delta_4 \end{array}$$

and $M_i = M_{UF}/2$ for $i = 1, 2$ or $M_i = M_{UR}/2$ for $i = 3, 4$.

Inertia forces for a beam axle suspension are approximated by means of a thin rod representation as illustrated in Figure 3.2. For this case, the inertial force is given by:

$$F_{Iy_i} = \gamma \int_{-y_i}^{y_i} a_{y_i} dl = \gamma \int_{-y_i}^{y_i} [\dot{v} + uR - wP + \ddot{y}_i - 2P\dot{z}_i + x_i(PQ + \dot{R}) - y_i(P^2 + R^2) + z_i(QR - \dot{P})] dl \quad (12)$$

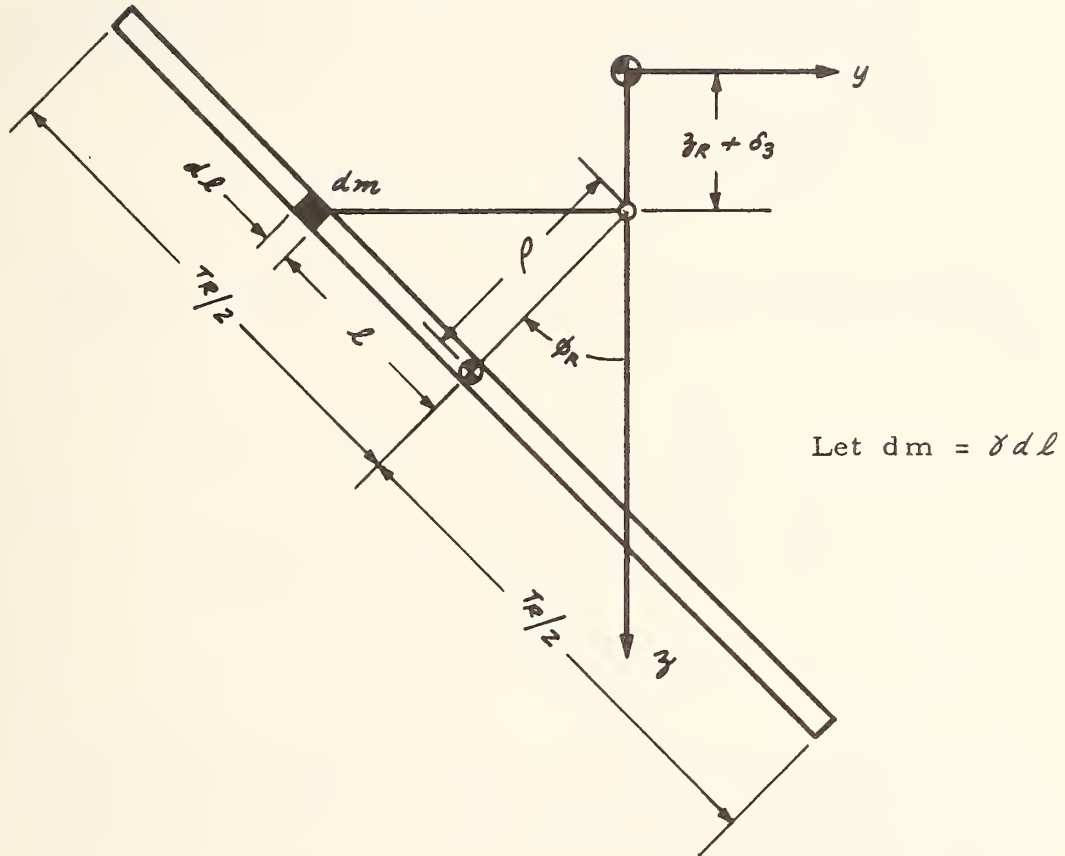


Figure 3.2 THIN ROD APPROXIMATION OF REAR AXLE INERTIAL PROPERTIES

and

$$\begin{array}{lll}
 x_1 = a & y_1 = -\rho_F \sin \phi_F - l \cos \phi_F & z_1 = z_F + \delta_1 + \rho_F \cos \phi_F - l \sin \phi_F \\
 & \dot{y}_1 = -\rho_F \dot{\phi}_F \cos \phi_F + l \dot{\phi}_F \sin \phi_F & \dot{z}_1 = \dot{\delta}_1 - \rho_F \dot{\phi}_F \sin \phi_F - l \dot{\phi}_F \cos \phi_F \\
 & \ddot{y}_1 = \rho_F \dot{\phi}_F^2 \sin \phi_F + l \dot{\phi}_F^2 \cos \phi_F & \\
 & -\rho_F \ddot{\phi}_F \cos \phi_F + l \ddot{\phi}_F \sin \phi_F & \\
 \\
 x_3 = -b & y_3 = -\rho \sin \phi_R - l \cos \phi_R & z_3 = z_R + \delta_3 + \rho \cos \phi_R - l \sin \phi_R \\
 & \dot{y}_3 = -\rho \dot{\phi}_R \cos \phi_R + l \dot{\phi}_R \sin \phi_R & \dot{z}_3 = \dot{\delta}_3 - \rho \dot{\phi}_R \sin \phi_R - l \dot{\phi}_R \cos \phi_R \\
 & \ddot{y}_3 = \rho \dot{\phi}_R^2 \sin \phi_R + l \dot{\phi}_R^2 \cos \phi_R & \\
 & -\rho \ddot{\phi}_R \cos \phi_R + l \ddot{\phi}_R \sin \phi_R &
 \end{array}$$

Substituting into (12) and assuming ϕ_F and ϕ_R to be small angles yields:

$$\begin{aligned}
 F_{Iy_1} = M_{UF} [& \dot{v} + uR - wP + \rho_F \phi_F \dot{\phi}_F^2 - \rho_F \ddot{\phi}_F - 2P\dot{\delta}_1 + 2P\rho_F \phi_F \dot{\phi}_F + a(PQ + \dot{R}) \\
 & + \rho_F \phi_F (P^2 + R^2) + (z_F + \delta_1 + \rho_F)(QR - \dot{P})] \quad (13)
 \end{aligned}$$

$$\begin{aligned}
 F_{Iy_3} = M_{UR} [& \dot{v} + uR - wP + \rho \phi_R \dot{\phi}_R^2 - \rho \ddot{\phi}_R - 2P\dot{\delta}_3 + 2P\rho \phi_R \dot{\phi}_R - b(PQ + \dot{R}) \\
 & + \rho \phi_R (P^2 + R^2) + (z_R + \delta_3 + \rho)(QR - \dot{P})] \quad (14)
 \end{aligned}$$

Substitution of the appropriate inertial force equations into (9) for the different suspension options yields the equation for vehicle acceleration in the y direction as defined by the second row of matrices $\|D\|$ and $\|E\|$ in Section 3.1.5.

For the case of sprung mass accelerations in the z direction, interaction with the unsprung masses takes place through the mechanism of the suspension forces. Therefore, the corresponding equation of motion can be written directly as

$$M_s(\dot{w} + vP - uQ) = -\sum F_{zi} + \sum F_{zs} + M_s g \cos \theta \cos \phi \quad (15)$$

This equation appears in the third row of matrices $\|D\|$ and $\|E\|$ in Section 3.1.5.

The equations defining angular motions are derived in a similar manner. That is, the preceding definitions of the unsprung mass acceleration components are substituted in the following equations.

$$\begin{aligned} I_x \dot{P} - I_{xz} \dot{R} - QR(I_y - I_z) - QPI_{xz} &= \sum N_{\phi u} + \sum N_{\phi s} + \sum F_{Iy_i} z_i \\ &\quad - \sum M_i z_i g \cos \theta \sin \phi \end{aligned} \quad (16)$$

where F_{Iy_i} are defined by (11) or (12) for either independent suspension or beam axle suspension unsprung masses. For independent suspension z_i are given by:

$$\begin{aligned} z_1 &= z_F + \delta_1 \\ z_2 &= z_F + \delta_2 \\ z_3 &= z_R + \delta_3 \\ z_4 &= z_R + \delta_4 \end{aligned} \quad (17)$$

and for beam axles:

$$\begin{aligned} z_1 &= z_F + \delta_1 \\ z_3 &= z_R + \delta_3 \end{aligned} \quad (18)$$

$$\begin{aligned} I_y Q - (R^2 - P^2) I_{xz} - RP(I_z - I_x) &= \sum N_{\theta u} + \sum N_{\theta s} - \sum F_{Ix_i} z_i \\ &\quad - \sum M_i z_i g \sin \theta \end{aligned} \quad (19)$$

where F_{Ix_i} are given by (7) and (8), z_i by (17) for the independent suspension and by

$$z_1 = z_F + \delta_1 + \rho_F$$

$$z_3 = z_R + \delta_3 + \rho$$

for the beam axle suspension option.

$$\begin{aligned} -I_{xz}\dot{P} + (I_x + I_R)\dot{R} - PQ(I_x - I_y) + QR\dot{I}_{xz} &= \sum N\psi_u + \sum N\psi_s + \sum F_{Ix_i} y_i \\ -\sum F_{Iy_i} x_i + \sum M_i x_i g \cos\theta \sin\phi + \sum M_i y_i g \sin\theta \end{aligned} \quad (20)$$

where F_{Ix_i} , F_{Iy_i} are given by (7), (8), (11) and (12) for either

suspension type, $x_i = a$ for $i = 1, 2$ and $x_i = -b$ for $i = 3, 4$.

For independent suspension,

$$y_1 = T_F/2$$

$$y_2 = -T_F/2$$

$$y_3 = T_R/2$$

$$y_4 = -T_R/2$$

and for beam axle suspension

$$y_1 = -\rho_F \phi_F$$

$$y_3 = -\rho \phi_R$$

Appropriate substitutions lead to the fourth, fifth and sixth rows of matrixies $\|D\|$ and $\|E\|$ in Section 3.1.5.

3.1.2 Unsprung Masses

In the following derivations, the general procedure that is applied to aircraft control systems in Reference 1 is followed. That is, the equations of motion are obtained by application of Lagrange's equation of motion in a moving frame of reference:

$$\frac{d}{dt} \left(\frac{\partial T}{\partial \dot{q}_k} \right) - \frac{\partial T}{\partial q_k} = \mathcal{F} \quad (21)$$

where T = kinetic energy relative to the vehicle-fixed axis system of that portion of the total unsprung mass that has q_k for a degree of freedom,

$$\mathcal{F} = \frac{\partial W}{\partial q_k} = \text{generalized force, or moment,}$$

W = work done on the unsprung mass system, in degree of freedom q_k , by the external forces which act upon it, including the effects of the inertia force field produced by acceleration and rotation of the vehicle-fixed axis system, and q_k = generalized coordinate (i.e., degree of freedom) relative to the vehicle-fixed axes.

Independent Suspension Unsprung Masses

The kinetic energy of an independently suspended unsprung mass relative to the vehicle-fixed system (in its assumed form of a point mass and neglecting wheel rotation) can be expressed as

$$T = \frac{1}{2} \left(\frac{M_{ui}}{Z} \right) \dot{\delta}_i^2 \quad (22)$$

where the subscript i refers to the mass number (1 = right front, 2 = left front, 3 = right rear, 4 = left rear) and the subscript j identifies the front or rear.

The generalized force, \mathcal{F} , is obtained by means of determination of the virtual work done by external forces, including inertia forces, during a virtual displacement of the right front unsprung mass:

$$\delta W = \left(F_{3ui} + S_i + \frac{M_{ui} g}{Z} \cos \theta \cos \phi \right) \delta(\delta_i) + \delta(W_i) \quad (23)$$

where δW_i = work done by the inertia forces.

Let the acceleration of the right front unsprung mass relative to the space-fixed axes be $\bar{\alpha}$, and relative to the vehicle-fixed axes be $\bar{\alpha}'$. Then the acceleration due to motion of the vehicle is $(\bar{\alpha} - \bar{\alpha}')$ and the corresponding inertia force is

$$d\bar{F}_i = -(\bar{\alpha} - \bar{\alpha}') dm \quad (24)$$

The components of $d\bar{F}_i$ in the x and y directions are perpendicular to the virtual displacement, $\delta(\delta_i)$, and can, therefore, do no work during the displacement. The scalar component of $d\bar{F}_i$ in the z direction can be expressed as follows:

$$\begin{aligned} dF_{zi} = & - \left[\dot{w} + vP - uQ + x_i(PR - \dot{Q}) + y_i(QR + \dot{P}) \right. \\ & \left. - (z_j + \delta_i)(P^2 + Q^2) \right] dm \end{aligned} \quad (25)$$

Since the front independently suspended unsprung masses are treated as point masses, the virtual work due to inertial forces is given by

$$\begin{aligned} \delta W_i = & - \frac{M_{uj}}{2} \left[\dot{w} + vP - uQ + x_i(PR - \dot{Q}) + y_i(QR + \dot{P}) \right. \\ & \left. - (z_j + \delta_i)(P^2 + Q^2) \right] \delta(\delta_i) \end{aligned} \quad (26)$$

Application of Equations (22), (23) and (26) in Equation (21) yields the equations for independently unsprung masses in the matrices $\|D\|$ and $\|E\|$ in Section 3.1.5.

Beam Axle Unsprung Mass

From Figure 3.3, the motions of the center of gravity of the axle are defined by the following relationships (note that the subscript j is used here to indicate either the front or rear axle):

$$\begin{aligned} y &= -\rho_j \sin \phi_j & \bar{z} &= \bar{z}_j + \delta_j + \rho_j \cos \phi_j \\ \dot{y} &= -\rho_j \dot{\phi}_j \cos \phi_j & \dot{\bar{z}} &= \dot{\delta}_j - \rho_j \dot{\phi}_j \sin \phi_j \\ \ddot{y} &= \rho_j (\dot{\phi}_j^2 \sin \phi_j - \ddot{\phi}_j \cos \phi_j) & \ddot{\bar{z}} &= \ddot{\delta}_j - \rho_j (\dot{\phi}_j^2 \cos \phi_j + \ddot{\phi}_j \sin \phi_j) \end{aligned}$$

The kinetic energy of the axle, relative to the axis system fixed in the sprung mass can be expressed:

$$\begin{aligned} T &= \frac{1}{2} I_j \dot{\phi}_j^2 + \frac{1}{2} M_{uj} (\dot{y}^2 + \dot{\bar{z}}^2) , \text{ or} \\ T &= \frac{1}{2} I_j \dot{\phi}_j^2 + \frac{1}{2} M_{uj} (\rho_j^2 \dot{\phi}_j^2 + \dot{\delta}_j^2 - 2\rho_j \dot{\phi}_j \dot{\delta}_j \sin \phi_j) \end{aligned} \quad (27)$$

Evaluation of the left side of Equation (21) for each of the axle degrees of freedom, and a subsequent assumption of a small angle restriction on ϕ_j , yields:

$$\frac{d}{dt} \left(\frac{\partial T}{\partial \dot{\phi}_j} \right) - \frac{\partial T}{\partial \phi_j} = (I_j + M_{uj} \rho_j^2) \ddot{\phi}_j - (M_{uj} \rho_j \phi_j) \ddot{\delta}_j \quad (28)$$

$$\frac{d}{dt} \left(\frac{\partial T}{\partial \dot{\delta}_j} \right) - \frac{\partial T}{\partial \delta_j} = M_{uj} (\ddot{\delta}_j - \rho_j \dot{\phi}_j^2 - \rho_j \phi_j \ddot{\phi}_j) \quad (29)$$

The work done by the inertia forces produced by vehicle motions during a virtual displacement, $\delta (-\delta_j)$, is determined as follows (see Figure 3.3 and Equation (22)).

$$\frac{\delta W_i}{\delta (\delta_j)} = \int_{-\delta_j/2}^{+\delta_j/2} dF_3 = -\gamma \int_{-\delta_j/2}^{+\delta_j/2} (a_3 - \ddot{z}) d\ell \quad (30)$$

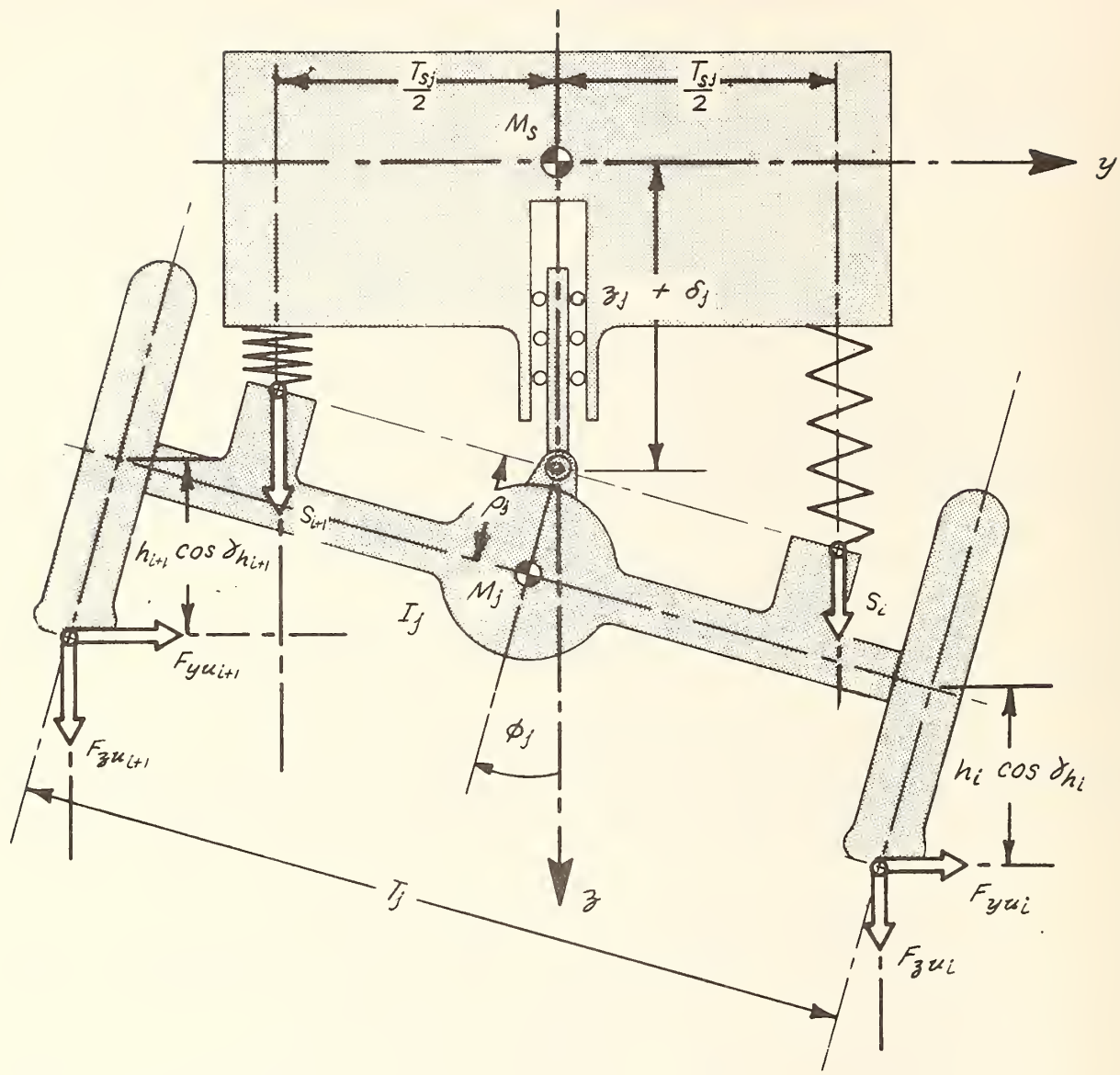


Figure 3.3 AXLE REPRESENTATION

The scalar component of acceleration of element dl in the \mathcal{Z} direction, due to motion of the vehicle, is defined by the following expression:

$$\begin{aligned}
 a_3 - \ddot{z} &= \dot{w} + Pv - Qu - 2P\rho_j\dot{\phi}_j \cos \phi_j + x(PR - Q) \\
 &\quad - (\rho_j \sin \phi_j + l \cos \phi_j)(QR + P) \\
 &\quad - (z_j + \delta_j + \rho_j \cos \phi_j - l \sin \phi_j)(P^2 + Q^2)
 \end{aligned} \tag{31}$$

Substitution of (31) into (30), integration of (30) where $x = a$ for the front and $x = -b$ for the rear, and subsequent assumption of a small angle restriction on ϕ_j , yields the portion of the generalized force that corresponds to inertial forces produced by vehicle motions. When this results and Equation (29) are substituted in the following relationship, the equation of motion for the vertical acceleration of the beam axle is obtained:

$$\begin{aligned}
 \frac{d}{dt} \left(\frac{\partial T}{\partial \dot{\phi}_j} \right) - \frac{\partial T}{\partial \phi_j} &= \frac{\delta(W_j)}{\delta(\phi_j)} + F_{3u_L} + F_{3u_{L+1}} \\
 &\quad + S_i + S_{i+1} + M_{u_j} g \cos \theta \cos \phi
 \end{aligned} \tag{32}$$

The work done by the inertia forces produced by vehicle motions during a virtual displacement, $\delta(\phi_j)$, is determined as follows (see Figure 3.3 and Equation (24)).

$$\begin{aligned}
 \frac{\delta(W_j)}{\delta(\phi_j)} &= - \int_{-T_j/2}^{+T_j/2} \left[dF_y (\rho_j \cos \phi_j - l \sin \phi_j) + dF_z (\rho_j \sin \phi_j + l \cos \phi_j) \right] \\
 &= \delta \int_{-T_j/2}^{+T_j/2} \left[(a_y - \ddot{y})(\rho_j \cos \phi_j - l \sin \phi_j) \right. \\
 &\quad \left. + (a_3 - \ddot{z})(\rho_j \sin \phi_j + l \cos \phi_j) \right] dl
 \end{aligned} \tag{33}$$

The scalar component of acceleration of element dl in the z direction, due to motion of the vehicle, is defined by Equation (31). The corresponding component in the y direction is defined by the following expression:

$$\begin{aligned} a_y - \ddot{\gamma} &= \dot{v} + Ru - Pw - 2P(\dot{\delta}_j - \rho_j \dot{\phi}_j \sin \phi_j) - (PQ + R\dot{r}) \\ &\quad + (\rho_j \sin \phi_j + l \cos \phi_j)(P^2 + R^2) \\ &\quad + (z_j + \delta_j + \rho_j \cos \phi_j - l \sin \phi_j)(QR - \dot{r}) \end{aligned} \quad (34)$$

Substitution of (31) and (34) into (33), integration of (33) and subsequent assumption of a small angle restriction on ϕ_j , yields the portion of the generalized moment that corresponds to inertial force produced by vehicle motions. When this result and Equation (28) are substituted in the following relationship, the equation of motion for the angular acceleration of the beam axle is obtained.

$$\frac{d}{dt} \left(\frac{\partial T}{\partial \dot{\phi}_j} \right) - \frac{\partial T}{\partial \phi_j} = \frac{\delta(W_j)}{\delta(\phi_j)} + N_{\phi_j} \quad (35)$$

3.1.3 Steering System

The steer mode degree of freedom is defined by the following relationships with the assumption that inertial coupling effects are negligible:

$$\begin{aligned} I_\psi \ddot{\psi}_F + T_1 \psi + T_2 \psi &= F_{yu1}(h_1 \cos \alpha_{h1} - \bar{P} \cos \psi'_1 \cos \theta_{xG1}) \\ &\quad + F_{yu2}(h_2 \cos \alpha_{h2} - \bar{P} \cos \psi'_2 \cos \theta_{xG2}) \\ &\quad - F_{xu1} h_1 (\cos \beta_{h1} + \phi_1 \cos \gamma_{h1}) - F_{xu2} h_2 (\cos \beta_{h2} + \phi_2 \cos \gamma_{h2}) \\ &\quad + F_{zu1} \phi_1 h_1 \cos \alpha_{h1} + F_{zu2} \phi_2 h_2 \cos \alpha_{h2} \end{aligned} \quad (36)$$

where

$$T_1\psi = \begin{cases} 0 & , \text{ for } |\dot{\psi}_F| \leq \epsilon_\psi \\ C'_\psi \operatorname{sgn} \dot{\psi}_F & , \text{ for } |\dot{\psi}_F| > \epsilon_\psi \end{cases}$$

$$T_2\psi = \begin{cases} 0 & , \text{ for } |\psi_F| \leq \Omega_\psi, \text{ or } \operatorname{sgn} \dot{\psi}_F \neq \operatorname{sgn} \dot{\psi}_e \\ \operatorname{sgn} \dot{\psi}_F K_\psi (|\psi_F| - \Omega_\psi) & , \text{ for } |\psi_F| > \Omega_\psi \end{cases}$$

The assumed form of the steer angle stops is depicted in Figure 3.4.

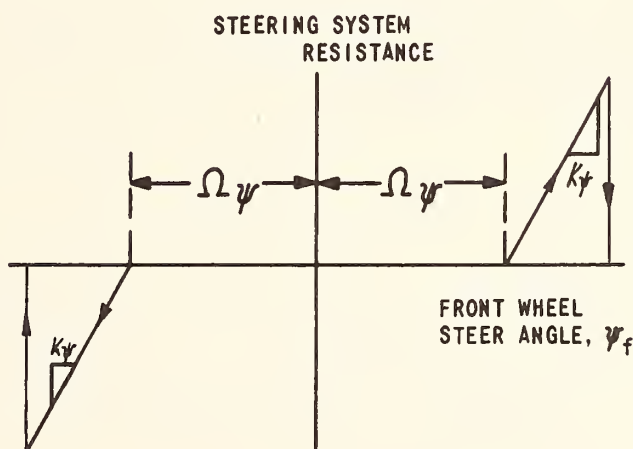


Figure 3.4 STEERING SYSTEM RESISTANCE VS STEER ANGLE

In the HVOSM-VD2 program version, torques generated within the steering system by gyroscopic precession of the spinning front wheels are approximated by means of the following added term in Equation (36):

$$I_{\psi} \ddot{\psi}_F + T_1 \dot{\psi} + T_2 \dot{\psi} = \dots + I_{WF} [(RPS)_1 \left(P + \frac{d\phi_1}{d\delta_1} \dot{\delta}_1 \right) \cos \psi_1 + (RPS)_2 \left(P + \frac{d\phi_2}{d\delta_2} \dot{\delta}_2 \right) \cos \psi_2] \quad (37)$$

3.1.4 Wheel Spin (HVOSM-VD2 Program Version)

The inertial coupling of the drive wheels, through the differential gears, and the associated effects of drive-line inertia can exert a significant influence on the occurrence of wheel lock. Therefore, it was necessary to derive differential equations for the rotational motions of the drive wheels, that would include these effects. Since the developed program, for generality, permits the simulation of either rear or front wheel drive, the derived equations are applied to both ends of the vehicle. The coupling effects are suppressed at the nondriving end by means of the input of a zero value for the associated drive line inertia.

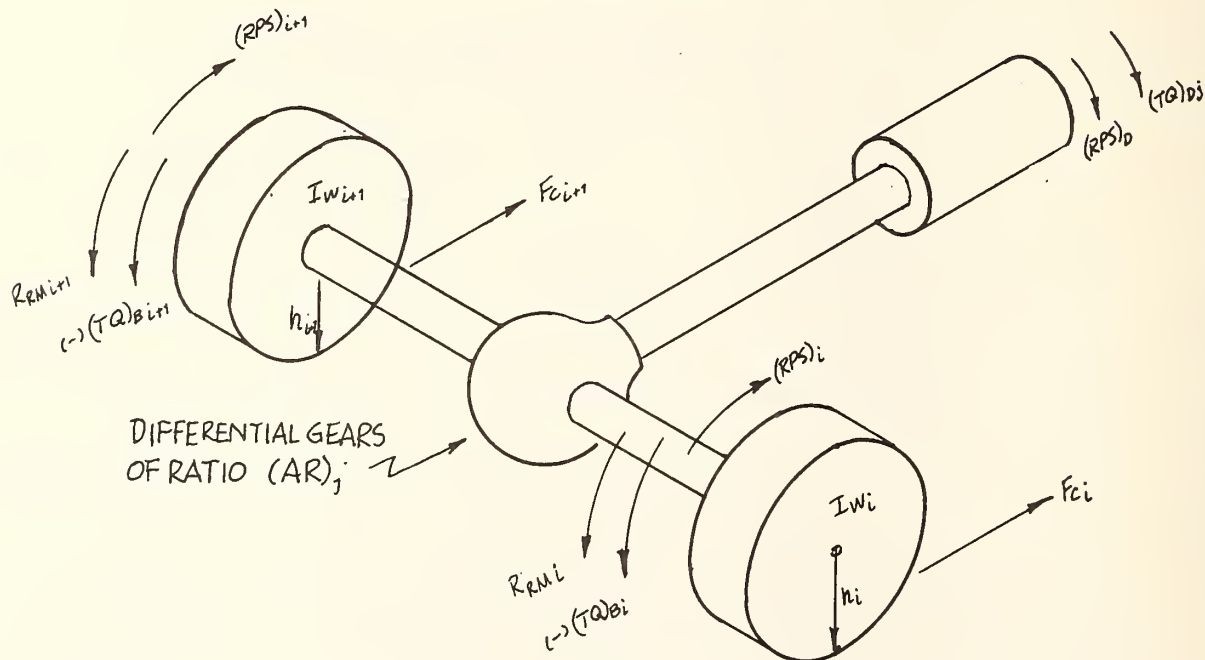


Figure 3.5 INERTIAL COUPLING OF DRIVE WHEELS

The kinetic energy of the system depicted in Figure 3.5 can be expressed

$$\Gamma = \frac{1}{2} I_{W_i} (RPS)_i^2 + \frac{1}{2} I_{W_{i+1}} (RPS)_{i+1}^2 + \frac{1}{2} I_{D_j} (RPS)_{Dj}^2 \quad (38)$$

Let $(RPS)_{Dj} = (AR)_j \left[\frac{(RPS)_i + (RPS)_{i+1}}{2} \right]$

then $\Gamma = \frac{1}{2} I_{W_i} (RPS)_i^2 + \frac{1}{2} I_{W_{i+1}} (RPS)_{i+1}^2 + \frac{1}{2} I_{Dj} (AR)_j^2 \left[\frac{(RPS)_i^2 + 2(RPS)_i (RPS)_{i+1} + (RPS)_{i+1}^2}{4} \right] \quad (39)$

Collecting terms, Equation (39) becomes

$$\Gamma = \left[\frac{I_{W_i}}{2} + \frac{I_{Dj} (AR)_j^2}{8} \right] (RPS)_i^2 + \left[\frac{I_{W_{i+1}}}{2} + \frac{I_{Dj} (AR)_j^2}{8} \right] (RPS)_{i+1}^2 + \frac{I_{Dj} (AR)_j^2}{4} (RPS)_i (RPS)_{i+1} \quad (40)$$

The potential energy of the system, V , in the rotational mode (i.e., torsional wind-up of axle and propeller shafts, elastic distortion of tires) is assumed to be negligible. Therefore,

$$V = 0 \quad (41)$$

Energy dissipation may be expressed in the following form:

$$D = -12(TQ)_{Dj} (RPS)_{Dj} + [F_{ci} h_i + R_{RMi} - 12(TQ)_{Bi}] (RPS)_i + [F_{ci+1} h_{i+1} + R_{RMi+1} - 12(TQ)_{Bi+1}] (RPS)_{i+1} \quad (42)$$

Substitution for and collection of terms yields

$$\begin{aligned} D = & [F_{ci} h_i - 6(TQ)_{Dj} (AR)_j + R_{RMi} - 12(TQ)_{Bi}] (RPS)_i \\ & + [F_{ci+1} h_{i+1} - 6(TQ)_{Dj} (AR)_j + R_{RMi+1} - 12(TQ)_{Bi+1}] (RPS)_{i+1} \end{aligned} \quad (43)$$

Application of Langrange's equation of motion to Equation (40), (41) and (43) yields:

$$\left[I_{W_i} + \frac{I_{Dj}(AR)_j^2}{4} \right] \left[\frac{d}{dt} (RPS)_i \right] + \left[\frac{I_{Dj}(AR)_j^2}{4} \right] \left[\frac{d}{dt} (RPS)_{i+1} \right] = -F_{ci} h_i + 12(TQ)_{Bi} + 6(AR)_j (TQ)_{Dj} + R_{RMi} \quad (44)$$

$$\left[\frac{I_{Dj}(AR)_j^2}{4} \right] \left[\frac{d}{dt} (RPS)_i \right] + \left[I_{W_{i+1}} + \frac{I_{Dj}(AR)_j^2}{4} \right] \left[\frac{d}{dt} (RPS)_{i+1} \right] = -F_{ci+1} h_{i+1} + 12(TQ)_{Bi+1} + 6(AR)_j (TQ)_{Dj} + R_{RMi+1} \quad (45)$$

The rates of change of the wheel angular velocities are integrated directly.

$$(RPS)_i = (RPS)_{i_0} + \int_0^t \frac{d}{dt} (RPS)_i \ dt \quad (46)$$

where

$$(RPS)_{i_0} = \frac{u_{gi_0} \cos \psi'_{i_0} + v_{gi_0} \sin \psi'_{i_0}}{h_{i_0}}$$

3.1.5 Summary of Equations of Motion for Sprung and Unsprung Masses

3.1.5.1 Independent Front Suspension - Berm Axle Rear Suspension Equations of Motion

The equations of motion are simplified by the use of the following combinations of inertial terms:

$$\begin{aligned}
 \Sigma M &= M_s + M_{uf} + M_{ur} \\
 (I'_x)_t &= M_{uf} \left[\dot{z}_f^2 + z_f (\delta_1 + \delta_2) + \frac{\delta_1^2 + \delta_2^2}{2} \right] + M_{ur} (\dot{z}_R + \delta_3)^2 + \rho M_{ur} (\dot{z}_R + \delta_3) \\
 (I'_y)_t &= (I'_x)_t + \rho M_{ur} (\dot{z}_R + \delta_3 + \rho) \\
 (I'_z)_t &= M_{uf} \left[a^2 + \left(\frac{T_f}{2} \right)^2 \right] + M_{ur} (b^2 + \rho^2 \phi_R^2) \\
 (I'_{yz})_t &= M_{uf} a \left(\dot{z}_f + \frac{\delta_1 + \delta_2}{2} \right) - M_{ur} b (\dot{z}_R + \delta_3) \\
 (I'_{y3})_t &= \frac{M_{uf} T_f}{4} (\delta_1 - \delta_2) - M_{ur} \rho \phi_R (\dot{z}_R + \rho + \delta_3) \\
 \delta_1 &= M_{uf} a - M_{ur} b \\
 (\dot{\delta}_2)_t &= M_{uf} \left(\dot{z}_f + \frac{\delta_1 + \delta_2}{2} \right) + M_{ur} (\dot{z}_R + \rho + \delta_3) \\
 (\dot{\delta}_3)_t &= (\dot{\delta}_2)_t - M_{ur} \rho \\
 (\dot{\delta}_4)_t &= (I'_{yz})_t + M_{ur} \rho^2 \phi_R \\
 (\dot{\delta}_5)_t &= M_{uf} \left[a^2 - \left(\frac{T_f}{2} \right)^2 \right] + M_{ur} \left[b^2 - \rho^2 \phi_R^2 \right] \\
 (\dot{\delta}_6)_t &= 2 \left[\frac{M_{uf}}{2} (\dot{\delta}_1 + \dot{\delta}_2) + M_{ur} (\dot{\delta}_3 - \rho \phi_R \dot{\phi}_R) \right] \\
 (\dot{\delta}_7)_t &= 2 \left\{ \frac{M_{uf}}{2} \left[\dot{z}_f (\dot{\delta}_1 + \dot{\delta}_2) + \delta_1 \dot{\delta}_1 + \delta_2 \dot{\delta}_2 \right] + M_{ur} (\dot{z}_R + \delta_3) (\dot{\delta}_3 - \rho \phi_R \dot{\phi}_R) \right\} \\
 (\dot{\delta}_8)_t &= 2 \left[\frac{M_{uf} T_f}{4} (\dot{\delta}_1 - \dot{\delta}_2) - M_{ur} \rho \phi_R (\dot{\delta}_3 - \rho \phi_R \dot{\phi}_R) \right] \\
 (\dot{\delta}_9)_t &= 2 \left[\frac{M_{uf} a}{2} (\dot{\delta}_1 + \dot{\delta}_2) - M_{ur} b (\dot{\delta}_3 - \rho \phi_R \dot{\phi}_R) \right]
 \end{aligned} \tag{47}$$

$$\begin{array}{c}
\boxed{\begin{array}{cccccc}
\Sigma M & 0 & 0 & 0 & \delta_2 & \rho M_{ur} \phi_K & 0 \\
\Sigma M & 0 & -\gamma_2 & 0 & 0 & 0 & 0 \\
0 & 0 & M_s & 0 & 0 & 0 & 0 \\
0 & -\gamma_3 & 0 & I_x + I_z' & 0 & -I_{xz} - I_{zy}' & \rho M_{ur}(\beta_{\alpha} + \delta_3) \\
\delta_2 & 0 & 0 & 0 & 0 & 0 & 0 \\
\rho M_{ur} \phi_K & \gamma_1 & 0 & I_y + I_y' & -I_z' & 0 & 0 \\
0 & 0 & 0 & -I_{yz} - I_{xy}' + \rho M_{ur} b & -I_{yz} & 0 & 0 \\
0 & 0 & \frac{M_{ur}}{2} & \frac{M_{ur} T_x}{4} & 0 & \frac{M_{ur} a}{2} & 0 \\
0 & 0 & \frac{M_{ur}}{2} & -\frac{M_{ur} T_x}{4} & 0 & -\frac{M_{ur} a}{2} & 0 \\
0 & 0 & 0 & M_{ur} & -\rho M_{ur} \phi_K & b M_{ur} & 0 \\
0 & -\rho M_{ur} & -\rho M_{ur} \phi_K & I_x + \rho M_{ur}(\beta_{\alpha} + \delta_3) & -\rho M_{ur} b \phi_K & \rho M_{ur} b & 0 \\
0 & 0 & 0 & -\rho M_{ur} & 0 & 0 & -\rho M_{ur} \phi_K & I_x + M_{ur} \rho^2
\end{array}} = \boxed{\begin{array}{c} \dot{u} \\ \dot{v} \\ \dot{w} \\ \dot{p} \\ Q \\ E \end{array}}
\end{array}$$

$$\begin{aligned}
& \left(\Sigma M \right) (vR - wQ - g \sin \theta) - \delta_2 PR + \rho M_{ue} \phi_e PQ + \delta_1 (Q^2 + R^2) - \delta_6 Q - 2M_{ue} \rho \dot{\phi}_e R + \Sigma F_{xz} + \Sigma F_{zu} \\
& \left(\Sigma M \right) (wP - uR + g \cos \theta \sin \phi) + \delta_2 P - \delta_1 PQ - \delta_2 QR - \rho M_{ue} \phi_e (P^2 + R^2 + \dot{\phi}_e^2) + \Sigma F_{yz} + \Sigma F_{yu} \\
& M_s (uQ - vP + g \cos \theta \cos \phi) - \Sigma F_{yz} + \Sigma F_{zs} \\
& \delta_3 (uR - wP - g \cos \theta \sin \phi) + (I_{xz} + I'_{xz}) PQ - \delta_1 P + (I_y - I_z + I'_z) QR - \delta_4 (P^2 + R^2) + \rho M_{ue} \phi_e (\delta_x + \delta_z) \dot{\phi}_e^2 + \Sigma N \phi_s + \Sigma N \phi_u \\
& I_{xz} (R^2 - P^2) + (I_3 - I_x - I'_y) PR + \delta_2 (vR - wQ - g \sin \theta) - \delta_1 v z M_{ue} \rho (\delta_3 - \rho M_{ue} b) (Q^2 + R^2) - I'_{yz} PQ \\
& - 2M_{ue} (\delta_R + \rho + \delta_3) \rho \dot{\phi}_e R + \Sigma N_{bs} + \Sigma N_{bu} \\
& (I_z - I_y) PQ - (I_{xz} + I'_{xz} - M_{ue} \rho b) QR + \delta_2 Q + I'_{yz} PR + \delta_2 P + \rho M_{ue} \phi_e [vR - wQ - 2R \dot{\phi}_e^2 - b(Q^2 - P^2 \dot{\phi}_e^2) - g \sin \theta] \\
& + \delta_1 (wP - uR + g \cos \theta \sin \phi) + \Sigma N_{ys} + \Sigma N_{yu} \\
& \frac{M_{ue}}{2} [uQ - vP - aPR - \frac{I'_x}{2} QR + (\delta_x + \delta_z) (P^2 + Q^2) + g \cos \theta \cos \phi] + F_{yu} + S_r \\
& \frac{M_{ue}}{2} [uQ - vP - aPR + \frac{I'_x}{2} QR + (\delta_x + \delta_z) (P^2 + Q^2) + g \cos \theta \cos \phi] + F_{zu} + S_z \\
& M_{ue} [uQ - vP + \rho \dot{\phi}_e^2 + 2PR \dot{\phi}_e + bPR + \rho \phi_e QR + (\delta_x + \delta_3 + \rho) (P^2 + Q^2) + g \cos \theta \cos \phi] + F_{uz} + F_{u4} + S_3 + S_4 \\
& \rho M_{ue} [uR - wP - 2P \dot{\phi}_3 + 2PP \phi_e \dot{\phi}_e - bPQ + \rho \phi_e (P^2 + R^2) + (\delta_x + \delta_3 + \rho) QR - g \cos \theta \sin (\phi + \phi_e)] + \rho M_{ue} \phi_e [vP - uQ - 2P \rho \dot{\phi}_e \\
& - bPR - \rho \phi_e QR - (\delta_x + \delta_3 + \rho) (P^2 + Q^2)] - I_e \phi_e (R^2 - Q^2) - I'_e QR + \Sigma N \phi_e
\end{aligned}$$

3.1.5.2 Independent Front and Rear Suspension
 Equations of Motion

$$I'_x = \frac{M_{UF}}{2} \left[(z_F + \delta_1)^2 + (z_F + \delta_2)^2 \right] + \frac{M_{UR}}{2} \left[(z_R + \delta_3)^2 + (z_R + \delta_4)^2 \right]$$

$$I'_y = I'_x$$

$$I'_z = M_{UF} \left[a^2 + \left(\frac{T_F}{2} \right)^2 \right] + M_{UR} \left[b^2 + \left(\frac{T_R}{2} \right)^2 \right]$$

$$I'_{xz} = \frac{M_{UF}}{2} \left[a(z_F + \delta_1) + a(z_F + \delta_2) \right] - \frac{M_{UR}}{2} \left[b(z_R + \delta_3) + b(z_R + \delta_4) \right]$$

$$I'_{yz} = \frac{M_{UF}}{2} \left[\frac{T_F}{2}(z_F + \delta_1) - \frac{T_F}{2}(z_F + \delta_2) \right] + \frac{M_{UR}}{2} \left[\frac{T_R}{2}(z_R + \delta_3) - \frac{T_R}{2}(z_R + \delta_4) \right]$$

$$\gamma_1 = M_{UF}a - M_{UR}b \quad (49)$$

$$\gamma_2 = M_{UF} \left[z_F + \left(\frac{\delta_1 + \delta_2}{2} \right) \right] + M_{UR} \left[z_R + \left(\frac{\delta_3 + \delta_4}{2} \right) \right]$$

$$\gamma_5 = M_{UF} \left[a^2 - \left(\frac{T_F}{2} \right)^2 \right] + M_{UR} \left[b^2 - \left(\frac{T_R}{2} \right)^2 \right]$$

$$\gamma_6 = M_{UF}(\dot{\delta}_1 + \dot{\delta}_2) + M_{UR}(\dot{\delta}_3 + \dot{\delta}_4)$$

$$\gamma_7 = M_{UF} \left[z_F (\dot{\delta}_1 + \dot{\delta}_2) + \delta_1 \dot{\delta}_1 + \delta_2 \dot{\delta}_2 \right] + M_{UR} \left[z_R (\dot{\delta}_3 + \dot{\delta}_4) + \delta_3 \dot{\delta}_3 + \delta_4 \dot{\delta}_4 \right]$$

$$\gamma_8 = \frac{M_{UF} T_F}{2} (\dot{\delta}_1 - \dot{\delta}_2) + \frac{M_{UR} T_R}{2} (\dot{\delta}_3 - \dot{\delta}_4)$$

$$\gamma_9 = M_{UF}a(\dot{\delta}_1 + \dot{\delta}_2) - M_{UR}b(\dot{\delta}_3 + \dot{\delta}_4)$$

Inertial Term Definitions for Independent
 Rear Suspension Option

$$\begin{bmatrix}
 \ddot{x} & \ddot{y} & \ddot{z} & \dot{w} & \dot{\rho} & \dot{Q} & \dot{R} & \ddot{\delta_1} & \ddot{\delta_2} & \ddot{\delta_3} & \ddot{\delta_4} \\
 \end{bmatrix} = \begin{bmatrix} E \end{bmatrix}$$

$$\begin{bmatrix}
 0 & 0 & 0 & 0 & 0 & 0 & 0 & 0 & 0 & 0 & 0 \\
 0 & \Sigma M & 0 & -\gamma_2 & 0 & \gamma_1 & 0 & 0 & 0 & 0 & 0 \\
 0 & 0 & M_s & 0 & 0 & 0 & 0 & 0 & 0 & 0 & 0 \\
 0 & 0 & -\gamma_2 & 0 & I_x + I_x' & 0 & -I_{xz} - I_{x'z} & 0 & 0 & 0 & 0 \\
 0 & \gamma_2 & 0 & 0 & 0 & I_y + I_y' & -I_{yz} & 0 & 0 & 0 & 0 \\
 0 & \gamma_1 & 0 & -I_{xz} - I_{x'z} & 0 & -I_{yz} & -I_{z'z} & 0 & 0 & 0 & 0 \\
 0 & 0 & \frac{M_{UF}}{2} & \frac{M_{UF}T_F}{4} & -\frac{M_{UF}a}{2} & 0 & \frac{M_{UF}}{2} & 0 & 0 & 0 & 0 \\
 0 & 0 & \frac{M_{UR}}{2} & \frac{M_{UR}T_R}{4} & -\frac{M_{UR}b}{2} & 0 & \frac{M_{UF}}{2} & 0 & 0 & 0 & 0 \\
 0 & 0 & \frac{M_{UR}}{2} & -\frac{M_{UR}}{4} & \frac{M_{UR}b}{2} & 0 & 0 & 0 & 0 & 0 & \frac{M_{UR}}{2}
 \end{bmatrix}$$

(50)

Matrix Equations of Motion for Independent Rear Suspension Option

$$\Sigma M(vR - uQ - g \sin\theta) + \chi_1(Q^2 + R^2) - \chi_2 PR - \chi_6 Q + \Sigma F_{xu} + \Sigma F_{xs}$$

$$\Sigma M(wP - uR + g \cos\theta \sin\phi) - \chi_1 PQ - \chi_2 QR + \chi_6 P + \Sigma F_{yu} + \Sigma F_{ys}$$

$$M_s(uQ - vP + g \cos\theta \cos\phi) - \Sigma F_{zi} + \Sigma F_{zs}$$

$$-\chi_2(wP - uR + g \cos\theta \sin\phi) + (I_{xz} + I'_{xz})PQ - I'_{yz}(P^2 + R^2) + (I_y - I_z + I'_x)QR - \chi_1 P + \Sigma N_{yu} + \Sigma N_{ys}$$

$$\chi_2(vR - wQ - g \sin\theta) - (I_x - I_z + I'_x)PR - \chi_1 Q + I'_{xz}(Q^2 + R^2) - I'_{yz}PQ + I_{xz}(R^2 - P^2) + \Sigma N_{eu} + \Sigma N_{es}$$

$$\chi_1(wP - uR + g \cos\theta \sin\phi) + (I_x - I_z - \chi_5)PQ - I_{xz} + I'_{xz})QR + \chi_6 Q + I'_{yz}PR + \chi_1 P + \Sigma N_{yu} + \Sigma N_{ys}$$

$$\frac{M_{uf}}{2} [uQ - vP + g \cos\theta \cos\phi - \alpha PR + (z_f + \delta_f)(P^2 + R^2) - \frac{T_f}{2} QR] + F_{zu1} + S_1$$

$$\frac{M_{ur}}{2} [uQ - vP + g \cos\theta \cos\phi - \alpha PR + (z_f + \delta_f)(P^2 + R^2) + \frac{T_f}{2} QR] + F_{zu2} + S_2$$

$$\frac{M_{ur}}{2} [uQ - vP + g \cos\theta \cos\phi + b PR + (z_r + \delta_j)(P^2 + R^2) - \frac{T_r}{2} QR] + F_{zu3} + S_3$$

$$\frac{M_{ur}}{2} [uQ - vP + g \cos\theta \cos\phi + b PR + (z_r + \delta_j)(P^2 + R^2) + \frac{T_r}{2} QR] + F_{zu4} + S_4$$

$$[E] =$$

3.1.5.3 Beam Axle Front and Rear Suspension
Equations of Motion

$$I'_x = M_{UF}(z_F + \delta_F)^2 + \rho_F M_{UF}(z_F + \delta_F) + M_{UR}(z_R + \delta_R)^2 + \rho_R M_{UR}(z_R + \delta_R)$$

$$I'_y = I'_x + \rho_F M_{UF}(z_F + \delta_F + \rho_F) + \rho_R M_{UR}(z_R + \delta_R + \rho_R)$$

$$I'_z = M_{UF}(a^2 + \rho_F^2 \dot{\phi}_F^2) + M_{UR}(b^2 + \rho_R^2 \dot{\phi}_R^2)$$

$$I'_{xz} = M_{UF}a(z_F + \delta_F) - M_{UR}b(z_R + \delta_R)$$

$$I'_{yz} = -M_{UF}\rho_F \dot{\phi}_F(z_F + \rho_F + \delta_F) - M_{UR}\rho_R \dot{\phi}_R(z_R + \rho_R + \delta_R)$$

$$\gamma_1 = M_{UF}a - M_{UR}b$$

$$\gamma_2 = M_{UF}(z_F + \rho_F + \delta_F) + M_{UR}(z_R + \rho_R + \delta_R)$$

$$\gamma_3 = \gamma_2 - M_{UR}\rho_R - M_{UF}\rho_F$$

$$\gamma_4 = I'_{yz} + \rho_F^2 \dot{\phi}_F M_{UF} + \rho_R^2 \dot{\phi}_R M_{UR}$$

$$\gamma_5 = M_{UF}(a^2 - \rho_F^2 \dot{\phi}_F^2) + M_{UR}(b^2 - \rho_R^2 \dot{\phi}_R^2)$$

$$\gamma_6 = 2M_{UF}(\dot{\delta}_F - \rho_F \dot{\phi}_F \dot{\phi}_F) + 2M_{UR}(\dot{\delta}_R - \rho_R \dot{\phi}_R \dot{\phi}_R)$$

$$\gamma_7 = 2M_{UF}(z_F + \delta_F)(\dot{\delta}_F - \rho_F \dot{\phi}_F \dot{\phi}_F) + 2M_{UR}(z_R + \delta_R)(\dot{\delta}_R - \rho_R \dot{\phi}_R \dot{\phi}_R)$$

$$\gamma_8 = -2M_{UF}\rho_F \dot{\phi}_F(\dot{\delta}_F - \rho_F \dot{\phi}_F \dot{\phi}_F) + 2M_{UR}\rho_R \dot{\phi}_R(\dot{\delta}_R - \rho_R \dot{\phi}_R \dot{\phi}_R)$$

$$\gamma_9 = 2M_{UF}a(\dot{\delta}_F - \rho_F \dot{\phi}_F \dot{\phi}_F) - 2M_{UR}b(\dot{\delta}_R - \rho_R \dot{\phi}_R \dot{\phi}_R)$$

Inertial Term Definitions for Solid
Front Axle Option

$$\begin{aligned}
& \left[\begin{aligned}
& 2M(vRP-wQ-g\sin\theta) - Y_2' PR + p_F M_{RF} \dot{\phi}_F PQ + p_F M_{RF} \dot{\phi}_F QR + Y_1(Q^2+R^2) - Y_1' (Q^2+R^2) - Y_1 (Q^2+R^2) \\
& - 2Mv\dot{\phi}_F \dot{\phi}_F R + Z F_{xS} + Z F_{xU} \\
& - ZM(wP-UR+g\cos\theta\sin\phi) + Y_6 P - Y_1 PQ - Y_2 QR - p_F M_{RF} \dot{\phi}_F (P^2+R^2+\dot{\phi}_F^2) \\
& - p_F M_{RF} \dot{\phi}_F (P^2+R^2+\dot{\phi}_F^2) + Z F_{yS} + Z F_{yU}
\end{aligned} \right] \\
& M_S(uQ-vP+g\cos\theta\cos\phi) - Z F_{zI} + Z F_{zS} \\
& - Y_3(wR-wP-g\cos\theta\sin\phi) + (I_{xz}+I_{xz}') PQ - Y_7 P + (I_y - I_z + I_x') QR - Y_4(P^2+R^2) \\
& + p_F M_{RF} \dot{\phi}_F (Z_F + \dot{\phi}_F) \dot{\phi}_F^2 + Z N \dot{\phi}_S + Z N \dot{\phi}_U \\
& - Y_2(wR-wQ-g\sin\theta) + I_{xz}(R^2-P^2) + (I_z - I_x - I_y) PR - Y_7 Q - 2Q \dot{\phi}_F M_{RF} (\dot{\phi}_F - p_F \dot{\phi}_F \dot{\phi}_F) \\
& + (I_{xz}' - p_F M_{RF} b + p_F M_{RF} a)(Q^2+R^2) - I_{yz}' PQ - 2Mv\dot{\phi}_F (Z_F + \dot{\phi}_F + \dot{\phi}_U) \dot{\phi}_F R - 2Mv\dot{\phi}_F (Z_F + \dot{\phi}_F + \dot{\phi}_U) \dot{\phi}_F R + Z N \dot{\phi}_S + Z N \dot{\phi}_U \\
& - Y_1(wP-vR+wQ-2R\dot{\phi}_F \dot{\phi}_U - b(Q^2-P^2-\dot{\phi}_F^2) - g\sin\theta) + p_F M_{RF} \dot{\phi}_F [vR - wQ - 2R\dot{\phi}_F \dot{\phi}_U + a(Q^2-P^2-\dot{\phi}_F^2) - g\sin\theta] + Z N \dot{\phi}_S + Z N \dot{\phi}_U \\
& - M_{RF}[uQ-vP+p_F \dot{\phi}_F^2 + 2P \dot{\phi}_F \dot{\phi}_U - \alpha PR + \beta \dot{\phi}_F QR + (I_{xz} + I_{xz}') PR + Y_8 Q + I_{yz}' PR + Y_9 P \\
& + F_{zu1} + F_{zu2} + S_1 + S_2 \\
& - p_F M_{RF} [uR - wP - 2P \dot{\phi}_F \dot{\phi}_U + 2P \dot{\phi}_F \dot{\phi}_U + a PQ + \alpha \dot{\phi}_F (P^2 + R^2) + (Z_F + \dot{\phi}_F + \dot{\phi}_U) \dot{\phi}_F QR - g \cos\theta \sin(\phi + \theta_F)] \\
& + p_F M_{RF} \dot{\phi}_F [vP - uQ - 2P \dot{\phi}_F \dot{\phi}_U + a PR - (Z_F + \dot{\phi}_F + \dot{\phi}_U) (P^2 + Q^2)] - I_F \dot{\phi}_F (R^2 - Q^2) - I_F QR + Z N \dot{\phi}_F \\
& - M_{RF}[uQ-vP+p_F \dot{\phi}_F^2 + 2P \dot{\phi}_F \dot{\phi}_U + b PR + p_F \dot{\phi}_F QR + (Z_F + \dot{\phi}_F + \dot{\phi}_U) (P^2 + Q^2) + g \cos\theta \cos\phi] \\
& + F_{zu3} + F_{zu4} + S_3 + S_4 \\
& - p_F M_{RF} [uR - wP - 2P \dot{\phi}_F \dot{\phi}_U + 2P \dot{\phi}_F \dot{\phi}_U + b PQ + p_F \dot{\phi}_F (P^2 + R^2) + (Z_F + \dot{\phi}_F + \dot{\phi}_U) \dot{\phi}_F QR - g \cos\theta \sin(\phi + \theta_F)] \\
& + p_F M_{RF} \dot{\phi}_F [vP - uQ - 2P \dot{\phi}_F \dot{\phi}_U - b PR - (Z_F + \dot{\phi}_F + \dot{\phi}_U) (P^2 + Q^2)] - I_F \dot{\phi}_F (R^2 - Q^2) - I_F QR + Z N \dot{\phi}_F
\end{aligned} \right]
\end{aligned}$$

$$\begin{bmatrix}
\ddot{u} \\
\dot{v} \\
\dot{w} \\
\dot{\rho} \\
\dot{Q} \\
\dot{R}
\end{bmatrix} = \begin{bmatrix}
E
\end{bmatrix}$$

$$\begin{bmatrix}
ZM & 0 & 0 & \rho_{FMF}g_F + \rho_{MMF}g_F & 0 & 0 & 0 \\
0 & ZM & 0 & -\chi_2 & 0 & \rho_{FMF} & 0 \\
0 & 0 & M_s & 0 & 0 & 0 & \rho_{MMF} \\
0 & -\chi_3 & 0 & I_x + I_x' & 0 & -(\bar{I}_{xz} + \bar{I}_{xz}') & 0 \\
0 & 0 & 0 & I_y + I_y' & -I_{yz}' & 0 & \rho_{MMF}(z_F t_F) \\
\delta_2 & 0 & 0 & -I_{xz} - I_{xz}' & I_z + I_R & 0 & 0 \\
\rho_{MMF}g_F & \rho_{MMF}g_F & \chi_1 & 0 & +\rho_{MMF}b & 0 & \rho_{MMF}b \\
0 & 0 & M_F & \rho_{FMF}g_F & -\alpha_{MF} & 0 & \rho_{FMF}g_F \\
0 & -\rho_{FMF} & -\rho_{FMF}g_F & (Z_F + \delta_F t_F) & \rho_{MMF}g_F & \rho_{MMF}g_F^2 & 0 \\
0 & 0 & M_F & \rho_{MMF}g_F & b_{MF} & 0 & \rho_{MMF}g_F \\
0 & -\rho_{MMF} & -\rho_{MMF}g_F & (Z_F + \delta_F t_F) & \rho_{MMF}b & 0 & 0
\end{bmatrix}$$

Matrix Equations of Motion for Solid Front Axle Option

3.2 Vehicle Position and Orientation

3.2.1 Sprung Mass

The transformation matrix from the coordinate system fixed in the vehicle sprung mass to the inertial coordinate system according to the rotational sequence ψ , θ and ϕ is:

$$\| A \| = \begin{vmatrix} \cos \theta \cos \psi & -\cos \phi \sin \psi + \sin \phi \sin \theta \cos \psi & \sin \phi \sin \psi + \cos \phi \sin \theta \cos \psi \\ \cos \theta \sin \psi & \cos \phi \cos \psi + \sin \phi \sin \theta \sin \psi & -\cos \psi \sin \phi + \cos \phi \sin \theta \sin \psi \\ -\sin \theta & \cos \theta \sin \phi & \cos \theta \cos \phi \end{vmatrix} \quad (53)$$

where $\theta' = \theta_t$, $\phi' = \phi_t$, and $\psi' = \psi_t$

In order to obtain the Euler angles required it is necessary to integrate the components of the rotational velocities (P , Q , R) along the axes of rotation of the Euler angles. These components are given by:

$$\dot{\theta}'_t = Q \cos \phi'_t - R \sin \phi'_t \quad (54)$$

$$\dot{\phi}'_t = P + (Q \sin \phi'_t + R \cos \phi'_t) \tan \theta'_t \quad (55)$$

$$\dot{\psi}'_t = (Q \sin \phi'_t + R \cos \phi'_t) \sec \theta'_t \quad (56)$$

Note that the presence of the $\tan \theta'_t$ and $\sec \theta'_t$ in these expressions result in a singularity at $\theta'_t = \pi/2$.

An indexing scheme that allows unlimited angular excursions of the vehicle involves the use of three sets of Euler angles:

- (1) ψ_t , θ_t , ϕ_t are the Euler angles that define the orientation of the vehicle with respect to the inertial axis system in which the x' and y' axes are horizontal and z' is vertically downward.

- (2) ψ'_t , θ'_t , ϕ'_t are the Euler angles that define the orientation of the vehicle with respect to an intermediate system (the indexed axis system). Note that this axis system is fixed in space either coincident with the initial orientation of the vehicle or is oriented colinear with the vehicle axes at the time of most recent indexing.
- (3) ψ'_n , θ'_n , ϕ'_n are the Euler angles that define the orientation of the indexed axis system with respect to the inertial system.

Thus, it can be seen from Equations (54), (55) and (56) that the rates of change of the Euler angles that are calculated are written with respect to the indexed axes and integrated:

$$\theta'_t = \theta'_n + \int \dot{\theta}'_t dt \quad (57)$$

$$\phi'_t = \phi'_n + \int \dot{\phi}'_t dt \quad (58)$$

$$\psi'_t = \psi'_n + \int \dot{\psi}'_t dt \quad (59)$$

These angles are then related to the vehicle Euler angles with respect to the space axes by the following logic.

If $\theta_o = \phi_o = 0$ and coordinate system indexing has not occurred,

$$\theta_t = \theta'_t$$

$$\phi_t = \phi'_t$$

$$\psi_t = \psi'_t$$

If $\theta_o \neq 0$, $\phi_o \neq 0$, or coordinate system indexing has occurred,

(1) For first time increment of a given run only, set

$$\psi_{t-1} = \psi'_n , \quad \theta_{t-1} = \theta'_n , \quad \phi_{t-1} = \phi'_n$$

(2) Let $\|B_n\| = \|A\|$ with $\psi = \psi'_n$, $\theta = \theta'_n$,
 $\phi = \phi'_n$ (note that $\|B_n\|$ remains constant between times of indexing).

Let $\|C_n\| = \|A\|$ with $\psi = \psi'_t$, $\theta = \theta'_t$,
 $\phi = \phi'_t$.

Therefore, $\|B_n\|$ transforms a vector in the indexed coordinate system (\bar{v}'') to the space fixed coordinate system

$$\bar{v}' = \|B_n\| \bar{v}''$$

and $\|C_n\|$ transforms a vector in the vehicle coordinate system (\bar{v}) to the indexed coordinate system

$$\bar{v}'' = \|C_n\| \bar{v}$$

Therefore

$$\bar{v}' = \|B_n\| \cdot \|C_n\| \bar{v}$$

and, by definition,

$$\|A\| = \|B_n\| \cdot \|C_n\|$$

- (3) By inspection of the elements of $\|A\|$, (Equation (53)), it is seen that:

$$\tan \psi_t = A_{21}/A_{11}$$

Therefore,

$$\psi_t = \arctan \left[\frac{B_{21}C_{11} + B_{22}C_{21} + B_{23}C_{31}}{B_{11}C_{11} + B_{12}C_{21} + B_{13}C_{31}} \right] \quad (60)$$

- (4) Number of revolutions is integer value

$$IV = \frac{\psi_{t-1}}{2\pi}$$

- (5) Define four possible values for testing

$$\begin{aligned} TRYPSI_1 &= \psi_t + 2\pi(IV) \\ TRYPSI_2 &= \psi_t + \pi + 2\pi(IV) \\ TRYPSI_3 &= \psi_t - \pi + 2\pi(IV) \\ TRYPSI_4 &= \psi_t - 2\pi + 2\pi(IV) \quad \text{for positive } \psi_t, \\ &= \psi_t + 2\pi + 2\pi(IV) \quad \text{for negative } \psi_t. \end{aligned}$$

(6) Test each of the four possible angles to seek correct one. For $i = 1, 2, 3, 4$

$$\text{DIFF}_i = \text{TRYPSI}_i - \psi_{t-1}$$

(a) If $|\text{DIFF}_i| < \frac{\pi}{4}$, TRYPSI_i is the correct one. SET $\psi_t = \text{TRYPSI}_i$.

(b) If none of the four values of $|\text{DIFF}_i| < \frac{\pi}{4}$, let $IV = \psi_{t-1} / 2\pi + 1 \text{ sgn } (\psi_{t-1} / 2\pi)$. Return to (5).

(7) (a) For $|\sin \psi_t| > 0.07$.

$$\theta_t = \arctan \left[\frac{-\cos \psi_t (B_{31}C_{11} + B_{32}C_{21} + B_{33}C_{31})}{B_{11}C_{11} + B_{12}C_{21} + B_{13}C_{31}} \right] \quad (61)$$

(b) For $0.7 < |\sin \psi_t|$.

$$\theta_t = \arctan \left[\frac{-\sin \psi_t (B_{31}C_{11} + B_{32}C_{21} + B_{33}C_{31})}{B_{21}C_{11} + B_{22}C_{21} + B_{23}C_{31}} \right] \quad (62)$$

$$(8) \phi_t = \arctan \left[\frac{B_{31}C_{12} + B_{32}C_{22} + B_{33}C_{32}}{B_{31}C_{13} + B_{32}C_{23} + B_{33}C_{33}} \right] \quad (63)$$

(9) Repeat steps (4) through (6) for θ_t , ϕ_t .

The values of the angles ψ_t , θ_t , ϕ_t at the time of indexing are saved as ψ'_n , θ'_n , ϕ'_n , and the angles ψ'_t , θ'_t , and ϕ'_t are set to zero.

The position of the sprung mass center of gravity is determined by integration of the velocity components in the space-fixed axis system, u' , v' , and w' , where

$$\begin{vmatrix} u' \\ v' \\ w' \end{vmatrix} = \|A\| \cdot \begin{vmatrix} u \\ v \\ w \end{vmatrix} \quad (64)$$

u , v , and w are obtained from the differential equations or initial conditions, and

$$x'_c = x'_{co} + \int_0^t u' dt \quad (65)$$

$$y'_c = y'_{co} + \int_0^t v' dt \quad (66)$$

$$z'_c = z'_{co} + \int_0^t w' dt \quad (67)$$

3.2.2 Unsprung Masses

3.2.2.1 Independent Front/Solid Axle Rear Suspension

Wheel Center Location

$$\begin{vmatrix} x'_1 \\ y'_1 \\ z'_1 \end{vmatrix} = \begin{vmatrix} x'_c \\ y'_c \\ z'_c \end{vmatrix} + \|A\| \cdot \begin{vmatrix} a \\ T_F/2 + \Delta T_{HF1} \\ z_F + \delta_1 \end{vmatrix} \quad \text{RIGHT FRONT} \quad (68)$$

$$\begin{vmatrix} x'_2 \\ y'_2 \\ z'_2 \end{vmatrix} = \begin{vmatrix} x'_c \\ y'_c \\ z'_c \end{vmatrix} + \|A\| \cdot \begin{vmatrix} a \\ -(T_F/2 + \Delta T_{HF2}) \\ z_F + \delta_1 \end{vmatrix} \quad \text{LEFT FRONT} \quad (69)$$

$$\begin{vmatrix} x'_3 \\ y'_3 \\ z'_3 \end{vmatrix} = \begin{vmatrix} x'_c \\ y'_c \\ z'_c \end{vmatrix} + \|A\| \cdot \begin{vmatrix} -b \\ T_R/2 - \rho \phi_R \\ z_R + \rho + (T_R/2) \phi_R + \delta_3 \end{vmatrix} \quad \text{RIGHT REAR} \quad (70)$$

$$\begin{vmatrix} x'_4 \\ y'_4 \\ z'_4 \end{vmatrix} = \begin{vmatrix} x'_c \\ y'_c \\ z'_c \end{vmatrix} + \|A\| \cdot \begin{vmatrix} -b \\ -T_R/2 - \rho \phi_R \\ z_R + \rho - (T_R/2) \phi_R + \delta_3 \end{vmatrix} \quad \begin{matrix} \text{LEFT} \\ \text{REAR} \end{matrix} \quad (71)$$

where ΔT_{HF1} , and ΔT_{HF2} are the front half-track changes from the static values of $T_F/2$ interpolated from the ΔT_{HF} table as a function of suspension deflection δ_1 and δ_2 .

Wheel Orientation

$\phi_3 = \phi_4 = \phi_R$, from differential equations of motion or initial conditions;

ϕ_1, ϕ_2 by interpolation of tabular inputs of ϕ_c as a function of δ_1, δ_2 ;

ψ_1, ψ_2 by interpolation of tabular inputs of ψ_F as a function of time, or from differential equation of $\ddot{\psi}_F$ if curb routine is active;

$\psi_3 = \psi_4 = K_{RS} \phi_R$ (Rear axle roll steer, positive values of K_{RS} produce roll understeer) (72)

3.2.2.2 Independent Front and Rear Suspension

Wheel Center Location

$$\begin{vmatrix} x'_1 \\ y'_1 \\ z'_1 \end{vmatrix} = \begin{vmatrix} x'_c \\ y'_c \\ z'_c \end{vmatrix} + \|A\| \cdot \begin{vmatrix} a \\ T_F/2 + \Delta T_{HF1} \\ z_F + \delta_1 \end{vmatrix} \quad (73)$$

$$\begin{vmatrix} x'_2 \\ y'_2 \\ z'_2 \end{vmatrix} = \begin{vmatrix} x'_c \\ y'_c \\ z'_c \end{vmatrix} + \|A\| \cdot \begin{vmatrix} a \\ -(T_F/2 + \Delta T_{HF2}) \\ z_F + \delta_2 \end{vmatrix} \quad (74)$$

$$\begin{vmatrix} x'_3 \\ y'_3 \\ z'_3 \end{vmatrix} = \begin{vmatrix} x'_c \\ y'_c \\ z'_c \end{vmatrix} + \|A\| \cdot \begin{vmatrix} -b \\ T_R/2 + \Delta T_{HR3} \\ z_R + \delta_3 \end{vmatrix} \quad (75)$$

$$\begin{vmatrix} x'_4 \\ y'_4 \\ z'_4 \end{vmatrix} = \begin{vmatrix} x'_c \\ y'_c \\ z'_c \end{vmatrix} + \|A\| \cdot \begin{vmatrix} -b \\ -(T_R/2 + \Delta T_{HR4}) \\ z_R + \delta_4 \end{vmatrix} \quad (76)$$

where ΔT_{HR3} and ΔT_{HR4} are the rear half-track changes from the static value of $T_R/2$ interpolated from the ΔT_{HR} table as a function of suspension deflection δ_3 and δ_4

Wheel Orientation

ϕ_1, ϕ_2 - interpolate ϕ_c vs. δ_1, δ_2

ϕ_3, ϕ_4 - interpolate ϕ_{CR} vs. δ_3, δ_4

ψ_1, ψ_2 - interpolate ψ_F vs. t or from $\ddot{\psi}_F$

$$\psi_3 = K_{\delta s} + K_{\delta s_1} \delta_3 + K_{\delta s_2} \delta_3^2 + K_{\delta s_3} \delta_3^3 \quad (77)$$

$$\psi_4 = -(K_{\delta s} + K_{\delta s_1} \delta_4 + K_{\delta s_2} \delta_4^2 + K_{\delta s_3} \delta_4^3) \quad (78)$$

where $K_{\delta s}, K_{\delta s_1}, K_{\delta s_2}, K_{\delta s_3}$ are input coefficients.

3.2.3

Beam Axle Front and Rear Suspension

Wheel Center Location

$$\begin{vmatrix} x'_1 \\ y'_1 \\ z'_1 \end{vmatrix} = \begin{vmatrix} x'_c \\ y'_c \\ z'_c \end{vmatrix} + \|A\| \cdot \begin{vmatrix} a \\ T_F/2 - \rho_F \phi_F \\ z_F + \rho_F + (T_F/2) \phi_F + \delta_1 \end{vmatrix} \quad (79)$$

$$\begin{vmatrix} x'_2 \\ y'_2 \\ z'_2 \end{vmatrix} = \begin{vmatrix} x'_c \\ y'_c \\ z'_c \end{vmatrix} + \|A\| \cdot \begin{vmatrix} a \\ -T_F/2 - \rho_F \phi_F \\ z_F + \rho_F - (T_F/2) \phi_F + \delta_1 \end{vmatrix} \quad (80)$$

$$\begin{vmatrix} x'_3 \\ y'_3 \\ z'_3 \end{vmatrix} = \begin{vmatrix} x'_c \\ y'_c \\ z'_c \end{vmatrix} + \|A\| \cdot \begin{vmatrix} -b \\ T_R/2 - \rho \phi_R \\ z_R + \rho + (T_R/2) \phi_R + \delta_3 \end{vmatrix} \quad (81)$$

$$\begin{vmatrix} x'_4 \\ y'_4 \\ z'_4 \end{vmatrix} = \begin{vmatrix} x'_c \\ y'_c \\ z'_c \end{vmatrix} + \|A\| \cdot \begin{vmatrix} -b \\ -T_R/2 - \rho \phi_R \\ z_R + \rho - (T_R/2) \phi_R + \delta_3 \end{vmatrix} \quad (82)$$

Wheel Orientation:

$$\begin{aligned}
 \phi_1, \phi_2 &= \phi_F \\
 \phi_3, \phi_4 &= \phi_R \\
 \psi_1, \psi_2 &= \psi_F \quad \text{from interpolation or } \ddot{\psi}_F \quad \text{equation} \\
 \psi_3, \psi_4 &= K_{RS} \phi_R
 \end{aligned} \tag{83}$$

3.3 Vehicle to Ground Orientation

The directional cosines of a line perpendicular to the ground in the local terrain region under wheel i are calculated by:

$$\begin{aligned}
 \cos \alpha_{GZ'_i} &= \cos \phi_{Gi} \sin \theta_{Gi} \\
 \cos \beta_{GZ'_i} &= -\sin \phi_{Gi} \\
 \cos \gamma_{GZ'_i} &= \cos \theta_{Gi} \cos \phi_{Gi}
 \end{aligned} \tag{84}$$

where θ_{Gi} , ϕ_{Gi} are the ground slopes under wheel i as determined in Section 3.4.

A normal to the wheel plane of wheel i is determined by the directional cosines:

$$\begin{vmatrix} \cos \alpha_{yw_i} \\ \cos \beta_{yw_i} \\ \cos \gamma_{yw_i} \end{vmatrix} = \|A\| \cdot \begin{vmatrix} -\sin \psi_i \\ \cos \phi_i \cos \psi_i \\ \sin \phi_i \cos \psi_i \end{vmatrix} \tag{85}$$

By subtracting the angle between the two above normal lines from $\pi/2$, the camber angle relative to the ground is obtained:

$$\begin{aligned}\phi_{CGi} &= \frac{\pi}{2} - \arccos \left[\cos \alpha_{yw_i} \cos \alpha_{Gz'_i} + \cos \beta_{yw_i} \cos \beta_{Gz'_i} \right. \\ &\quad \left. + \cos \gamma_{yw_i} \cos \gamma_{Gz'_i} \right]\end{aligned}\quad (86)$$

(Note that a + sign for ϕ_{CGi} corresponds to camber thrust in +y direction.)

The directional components of a line perpendicular to both the normals to the wheel plane and ground plane are calculated by taking the vector cross-product of the two normals:

$$\begin{aligned}D_{1i} &= \begin{vmatrix} \cos \beta_{yw_i} & \cos \gamma_{yw_i} \\ \cos \beta_{Gz'_i} & \cos \gamma_{Gz'_i} \end{vmatrix} \quad D_{2i} = \begin{vmatrix} \cos \gamma_{yw_i} & \cos \alpha_{yw_i} \\ \cos \gamma_{Gz'_i} & \cos \alpha_{Gz'_i} \end{vmatrix} \\ D_{3i} &= \begin{vmatrix} \cos \alpha_{yw_i} & \cos \beta_{yw_i} \\ \cos \alpha_{Gz'_i} & \cos \beta_{Gz'_i} \end{vmatrix}\end{aligned}\quad (87)$$

Front and rear wheel steer angles in the plane of the ground are obtained by modifying the respective steer angles relative to the vehicle by the cosine of the angle between the assumed axis of rotation of the wheel (in steer) and the normal to the ground plane at the individual wheel, where

$$\begin{vmatrix} \cos \alpha_{zw_i} \\ \cos \beta_{zw_i} \\ \cos \gamma_{zw_i} \end{vmatrix} = \|A\| \cdot \begin{vmatrix} 0 \\ -\sin \phi_i \\ \cos \phi_i \end{vmatrix}\quad (88)$$

are the directional cosines of the assumed axis of rotation of the wheel (kingpin axis assumed to lie in wheel plane).

Thus:

$$\psi'_i = \psi_i (\cos \alpha_{GZ'_i} \cos \alpha_{zw_i} + \cos \beta_{GZ'_i} \cos \beta_{zw_i} + \cos \delta_{GZ'_i} \cos \delta_{zw_i}) \quad (89)$$

In order to determine appropriate slip angles to be used in the calculation of tire side forces, the forward and lateral velocities of the tire contact point in the plane of the ground under wheel i must first be calculated. This is done by determining velocity components along the vehicle x and y axes projected onto the ground plane under wheel i

The velocities of the tire contact point along the vehicle axes are first calculated by the expressions given for each suspension option.

Independent Front/Solid Axle Rear Suspension

Forward velocities of hubs (along x -axis)

$$\begin{aligned} u_1 &= u - (T_F/2 + \Delta T_{HF1})R + (z_F + \delta_1)Q \\ u_2 &= u + (T_F/2 + \Delta T_{HF2})R + (z_F + \delta_1)Q \\ u_3 &= u - (T_R/2)R + (z_R + \delta_3 + \rho + T_R \phi_R/2)Q \\ u_4 &= u + (T_R/2)R + (z_R + \delta_3 + \rho - T_R \phi_R/2)Q \end{aligned} \quad (90)$$

Lateral velocities of contact points (along y -axis)

$$\begin{aligned} v_1 &= v + aR - (z_F + \delta_1)P - (h_1 \cos \gamma_{h1})(P + \frac{d\phi_1}{d\delta_1} \dot{\delta}_1) + \frac{d\Delta T_{HF1}}{d\delta_1} \dot{\delta}_1 \\ v_2 &= v + aR - (z_F + \delta_2)P - (h_2 \cos \gamma_{h2})(P + \frac{d\phi_2}{d\delta_2} \dot{\delta}_2) - \frac{d\Delta T_{HF2}}{d\delta_2} \dot{\delta}_2 \\ v_3 &= v - bR - (z_R + \delta_3)P - (\rho + T_R \phi_R/2 + h_3 \cos \gamma_{h3})(\dot{\phi}_R + P) \\ v_4 &= v - bR - (z_R + \delta_3)P - (\rho - T_R \phi_R/2 + h_4 \cos \gamma_{h4})(\dot{\phi}_R + P) \end{aligned} \quad (91)$$

Vertical velocities of contact points (along z -axis)

$$\begin{aligned}
 w_1 &= w - aQ + (T_F/2 + \Delta T_{HF1})P + \dot{\delta}_1 + h_1 \cos \gamma_{h1} (P + \frac{d\phi_1}{d\delta_1} \dot{\delta}_1) \\
 w_2 &= w - aQ - (T_F/2 + \Delta T_{HF2})P + \dot{\delta}_2 + h_2 \cos \gamma_{h2} (P + \frac{d\phi_2}{d\delta_2} \dot{\delta}_2) \\
 w_3 &= w + bQ + \dot{\delta}_3 - (\rho \phi_R - T_R/2 - h_3 \cos \beta_{h3}) (\dot{\phi}_R + P) \\
 w_4 &= w + bQ + \dot{\delta}_4 - (\rho \phi_R + T_R/2 - h_4 \cos \beta_{h4}) (\dot{\phi}_R + P)
 \end{aligned} \tag{92}$$

Independent Front and Rear Suspension

Forward Velocity of Hubs:

$$\begin{aligned}
 u_1 &= u - (T_F/2 + \Delta T_{HF1})R + (z_F + \delta_1)Q \\
 u_2 &= u + (T_F/2 + \Delta T_{HF2})R + (z_F + \delta_2)Q \\
 u_3 &= u - (T_R/2 + \Delta T_{HR3})R + (z_R + \delta_3)Q \\
 u_4 &= u + (T_R/2 + \Delta T_{HR4})R + (z_R + \delta_4)Q
 \end{aligned} \tag{93}$$

Lateral Velocity of Contact Points:

$$\begin{aligned}
 v_1 &= v + aR - (z_F + \delta_1)P - (h_1 \cos \gamma_{h1}) (P + \frac{d\phi_1}{d\delta_1} \dot{\delta}_1) + \frac{d\Delta T_{HF1}}{d\delta_1} \dot{\delta}_1 \\
 v_2 &= v + aR - (z_F + \delta_2)P - (h_2 \cos \gamma_{h2}) (P + \frac{d\phi_2}{d\delta_2} \dot{\delta}_2) - \frac{d\Delta T_{HF2}}{d\delta_2} \dot{\delta}_2 \\
 v_3 &= v - bR - (z_R + \delta_3)P - (h_3 \cos \gamma_{h3}) (P + \frac{d\phi_3}{d\delta_3} \dot{\delta}_3) + \frac{d\Delta T_{HR3}}{d\delta_3} \dot{\delta}_3 \\
 v_4 &= v - bR - (z_R + \delta_4)P - (h_4 \cos \gamma_{h4}) (P + \frac{d\phi_4}{d\delta_4} \dot{\delta}_4) - \frac{d\Delta T_{HR4}}{d\delta_4} \dot{\delta}_4
 \end{aligned} \tag{94}$$

Vertical Velocity of Occupant Points:

$$\begin{aligned}
 w_1 &= w - aQ + (T_F/2 + \Delta T_{HF1})P + \dot{\delta}_1 + h_1 \cos \beta_{n1} (P + \frac{d\phi_1}{d\delta_1} \dot{\delta}_1) \\
 w_2 &= w - aQ - (T_F/2 + \Delta T_{HF2})P + \dot{\delta}_2 + h_2 \cos \beta_{n2} (P + \frac{d\phi_2}{d\delta_2} \dot{\delta}_2) \\
 w_3 &= w + bQ + (T_R/2 + \Delta T_{HR3})P + \dot{\delta}_3 + h_3 \cos \beta_{n3} (P + \frac{d\phi_3}{d\delta_3} \dot{\delta}_3) \\
 w_4 &= w + bQ - (T_R/2 + \Delta T_{HR4})P + \dot{\delta}_4 + h_4 \cos \beta_{n4} (P + \frac{d\phi_4}{d\delta_4} \dot{\delta}_4)
 \end{aligned} \tag{95}$$

Solid Front and Rear Axle

Forward Hub Velocity:

$$\begin{aligned}
 u_1 &= u - (T_F/2 - \rho_F \phi_F) + (z_F + \delta_1 + T_F \phi_F/2) Q \\
 u_2 &= u + (T_F/2 + \rho_F \phi_F) + (z_F + \delta_1 - T_F \phi_F/2) Q \\
 u_3 &= u - (T_R/2 - \rho \phi_R) + (z_R + \delta_3 + T_R \phi_R/2) Q \\
 u_4 &= u + (T_R/2 + \rho \phi_R) + (z_R + \delta_3 - T_R \phi_R/2) Q
 \end{aligned} \tag{96}$$

Lateral Contact Point Velocity:

$$\begin{aligned}
 v_1 &= v + aR - (z_F + \delta_1)P - (\rho_F + T_F \phi_F/2 + h_1 \cos \gamma_{n1}) (P + \dot{\phi}_F) \\
 v_2 &= v + aR - (z_F + \delta_1)P - (\rho_F - T_F \phi_F/2 + h_2 \cos \gamma_{n2}) (P + \dot{\phi}_F) \\
 v_3 &= v - bR - (z_R + \delta_3)P - (\rho + T_R \phi_R/2 + h_3 \cos \gamma_{n3}) (P + \dot{\phi}_R) \\
 v_4 &= v - bR - (z_R + \delta_3)P - (\rho - T_R \phi_R/2 + h_4 \cos \gamma_{n4}) (P + \dot{\phi}_R)
 \end{aligned} \tag{97}$$

Vertical Contact Point Velocity:

$$\begin{aligned}
 w_1 &= w + \dot{\delta}_1 - a Q - (\rho_F \phi_F - T_F/2 - h_1 \cos \beta_{h1})(P + \dot{\phi}_F) \\
 w_2 &= w + \dot{\delta}_1 - a Q - (\rho_F \phi_F + T_F/2 - h_2 \cos \beta_{h2})(P + \dot{\phi}_F) \\
 w_3 &= w + \dot{\delta}_3 + b Q - (\rho \phi_R - T_R/2 - h_3 \cos \beta_{h3})(P + \dot{\phi}_R) \\
 w_4 &= w + \dot{\delta}_3 + b Q - (\rho \phi_R + T_R/2 - h_4 \cos \beta_{h4})(P + \dot{\phi}_R)
 \end{aligned} \tag{98}$$

The angle between the vehicle x -axis and its projection onto the ground plane is then determined. By taking the vector cross-product of the y -axis and the normal to the ground, the directional components of the x -axis projection in the plane of the ground are obtained.

$$\begin{aligned}
 a_{xi} &= \begin{vmatrix} \cos \beta_y & \cos \delta_y \\ \cos \beta_{Gz'_i} & \cos \delta_{Gz'_i} \end{vmatrix} \\
 b_{xi} &= \begin{vmatrix} \cos \delta_y & \cos \alpha_y \\ \cos \delta_{Gz'_i} & \cos \alpha_{Gz'_i} \end{vmatrix} \\
 c_{xi} &= \begin{vmatrix} \cos \alpha_y & \cos \beta_y \\ \cos \alpha_{Gz'_i} & \cos \beta_{Gz'_i} \end{vmatrix}
 \end{aligned} \tag{99}$$

where

$$\begin{vmatrix} \cos \alpha_y \\ \cos \beta_y \\ \cos \delta_y \end{vmatrix} = \|A\| \cdot \begin{vmatrix} 0 \\ 1 \\ 0 \end{vmatrix}, \tag{100}$$

are the directional cosines of the y -axis.

The angle between the χ -axis and its projection onto the ground plane is then determined by the vector dot product:

$$\cos \theta_{xG_i} = \frac{(\cos \alpha_x) a_{xi} + (\cos \beta_x) b_{xi} + (\cos \gamma_x) c_{xi}}{\sqrt{a_{xi}^2 + b_{xi}^2 + c_{xi}^2}} \quad (101)$$

and,

$$\operatorname{sgn} \theta_{xG_i} = \operatorname{sgn} \left[\cos \gamma_x - \frac{c_{xi}}{\sqrt{a_{xi}^2 + b_{xi}^2 + c_{xi}^2}} \right]$$

where

$$\begin{vmatrix} \cos \alpha_x \\ \cos \beta_x \\ \cos \gamma_x \end{vmatrix} = \| A \| \cdot \begin{vmatrix} 1 \\ 0 \\ 0 \end{vmatrix}, \quad (102)$$

are the directional cosines of the χ -axis.

The forward velocity of the contact point in the ground plane is calculated as:

$$u_{G_i} = u_i \cos \theta_{xG_i} - w_i \sin \theta_{xG_i} \quad (103)$$

Similarly, the directional components of the y -axis projection onto the ground plane are:

$$\begin{aligned} a_{yi} &= \begin{vmatrix} \cos \gamma_x & \cos \beta_x \\ \cos \gamma_{GZ'_i} & \cos \beta_{GZ'_i} \end{vmatrix} \\ b_{yi} &= \begin{vmatrix} \cos \alpha_x & \cos \gamma_x \\ \cos \alpha_{GZ'_i} & \cos \gamma_{GZ'_i} \end{vmatrix} \\ c_{yi} &= \begin{vmatrix} \cos \beta_x & \cos \alpha_x \\ \cos \beta_{GZ'_i} & \cos \alpha_{GZ'_i} \end{vmatrix} \end{aligned} \quad (104)$$

And the angle between the y -axis and its projection onto the ground plane is:

$$\cos \phi_{yG_i} = \frac{(\cos \alpha_y) a_{y_i} + (\cos \beta_y) b_{y_i} + (\cos \delta_y) c_{y_i}}{\sqrt{a_{y_i}^2 + b_{y_i}^2 + c_{y_i}^2}} \quad (105)$$

and

$$\operatorname{sgn} \phi_{yG_i} = \operatorname{sgn} \left[\cos \delta_y - \frac{c_{y_i}}{\sqrt{a_{y_i}^2 + b_{y_i}^2 + c_{y_i}^2}} \right]$$

Finally, the lateral velocity of the contact point in the ground plane is:

$$v_{G_i} = v_i \cos \phi_{yG_i} - w_i \sin \phi_{yG_i} \quad (106)$$

3.4 Tire Contact with the Ground

3.4.1 Ground Contact Point

Determination of the tire "ground contact point" is accomplished by passing planes through the wheel centers (x'_i , y'_i , z'_i) perpendicular to both the wheel and ground planes at the individual wheels. At each wheel, the point that lies in all three planes is designated the "ground contact point". The characteristics of the ground under wheel are determined in Sections 3.4.2 through 3.4.5.

Thus,

$$\lambda_{x_i} = x'_i \cos \alpha_{yw_i} + y'_i \cos \beta_{yw_i} + z'_i \cos \delta_{yw_i} \quad (107)$$

$$\lambda_{y_i} = x'_i \cos \alpha_{Gz'_i} + y'_i \cos \beta_{Gz'_i} + z'_i \cos \delta_{Gz'_i} \quad (108)$$

(109)

$$\lambda_{z_i} = D_{x_i} x'_i + D_{y_i} y'_i + D_{z_i} z'_i$$

where Equation (107) is the equation for the plane of wheel i , (108) is the equation of the ground plane through the terrain point directly under the wheel center, (x'_i , y'_i , z'_i), and (109) is the equation of the plane through the wheel center perpendicular to both the wheel plane and ground plane.

Let

$$\|c_i\| = \begin{vmatrix} \cos \alpha_{yw_i} & \cos \beta_{yw_i} & \cos \gamma_{yw_i} \\ \cos \alpha_{GZ'_i} & \cos \beta_{GZ'_i} & \cos \gamma_{GZ'_i} \\ D_{1i} & D_{2i} & D_{3i} \end{vmatrix} \quad (110)$$

Then a point that lies in all three planes is determined from

$$\|c_i\| \cdot \begin{vmatrix} x'_{GPi} \\ y'_{GPi} \\ z'_{GPi} \end{vmatrix} = \begin{vmatrix} \lambda_{1i} \\ \lambda_{2i} \\ \lambda_{3i} \end{vmatrix} \quad (111)$$

The radial load on the tire is subsequently found by determining the deflection of the tire at the ground contact point.

$$\Delta_i = + \sqrt{(x'_i - x'_{GPi})^2 + (y'_i - y'_{GPi})^2 + (z'_i - z'_{GPi})^2} \quad (112)$$

where Δ_i is the distance between the wheel center and ground contact point; and

$$h_i = \begin{cases} \Delta_i, & \text{for } \Delta_i < R_w \\ R_w, & \text{for } R_w \leq \Delta_i \end{cases} \quad (113)$$

where h_i is the rolling radius of the tire.

Finally, the radial tire force is:

$$F_{R_i} = \begin{cases} 0, & \text{for } (R_w - h_i) = 0 \\ K_T (R_w - h_i), & \text{for } 0 < (R_w - h_i) < \sigma_T \\ K_T [\lambda_T (R_w - h_i) - (\lambda_T - 1) \sigma_T], & \text{for } \sigma_T \leq (R_w - h_i) \end{cases} \quad (114)$$

The directional cosines of the line of action of the tire radial force for wheel i are:

$$\begin{aligned} \cos \alpha_{R_i} &= \frac{x'_{GPi} - x'_i}{\Delta_i} \\ \cos \beta_{R_i} &= \frac{y'_{GPi} - y'_i}{\Delta_i} \\ \cos \gamma_{R_i} &= \frac{z'_{GPi} - z'_i}{\Delta_i} \end{aligned} \quad (115)$$

The corresponding direction cosines in the vehicle coordinate system are obtained from

$$\begin{vmatrix} \cos \alpha_{hi} \\ \cos \beta_{hi} \\ \cos \gamma_{hi} \end{vmatrix} = \|A^T\| \cdot \begin{vmatrix} \cos \alpha_{R_i} \\ \cos \beta_{R_i} \\ \cos \gamma_{R_i} \end{vmatrix} \quad (116)$$

3.4.2 Flat Terrain Ground Characteristics

The default terrain is defined as being flat and level at an elevation of 0.0. Therefore, the ground characteristics under wheel are defined as:

$$\begin{aligned} z'_{Gi} &= 0.0 \\ \phi_{Gi} &= 0.0 \\ \theta_{Gi} &= 0.0 \end{aligned}$$

3.4.3 Variable Terrain Ground Characteristics

Varying terrain is defined by the use of input terrain tables. Therefore, it is necessary to determine the characteristics of the terrain under wheel i as defined by z'_{Gi} , ϕ_{Gi} , θ_{Gi} by interpolation of terrain table data:

The calculational procedure for determining the elevation and slopes of the terrain under each wheel of the vehicle from tabular input data is described in detail below.

Step 1

The highest numbered terrain table (1 through 5) applicable to the wheel is determined by sequentially testing if the wheel is located within the X' and Y' bounds of each table. Note that in regions of overlapping tables, the program will use the terrain as defined in the highest numbered table. Therefore, if it is desired to use a small or "fine grid" table to describe in more detail terrain that is also within the bounds of another "coarse grid" table, the number of the "fine grid" table must be larger than that of the other table.

Step 2

The particular grid segment within which the wheel is located is determined and the corner points labeled as shown in Figure 3.6.

Step 3

Determine if an interpolation boundary cuts through the segment. For Y boundaries, a boundary cuts through the segment if

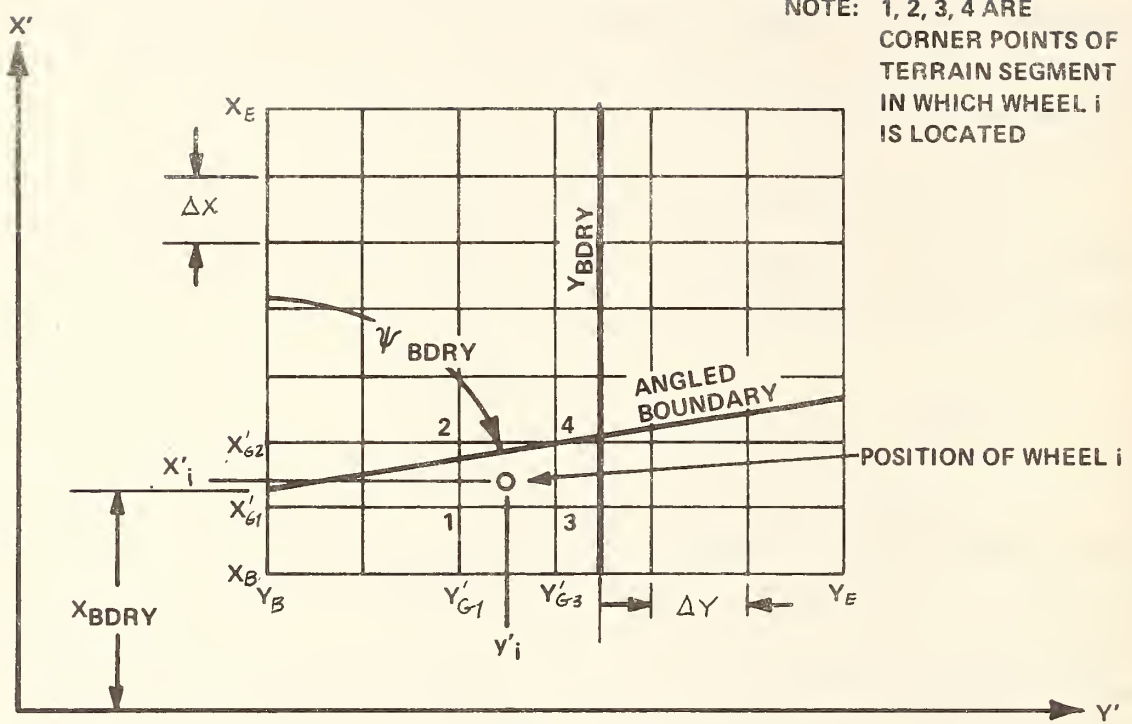


Figure 3.6 TERRAIN TABLE GRID

$$Y'_1 < Y_{BDRY} < Y'_3$$

(Note: Subscripts 1, 2, 3, 4 refer to corner points of grid segment.)

An angled boundary cuts through the segment if

$$X'_{G1} \leq X_{LCEPT} \leq X'_{G2} , \text{ or}$$

$$X_{LCEPT} \geq X'_{G2} \text{ and } X_{RCEPT} < X'_{G4} , \text{ or}$$

$$X_{LCEPT} \leq X'_{G1} \text{ and } X_{RCEPT} > X'_{G3}$$

where:

$$X_{LCEPT} = X_{BDRY} + (Y'_{G1} - Y'_B) \operatorname{ctn} \psi_{BDRY} \quad (117)$$

$$X_{RCEPT} = X_{BDRY} + (Y'_{G3} - Y'_B) \operatorname{ctn} \psi_{BDRY} \quad (118)$$

Step 4

If no boundaries cut through the segment, calculate z'_{Gi} by two-way interpolation using the elevations of the corner points of the segment z'_{G1} , z'_{G2} , z'_{G3} and z'_{G4} .

Then

$$\theta_{G1} = \arctan \left(\frac{z'_{G1} - z'_{G2}}{\Delta x} \right) \quad (119)$$

$$\theta_{G3} = \arctan \left(\frac{z'_{G3} - z'_{G4}}{\Delta x} \right) \quad (120)$$

$$\theta_{Gi} = \theta_{G1} + (\theta_{G3} - \theta_{G1}) \left(\frac{y'_i - Y'_{G1}}{\Delta Y} \right) \quad (121)$$

$$\phi_{6i} = \begin{cases} \arctan\left(\frac{z'_{G3,4} - z'_{6i}}{Y'_{G3} - y'_i}\right) \sec\theta_{6i} & , \text{for } Y'_{G3} \neq y'_i \geq Y'_{G1} \\ \arctan\left(\frac{z'_{G3,4} - z'_{6i,2}}{\Delta Y}\right) \sec\theta_{6i} & , \text{for } y'_i = Y'_{G3} \end{cases} \quad (122)$$

where $z'_{G1,2}$ and $z'_{G3,4}$ are "intermediate" terrain elevations at points on the Y' sides of the terrain segment at x'_i as determined in the first of the two-way interpolations.

Step 5

If there is only an angled boundary cutting through the segment, a determination is made as to whether or not the wheel has crossed the boundary. The wheel has crossed the boundary if

$$X_{BDRY} + (y'_i - Y'_B) \operatorname{ctn} \psi_{BDRY} < x'_i \quad (123)$$

(a) If the wheel has not crossed the boundary,

(1) starting with corner point 2, the first grid point along the Y'_{G1}, Y'_{G2} edge of the segment for which $X' < X_{LCEPT}$ is found and designated as point 2. Corner point 1 is then relabeled accordingly (one ΔX increment toward X_B).

(2) Starting with corner point 4, the first grid point along the Y'_{G3}, Y'_{G4} edge of the segment for which $X' < X_{RCEPT}$ is found and that point is designated point 4. Corner point 3 is relabeled accordingly (one ΔX increment toward X_B).

(3) If $X'_{G1} = X'_{G3}$, Z'_{Gi} , θ_{Gi} and ϕ_{Gi} are computed as in Step 4.

If $X'_{G2} = X'_{G3}$.

$$\theta_{Gi} = \arctan\left(\frac{Z'_{G3} - Z'_{G4}}{\Delta X}\right) \quad (124)$$

$$\phi_{Gi} = \arctan\left(\frac{Z'_{G3} - Z'_{G2}}{\Delta Y} \sec \theta_{Gi}\right) \quad (125)$$

$$Z'_{Gi} = Z'_{G2} + (y'_i - Y'_{G2}) \cos \theta_{Gi} \tan \phi_{Gi} - (x'_i - X'_{G2}) \tan \theta_{Gi} \quad (126)$$

If $X'_{G1} = X'_{G4}$,

$$\theta_{Gi} = \arctan\left(\frac{Z'_{G1} - Z'_{G2}}{\Delta X}\right) \quad (127)$$

$$\phi_{Gi} = \arctan\left(\frac{(Z'_{G4} - Z'_{G1})}{\Delta Y} \sec \theta_{Gi}\right) \quad (128)$$

Z'_{Gi} = Equation (126).

If $X'_{G2} < X'_{G3}$, designate the grid point one ΔX increment toward X_B from point 3 as point 5. Then

$$\theta_{Gi} = \text{Equation (124)}$$

$$\phi_{Gi} = \arctan\left(\frac{(Z'_{G5} - Z'_{G2})}{\Delta Y} \sec \theta_{Gi}\right) \quad (129)$$

$$Z'_{Gi} = \text{Equation (126)}$$

If $X'_{G1} > X'_{G4}$, designate the grid point one ΔX increment toward X_B from point 1 as point 5. Then

$$\theta_{G_i} = \text{Equation (127)}$$

$$\phi_{G_i} = \arctan \left(\frac{(Z'_{G_4} - Z'_{G_5})}{\Delta Y} \sec \theta_{G_i} \right) \quad (130)$$

$$Z'_{G_i} = \text{Equation (126)}$$

(b) If the wheel has crossed the boundary,

- (1) Starting with corner point 1, the first grid point along the Y'_{G_1}, Y'_{G_2} edge of the segment for which $X' > XLCEPT$ is found and designated as point 1. Corner point 2 is labeled accordingly (one ΔX increment toward X_E).
- (2) Starting with corner point 3, the first grid point along the Y'_{G_3}, Y'_{G_4} edge of the segment for which $X' > XRCEPT$ is found and designated as point 3. Corner point 4 is labeled accordingly (one ΔX increment toward X_E).
- (3) If $X'_{G_1} = X'_{G_3}$, Z'_{G_i} , θ_{G_i} and ϕ_{G_i} are computed as in step 4.

If $X'_{G_2} = X'_{G_3}$,

$$\theta_{G_i} = \text{Equation (127)}$$

$$\phi_{G_i} = \text{Equation (125)}$$

$$Z'_{G_i} = Z'_{G_1} + (y'_i - Y'_{G_1}) \cos \theta_{G_i} \tan \phi_{G_i} - (x'_i - X'_{G_1}) \tan \theta_{G_i} \quad (131)$$

If $X'_{G1} = X'_{G4}$,

$$\theta_{Gi} \quad = \text{Equation (124)}$$

$$\phi_{Gi} \quad = \text{Equation (128)}$$

$$z'_{Gi} \quad = \text{Equation (131)}$$

If $X'_{G2} < X'_{G3}$, designate the grid point one ΔX increment toward X_E from point 2 as point 5. Then

$$\theta_{Gi} \quad = \text{Equation (127)}$$

$$\phi_{Gi} = \arctan \left(\frac{(z'_{G3} - z'_{G5})}{\Delta Y} \sec \theta_{Gi} \right) \quad (132)$$

$$z'_{Gi} \quad = \text{Equation (131)}$$

If $X'_{G1} > X'_{G4}$, designate the grid point one ΔX increment toward X_E from point 4 as point 5. Then

$$\theta_{Gi} \quad = \text{Equation (124)}$$

$$\phi_{Gi} = \arctan \left(\frac{(z'_{G5} - z'_{G1})}{\Delta Y} \sec \theta_{Gi} \right) \quad (133)$$

$$z'_{Gi} \quad = \text{Equation (131)}$$

Step 6

If a Y' boundary cuts through the segment and

- (a) if $Y'_i \leq Y_{BDRY}$, the grid segment one ΔY increment toward Y_B is used with the corner points designated as shown in Figure 3.6. Proceed as in Steps 3 through 5.
- (b) If $Y'_i > Y_{BDRY}$, the grid segment one ΔY increment toward Y_E is used with the corner points designated as shown in Figure 3.6. Proceed as in Steps 3 through 5 using the following expression for the roll slope, ϕ_{Gi} , in Step 4.

$$\phi_{Gi} = \arctan \left(\frac{(Z'_{G1,2} - Z'_{Gi})}{(Y'_{G1} - y'_i)} \sec \theta_{Gi} \right) \quad , \text{for } y'_i < Y'_{G1}$$

When boundaries cut through the gird segment in which a wheel is located, the elevation and slopes of the terrain under the wheel are computed from data supplied for nearby terrain segments. To minimize errors that might result from use of grid points too far from the actual terrain segment in which the wheel is located, it is recommended that the angle, ψ_{BDRY} , be restricted to the following range:

$$(\pi - \arctan \frac{\Delta Y}{2\Delta X}) \geq \psi_{BDRY} \geq \arctan \frac{\Delta Y}{2\Delta X}$$

A minimum of two tabular values between like boundaries (i.e., two angled boundaries or two Y' boundaries) or between a boundary and the beginning or end of a terrain table must also be provided for proper operation of the subroutine.

3.4.4 Curb Impacts

The use of the curb impact subroutine is determined by a series of logical tests. If no curb impact input data are supplied, then this subroutine is not activated during the course of the computations. However, if input data are supplied, then each wheel center is tested for proximity to the curb immediately after the vehicle position and orientation subroutine has been completed.

If $R_w \leq (y'_{cl} - y'_i)$, then for wheel i ,

1. use tabular input of ψ_F until set to differential equation of $\ddot{\psi}_F$ by any one wheel,
2. bypass terrain input and set $z'_G = \theta_G = \phi_G = 0$,
3. retain coefficient of friction = AMU_i .

If $R_w \leq (y'_i - y'_{cl})$, where y'_{cl} is the location of the start of the last curb slope then for wheel i

1. continue to use differential equation for determination of ψ_F ,

2. bypass terrain input and set

$$z'_{Gi} = z'_{cl} + (y'_i - y'_{cl}) \tan \phi_{cl}$$

$$\theta_{Gi} = 0, \quad \phi_G = \phi_{cl}$$

3. reset coefficient of friction to the nominal ground value

4. if all wheels pass this test, reset calculation time increment to Δt ,
5. return to vehicle to ground orientation subroutine.

If $(y'_i - y'_{CL}) \leq R_w \geq (y'_{CI} - y'_i)$ then for wheel i , enter into curb impact subroutine calculations,

1. use differential equation for determination of ψ_F with most recent tabular value as initial condition,
2. set calculation time increment to Δt_c ,
3. modify the tire-ground friction coefficient by the curb friction multiplier, i.e., $\mu_{ci} = (\text{AMU}_i)(\text{AMUC})$

Let the matrix $\|A_j\|$ be defined as follows:

$$\|A_j\| = \begin{vmatrix} \cos\psi_i \cos\theta_j & -\sin\psi_i & \cos\psi_i \sin\theta_j \\ \cos\phi_i \sin\psi_i \cos\theta_j + \sin\phi_i \sin\theta_j & \cos\phi_i \cos\psi_i & \cos\phi_i \sin\psi_i \sin\theta_j - \sin\phi_i \cos\theta_j \\ \sin\phi_i \sin\psi_i \cos\theta_j - \cos\phi_i \sin\theta_j & \sin\phi_i \cos\psi_i & \sin\phi_i \sin\psi_i \sin\theta_j + \cos\phi_i \cos\theta_j \end{vmatrix} \quad (134)$$

where

$$\theta_j = 4(j), \quad j = -26, -25, \dots, 0, 1, \dots, 25, 26$$

(Note that the above matrix corresponds to the sequence ϕ_j , ψ_j , θ_j , which will apply the camber angle ϕ_i as a rotation about an axis parallel to the sprung mass x' axis.)

Let the matrix $\|B\|$ be defined as $\|A\| \cdot \|A_j\|$, and B_{23} , B_{33} represent elements of $\|B\|$ with the usual notation.

Solve each of the following expressions for h'_j :

$$1. \quad h'_j = - \frac{z'_i}{B_{33}} , \text{ for } y'_i < y'_{c1} \quad (135)$$

$$2. \quad h'_j = \frac{-z'_i + (y'_i - y'_{c1}) \tan \phi_{c1}}{B_{33} - B_{23} \tan \phi_{c1}} , \text{ for } y'_{c1} \leq y'_i < y'_{c2} \quad (136)$$

$$3. \quad h'_j = \frac{z'_{c2} - z'_i + (y'_i - y'_{c1}) \tan \phi_{c2}}{B_{33} - B_{23} \tan \phi_{c2}} , \text{ for } y'_{c2} \leq y'_i < y'_{c3} \quad (137)$$

$$4. \quad h'_j = \frac{z'_{c3} - z'_i + (y'_i - y'_{c3}) \tan \phi_{c3}}{B_{33} - B_{23} \tan \phi_{c3}} , \text{ for } y'_{c3} \leq y'_i < y'_{c4} \quad (138)$$

$$5. \quad h'_j = \frac{z'_{c4} - z'_i + (y'_i - y'_{c4}) \tan \phi_{c4}}{B_{33} - B_{23} \tan \phi_{c4}} , \text{ for } y'_{c4} \leq y'_i < y'_{c5} \quad (139)$$

$$6. \quad h'_j = \frac{z'_{c5} - z'_i + (y'_i - y'_{c5}) \tan \phi_{c5}}{B_{33} - B_{23} \tan \phi_{c5}} , \text{ for } y'_{c5} \leq y'_i < y'_{c6} \quad (140)$$

$$7. \quad h'_j = \frac{z'_{c6} - z'_i + (y'_i - y'_{c6}) \tan \phi_{c6}}{B_{33} - B_{23} \tan \phi_{c6}} , \text{ for } y'_{c6} \leq y'_i \quad (141)$$

Using each of the values of h'_j solve the following expression for three sets of (x'_j , y'_j , z'_j),

$$\begin{array}{c|c|c|c|c} x'_j & x'_i & & 0 \\ \hline y'_j & y'_i & + & 0 \\ \hline z'_j & z'_i & \cdot & h'_j \end{array} \quad (142)$$

Using the solutions of (x'_j , y'_j , z'_j) for each , test the value of h'_j for the range corresponding to its y'_j solution shown above. Retain only h'_j , x'_j , y'_j , z'_j for which is in the correct range for its h'_j solution.

Using the retained values above:

If $h'_j \geq R_{wi}$, then this individual radial spring is not in contact, index j by +1 if $j > 26$ proceed to calculation of radial tire forces.

If $h'_j < R_{wi}$, calculate and store the following:

$$\begin{aligned} \cos \alpha_j &= \frac{x'_i - x'_j}{h'_j} \\ \cos \beta_j &= \frac{y'_i - y'_j}{h'_j} \\ \cos \gamma_j &= \frac{z'_i - z'_j}{h'_j} \end{aligned} \quad (143)$$

Index j by +1 or, if $j > 26$, proceed to calculation of radial tire forces.

Calculation of radial tire forces:

For each h'_j , look up F'_j in input-generated table of F'_j versus $(R_{wi} - h'_j)$, calculate:

$$\sum F_R x'_i = \sum_{j=-26}^{+26} F'_j \cos \alpha_j \quad (144)$$

$$\sum F_R y'_i = \sum_{j=-26}^{+26} F'_j \cos \beta_j \quad (145)$$

$$\sum F_R z'_i = \sum_{j=-26}^{+26} F'_j \cos \gamma_j \quad (146)$$

and

$$F_{Ri} = +\sqrt{(\sum F_{Rx'i})^2 + (\sum F_{Ry'i})^2 + (\sum F_{Rz'i})^2} \quad (147)$$

Therefore, the directional cosines of the line of action of the tire radial force are:

$$\begin{aligned} \cos \alpha_{Ri} &= -\frac{\sum F_{Rx'i}}{F_{Ri}} \\ \cos \beta_{Ri} &= -\frac{\sum F_{Ry'i}}{F_{Ri}} \\ \cos \delta_{Ri} &= -\frac{\sum F_{Rz'i}}{F_{Ri}} \end{aligned} \quad (148)$$

An "equivalent" ground contact point and "equivalent" ground slopes are now determined for calculation and application of side and circumferential tire forces.

The equivalent rolling radius of the tire is

$$h_i = \begin{cases} R_w - \frac{F_{Ri}}{K_T}, & \text{for } (R_w - \sigma_T) < h_i \\ R_w - \left[\frac{F_{Ri}}{K_T \lambda_T} + \frac{(\lambda_T - 1) \sigma_T}{\lambda_T} \right], & \text{for } h_i < (R_w - \sigma_T) \end{cases} \quad (149)$$

and the corresponding y' and z' coordinates of the equivalent ground contact point are:

$$y'_{GPi} = y'_i + h_i \cos \beta_{Ri} \quad (150)$$

$$z'_{GPi} = z'_i + h_i \cos \delta_{Ri} \quad (151)$$

"Equivalent" terrain slopes for this case of nonplanar terrain contact are established by the use, as a normal to the equivalent terrain, of the projection of the normal to the actual terrain, at the equivalent ground contact point, in the plane determined by the radial force vector and a normal to the wheel plane. In this manner, the line of intersection between the equivalent ground plane and the wheel plane is made to remain perpendicular to the radial tire force vector.

Determination of the slopes of the equivalent ground plane is accomplished by means of application of the following relationships:

$$\phi_{gi} = \arcsin \left(\frac{-DN2_i}{\sqrt{DN1_i^2 + DN2_i^2 + DN3_i^2}} \right) \quad (152)$$

$$\theta_{gi} = \arctan \left(\frac{DN1_i}{DN3_i} \right) \quad (153)$$

where

$$\begin{aligned} DN1_i &= a_i b_i \sin \phi'_{gi} - a_i c_i \cos \phi'_{gi} \\ DN2_i &= -b_i c_i \cos \phi'_{gi} - (a_i^2 + c_i^2) \sin \phi'_{gi} \\ DN3_i &= (a_i^2 + b_i^2) \cos \phi'_{gi} + b_i c_i \sin \phi'_{gi} \end{aligned} \quad (154)$$

ϕ_{gi} and θ_{gi} are the equivalent ground slopes, ϕ'_{gi} is the actual ground slope at the equivalent tire contact point (note that $\theta'_{gi} = 0$ for the case of curb simulation), and

$$\begin{aligned}
 a_i &= \begin{vmatrix} \cos \beta_{Ri} & \cos \delta_{Ri} \\ \cos \beta_{yw_i} & \cos \delta_{yw_i} \end{vmatrix} \\
 b_i &= \begin{vmatrix} \cos \delta_{Ri} & \cos \alpha_{Ri} \\ \cos \delta_{yw_i} & \cos \alpha_{yw_i} \end{vmatrix} \\
 c_i &= \begin{vmatrix} \cos \alpha_{Ri} & \cos \beta_{Ri} \\ \cos \alpha_{yw_i} & \cos \beta_{yw_i} \end{vmatrix} \quad (155)
 \end{aligned}$$

are the directional components of a line perpendicular to both the normal to the wheel plane and F_{Ri} .

3.4.5 Road Roughness

The road roughness algorithm is based on the assumption that roughness data is in the form of small elevation changes from the ground plane and is supplied with a constant increment between elevation points. The roughness data is assumed to vary in the X' direction and is constant in the Y' direction. Tire enveloping effects are approximated through the use of the distributed radial spring tire model in a manner similar to that used in the curb impact model.

Let:

Δ_G be the distance increment between roughness elevation points

Z'_{Gm} be the mth elevation

The overall solution procedure involves determining the intersection between radial spring j and the straight line connecting elevation points m and $m+1$. If the point of intersection lies between the limits defined by the two elevation points, the solution is legitimate and the

radial spring deflection and force are computed. If the intersection is outside those limits m is incremented and the procedure repeated until an intersection is found. Note that the terrain outside of the limits of the data is assumed to be flat and level at an elevation of $Z'_G = 0.0$.

The transformation matrix between the radial spring j and space, $\|B\|$, is computed as $\|B\| = \|A\| \cdot \|A_j\|$ where $\|A_j\|$ is given by equation (134).

The intersection between radial spring j and the straight line between elevation points m and $m+1$ is:

$$x'_j = \frac{1}{1 - \frac{B_{13}}{B_{33}} \left(\frac{Z'_{Gm+1} - Z'_{Gm}}{\Delta G} \right)} \left\{ \left[x'_L + \frac{B_{13}}{B_{33}} Z'_{Gm} - x'_{Gm} \left(\frac{Z'_{Gm+1} - Z'_{Gm}}{\Delta G} \right) - z'_i \right] \right\} \quad (156)$$

If $x'_{Gm} \leq x'_j < x'_{Gm+1}$, the intersection occurs within the limits for this terrain segment and the distance between the wheel center and intersection point is computed:

$$h'_j = \frac{x'_i - x'_j}{B_{13}} \quad (157)$$

If $h'_j \geq R_{wi}$, the spring is not deflected, and calculations proceed for the next radial spring.

If $h'_j < R_{wi}$, the direction cosines for this spring are computed:

$$\begin{aligned} \cos \alpha_j &= \frac{x'_i - x'_j}{h'_j} \\ \cos \beta_j &= \frac{y'_i - y'_j}{h'_j} \\ \cos \gamma_j &= \frac{z'_i - z'_j}{h'_j} \end{aligned} \quad (158)$$

and the radial spring force, F_j' , is obtained through interpolation.

When calculations have been completed for all radial springs, the resultant force components are computed:

$$\sum F_{Rx'i} = \sum_j F_j' \cos \alpha_j \quad (159)$$

$$\sum F_{Ry'i} = \sum_j F_j' \cos \beta_j \quad (160)$$

$$\sum F_{Rz'i} = \sum_j F_j' \cos \gamma_j \quad (161)$$

and

$$F_{Ri} = \sqrt{(\sum F_{Rx'i})^2 + (\sum F_{Ry'i})^2 + (\sum F_{Rz'i})^2} \quad (162)$$

Therefore, the directional cosines of the line of action of the tire radial force are:

$$\begin{aligned} \cos \alpha_{Ri} &= - \frac{\sum F_{Rx'i}}{F_{Ri}} \\ \cos \beta_{Ri} &= - \frac{\sum F_{Ry'i}}{F_{Ri}} \\ \cos \gamma_{Ri} &= - \frac{\sum F_{Rz'i}}{F_{Ri}} \end{aligned} \quad (163)$$

An "equivalent" ground contact point and "equivalent" ground slopes are now determined for calculation and application of side and circumferential tire forces.

The equivalent rolling radius of the tire is

$$h_i = \begin{cases} R_{wi} - \frac{F_{ri}}{K_{Ti}}, & \text{for } (R_{wi} - \sigma_{Ti}) < h_i \\ R_{wi} - \left[\frac{F_{ri}}{K_{Ti} \lambda_{Ti}} + \frac{(\lambda_{Ti}-1) \sigma_{Ti}}{\lambda_{Ti}} \right], & \text{for } h_i < (R_{wi} - \sigma_{Ti}) \end{cases} \quad (164)$$

and the corresponding coordinates of the equivalent ground contact point are:

$$\begin{aligned} x'_{GPI} &= x'_i + h_i \cos \alpha_{ri} \\ y'_{GPI} &= y'_i + h_i \cos \beta_{ri} \end{aligned} \quad (165)$$

$$z'_{GPI} = z'_i + h_i \cos \gamma_{ri} \quad (166)$$

"Equivalent" terrain slopes for this case of nonplanar terrain contact are established by the use, as a normal to the equivalent terrain, of the projection of the normal to the actual terrain, at the equivalent ground contact point, in the plane determined by the radial force vector and a normal to the wheel plane. In this manner, the line of intersection between the equivalent ground plane and the wheel plane is made to remain perpendicular to the radial tire force vector.

Determination of the slopes of the equivalent ground plane is accomplished by means of application of the following relationships:

$$\phi_{gi} = \arcsin \left(\frac{-DN2_i}{\sqrt{DN1_i^2 + DN2_i^2 + DN3_i^2}} \right) \quad (167)$$

(168)

$$\theta_{gi} = \arctan \left(\frac{DN1_i}{DN3_i} \right)$$

where

$$\begin{aligned}
 DN1_i &= (c_i^2 + b_i^2) \sin \theta'_{Gi} - a_i c_i \cos \theta'_{Gi} \\
 DN2_i &= -a_i b_i \sin \theta'_{Gi} - c_i b_i \cos \theta'_{Gi} \\
 DN3_i &= (a_i^2 + b_i^2) \cos \theta'_{Gi} - a_i c_i \sin \theta'_{Gi}
 \end{aligned} \tag{169}$$

ϕ_{Gi} and θ_{Gi} are the equivalent ground slopes, θ'_{Gi} is the actual ground slope at the equivalent tire contact point (note $\phi'_{Gi} = 0$ for the case of road roughness), and

$$\begin{aligned}
 a_i &= \begin{vmatrix} \cos \beta_{Ri} & \cos \gamma_{Ri} \\ \cos \beta_{ywi} & \cos \gamma_{ywi} \end{vmatrix} \\
 b_i &= \begin{vmatrix} \cos \gamma_{Ri} & \cos \alpha_{Ri} \\ \cos \gamma_{ywi} & \cos \alpha_{ywi} \end{vmatrix} \\
 c_i &= \begin{vmatrix} \cos \alpha_{Ri} & \cos \beta_{Ri} \\ \cos \alpha_{ywi} & \cos \beta_{ywi} \end{vmatrix}
 \end{aligned} \tag{170}$$

are the directional components of a line perpendicular to both the normal to the wheel plane and F_{Ri}

3.5 Suspension Forces

Suspension forces include effects of viscous and coulomb damping, suspension stops, auxiliary roll stiffness, anti-pitch linkages and jacking forces, and are calculated based on suspension displacement and velocity.

3.5.1 Front Suspension

The displacement and velocity for front suspension force calculation are dependent on the suspension type. For independent front suspension they are:

$$\begin{aligned}\zeta_i &= \delta_i \\ \dot{\zeta}_i &= \dot{\delta}_i\end{aligned}\tag{171}$$

For a beam axle suspension, they are:

$$\begin{aligned}\zeta_i &= \delta_i - (-1)^i T_{SF} \phi_F / 2 \\ \dot{\zeta}_i &= \dot{\delta}_i - (-1)^i T_{SF} \dot{\phi}_F / 2\end{aligned}\tag{172}$$

The front suspension forces are given by:

$$S_i = \frac{b}{2(a+b)} M_s g - c_F \dot{\zeta}_i - F_{1Fi} - F_{2Fi} - F_{ARI} - F_{API} + F_{JFi}\tag{173}$$

where

$\frac{b}{2(a+b)} M_s g$ is the static sprung mass weight at wheel i

$c_F \dot{\zeta}_i$ is viscous damping force at wheel i

F_{1Fi} is the coulomb damping force at wheel i
given by

$$F_{1Fi} = \begin{cases} \frac{\dot{\zeta}_i}{\epsilon_F} C'_F & , \text{for } |\dot{\zeta}_i| < \epsilon_F \\ C'_F \text{sgn}(\dot{\zeta}_i) & , \text{for } |\dot{\zeta}_i| \geq \epsilon_F \end{cases}\tag{174}$$

is the combination of suspension force due to displacement from equilibrium and suspension stop force as illustrated in Figure 3.7 and given by:

$$F_{2FL} = \begin{cases} K_F \dot{\delta}_i & , \text{ for } \Omega_{FE} \geq \dot{\delta}_i \geq \Omega_{FC} \\ K_F \dot{\delta}_i + K_{FC} (\dot{\delta}_i - \Omega_{FC}) + K'_{FC} (\dot{\delta}_i - \Omega_{FC})^3 & , \text{ for } \dot{\delta}_i < \Omega_{FC} \text{ and } \operatorname{sgn} \dot{\delta}_i = \operatorname{sgn} \dot{\delta}_i \\ K_{FC} \dot{\delta}_i + \lambda_F [K_{FC} (\dot{\delta}_i - \Omega_{FC}) + K'_{FC} (\dot{\delta}_i - \Omega_{FC})^3] & , \text{ for } \dot{\delta}_i < \Omega_{FC} \text{ and } \operatorname{sgn} \dot{\delta}_i \neq \operatorname{sgn} \dot{\delta}_i \\ K_F \dot{\delta}_i + K_{FE} (\dot{\delta}_i - \Omega_{FE}) + K'_{FE} (\dot{\delta}_i - \Omega_{FE})^3 & , \text{ for } \dot{\delta}_i > \Omega_{FE} \text{ and } \operatorname{sgn} \dot{\delta}_i = \operatorname{sgn} \dot{\delta}_i \\ K_F \dot{\delta}_i + \lambda_F [K_{FE} (\dot{\delta}_i - \Omega_{FE}) + K'_{FE} (\dot{\delta}_i - \Omega_{FE})^3] & , \text{ for } \dot{\delta}_i > \Omega_{FE} \text{ and } \operatorname{sgn} \dot{\delta}_i \neq \operatorname{sgn} \dot{\delta}_i \end{cases}$$

(175)

F_{ARI} is the suspension force at wheel i due to auxiliary roll stiffness given by

$$F_{ARI} = -(-1)^i \left[\frac{R_F (\delta_2 - \delta_1)}{T_F^2} \right] \text{ for independent front suspension} \quad (176)$$

$$F_{ARI} = -(-1)^i \left[\frac{R_F \phi_i}{T_{SF}} \right] \text{ for beam axle front suspension} \quad (177)$$

F_{API} is the anti-pitch force at wheel i given by:

$$F_{APi} = - (AP_F)_{\dot{\delta}_i} \frac{F_{ci} h_i}{12} \cos \phi_i \cos \psi_i \quad (178)$$

where $(AP_F)_{\dot{\delta}_i}$ is the anti-pitch coefficient interpolated from the front anti-pitch table as a function of suspension deflection

$F_{JF,i}$ is an approximation of the jacking force induced on an independent suspension at wheel i given by:

$$F_{JF,i} = -(F_{yui} \cos\gamma_{hi} - F_{zui} \cos\beta_{hi})h_i \frac{d\phi_i}{ds_i} - (-1)^i F_{yui} \frac{d\Delta T_{HFC}}{ds_i} \quad (179)$$

Note that $F_{JF,i} = 0$ for beam axle suspension.

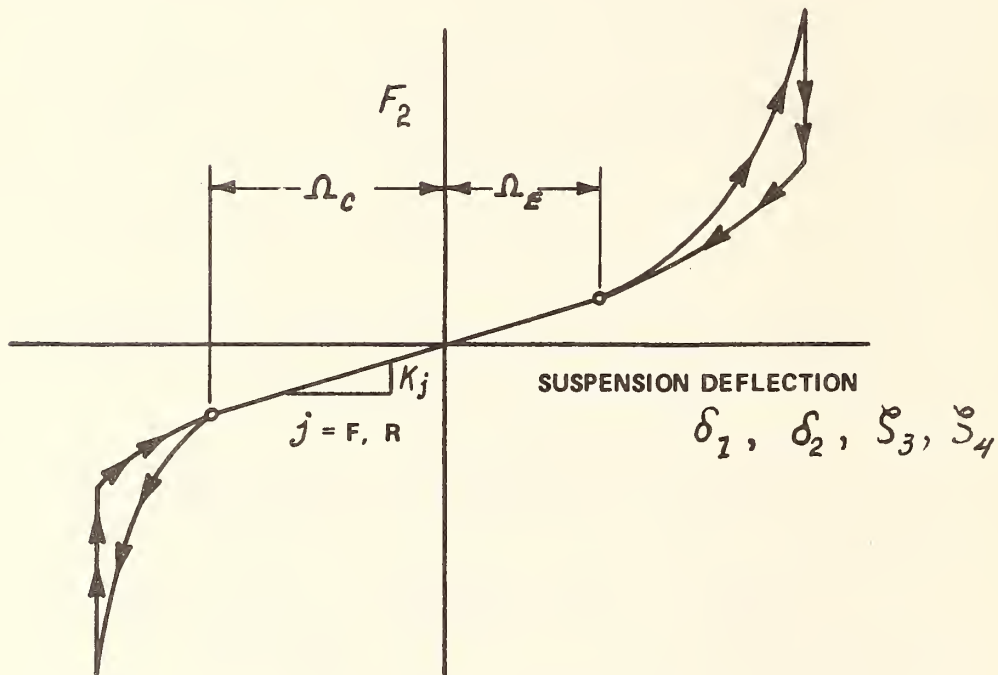


Figure 3.7 GENERAL FORM OF SIMULATED SUSPENSION LOAD-DEFLECTION CHARACTERISTICS
(REFERENCE 2)

3.5.2 Rear Suspension

The displacement and velocity for the rear suspension are similar to those of the front. For an independent rear suspension they are:

$$\begin{aligned}\delta_i &= \delta_i \\ \dot{\delta}_i &= \dot{\delta}_i\end{aligned}\tag{180}$$

And for a beam axle suspension:

$$\begin{aligned}\delta_i &= \delta_3 - (-1)^i T_s \phi_R / 2 \\ \dot{\delta}_i &= \dot{\delta}_3 - (-1)^i T_s \dot{\phi}_R / 2\end{aligned}\tag{182}$$

The rear suspension forces are given by:

$$S_i = \frac{a}{2(a+b)} M_s g - C_R \dot{\delta}_i - F_{1Ri} - F_{2Ri} - F_{ARI} - F_{API} + F_{JFI}\tag{183}$$

where

$\frac{a}{2(a+b)} M_s g$ is the static sprung mass weight at rear wheel, i

$C_R \dot{\delta}_i$ is the viscous damping force at rear wheel i

F_{1Ri} is the coulomb friction force at wheel i given by:

$$F_{1Ri} = \begin{cases} \frac{\dot{\delta}_i}{\epsilon_R} C'_R & , \text{ for } |\dot{\delta}_i| < \epsilon_R \\ C'_R \operatorname{sgn}(\dot{\delta}_i) & , \text{ for } |\dot{\delta}_i| \geq \epsilon_R \end{cases}\tag{184}$$

F_{ZRI} is the combination of suspension force due to displacement from equilibrium and suspension stop force as illustrated in Figure 3.7 and given by:

$$F_{ZRI} = \begin{cases} K_{Ri} s_i & , \text{for } \Omega_{RE} \geq s_i \geq \Omega_{RC} \\ K_R s_i + K_{RC}(s_i - \Omega_{RC}) + K'_{RC}(s_i - \Omega_{RC})^3 & , \text{for } s_i < \Omega_{RC} \text{ and } \text{sgn } s_i = \text{sgn } \dot{s}_i \\ K_R s_i + \lambda_R [K_{RC}(s_i - \Omega_{RC}) + K'_{RC}(s_i - \Omega_{RC})^3] & , \text{for } s_i < \Omega_{RC} \text{ and } \text{sgn } s_i \neq \text{sgn } \dot{s}_i \\ K_R s_i + K_{RE}(s_i - \Omega_{RE}) + K'_{RE}(s_i - \Omega_{RE})^3 & , \text{for } s_i > \Omega_{RC} \text{ and } \text{sgn } s_i = \text{sgn } \dot{s}_i \\ K_R s_i + \lambda_R [K_{RE}(s_i - \Omega_{RE}) + K'_{RE}(s_i - \Omega_{RE})^3] & , \text{for } s_i > \Omega_{RC} \text{ and } \text{sgn } s_i \neq \text{sgn } \dot{s}_i \end{cases} \quad (185)$$

F_{ARI} is the suspension force at wheel i due to auxiliary roll stiffness given by

$$F_{ARI} = (-1)^i \left[\frac{R_R (s_4 - s_3)}{T_R^2} \right] \quad \text{for independent front suspension} \quad (186)$$

$$F_{ARI} = -(-1)^i \left[\frac{R_R \phi_R}{T_S} \right] \quad \text{for beam axle front suspension} \quad (187)$$

F_{API} is the anti-pitch force at wheel i given by:

$$F_{API} = -(AP_R)_{s_i} \frac{F_{ci} h_i}{12} \cos\phi_i \cos\psi_i \quad (188)$$

where $(AP_R)_{s_i}$ is the anti-pitch coefficient interpolated from the front anti-pitch table as a function of suspension deflection

F_{JF_i} is an approximation of the jacking force induced on an independent suspension at wheel i given by:

$$F_{JF_i} = -(F_{yui} \cos \gamma_{hi} - F_{zui} \cos \beta_{hi}) h_i \frac{d\phi_i}{d\delta_i} - (-1)^i F_{yui} \frac{d\Delta T_{HRI}}{d\delta_i} \quad (189)$$

Note the $F_{JF_i} = 0$ for beam axle suspension.

Note that, the Anti-Pitch coefficient, AP_F or AP_R , is the ratio of the positive or negative jacking force (assumed positive for anti-pitch effects at the front and rear suspensions for forward braking) acting on the wheel to the corresponding moment of the applied circumferential force about a line parallel to the vehicle y axis. The units of the anti-pitch coefficient are lbs/lb-ft. Tabular entries of the coefficients correspond to given displacements of the wheel centers from their design positions.

Front and rear suspension jacking force, F_{JF_i} , approximated by the following derivation.

The y and z coordinates of the ground contact point of front wheel i may be expressed as

$$\begin{aligned} y_i &= -(-1)^i (T_f/2 + \Delta T_{HFI}) + h_i \cos \beta_{hi} \\ z_i &= z_j + \delta_i + h_i \cos \gamma_{hi} \end{aligned} \quad (190)$$

where

$$\begin{vmatrix} \cos \alpha_{hi} \\ \cos \beta_{hi} \\ \cos \gamma_{hi} \end{vmatrix} = \begin{vmatrix} \cos \psi_i \sin \theta_i \\ \cos \phi_i \sin \psi_i \sin \theta_i - \sin \phi_i \cos \theta_i \\ \sin \phi_i \sin \psi_i \sin \theta_i + \cos \phi_i \cos \theta_i \end{vmatrix} \quad (191)$$

Equating the work done by the tire forces, F_{yui} and F_{zui} , to that done by the suspension force, S_i , in a virtual displacement of the suspension $\Delta \delta_i$ yields:

$$-S_i = F_{yui} \frac{\partial y}{\partial \delta_i} + F_{zui} \frac{\partial z}{\partial \delta_i} \quad (192)$$

where

$$\begin{aligned} \frac{\partial y_i}{\partial \delta_i} &= -(-1)^i \frac{d\Delta T_{HF_i}}{d\delta_i} - h_i \cos \gamma_{ni} \frac{d\phi_i}{d\delta_i} \\ \frac{\partial z_i}{\partial \delta_i} &= 1 + h_i \cos \beta_{ni} \frac{d\phi_i}{d\delta_i} \end{aligned} \quad (193)$$

The suspension force is:

$$-S_i = F_{yui} - (-1)^i \frac{d\Delta T_{HF_i}}{d\delta_i} - h_i \cos \gamma_{ni} \frac{d\phi_i}{d\delta_i} + F_{zui} 1 + h_i \cos \beta_{ni} \frac{d\phi_i}{d\delta_i} \quad (194)$$

and the jacking component is given by:

$$F_{JFi} = -(S_i + F_{zui}) = -(F_{yui} \cos \gamma_{ni} - F_{zui} \cos \beta_{ni}) h_i \frac{d\phi_i}{d\delta_i} - (-1)^i F_{yui} \frac{d\Delta T_{HF_i}}{d\delta_i} \quad (195)$$

Similarly for the rear: $i = 3, 4$

$$F_{JFi} = -(F_{yui} \cos \gamma_{ni} - F_{zui} \cos \beta_{ni}) h_i \frac{d\phi_i}{d\delta_i} - (-1)^i F_{yui} \frac{d\Delta T_{HRi}}{d\delta_i} \quad (196)$$

where ΔT_{HF_i} , ΔT_{HRi} are the half-track changes input as tabular functions of suspension deflections.

3.6 Braking and Tractive Torques

3.6.1 HVOSM-RD2 Version

Braking and tractive torques in this program versions are interpolated from input front and rear torque tables (TQ_F , TQ_R) as functions of time.

3.6.2 HVOSM-VD2 Version

A general outline of the procedure used for generation of wheel torques (both tractive and braking) is depicted in Figure 3.8.

The form of the open loop control inputs (tabulated as functions of time) for speed control is illustrated in Figure 3.9. The detailed algorithms for generating wheel torques is discussed in the following sections.

3.6.2.1 Braking Torque

The brake torques at the individual wheels, $(TQ)_{Bi}$, are calculated for the specified brake type (i.e., 1, 2, 3, 4) based on analytical relationships given in References 3 and 4 using the input values for brake pushout pressure, P_{j0} , and the instantaneous values of brakeline pressure, P_j , and the lining fade coefficient, $(LF)_i$. The following relationships are applied:

1. P_c vs. t interpolated from direct tabular input.

2. $P_F \equiv P_c$

$$P_R = \begin{cases} P_c & , \text{for } 0 \leq P_c \leq P_1 \\ P_1 + K_1(P_c - P_1) & , \text{for } P_1 \leq P_c \leq P_2 \\ P_1 + K_1(P_2 - P_1) + K_2(P_c - P_2) & , \text{for } P_c > P_2 \end{cases} \quad (197)$$

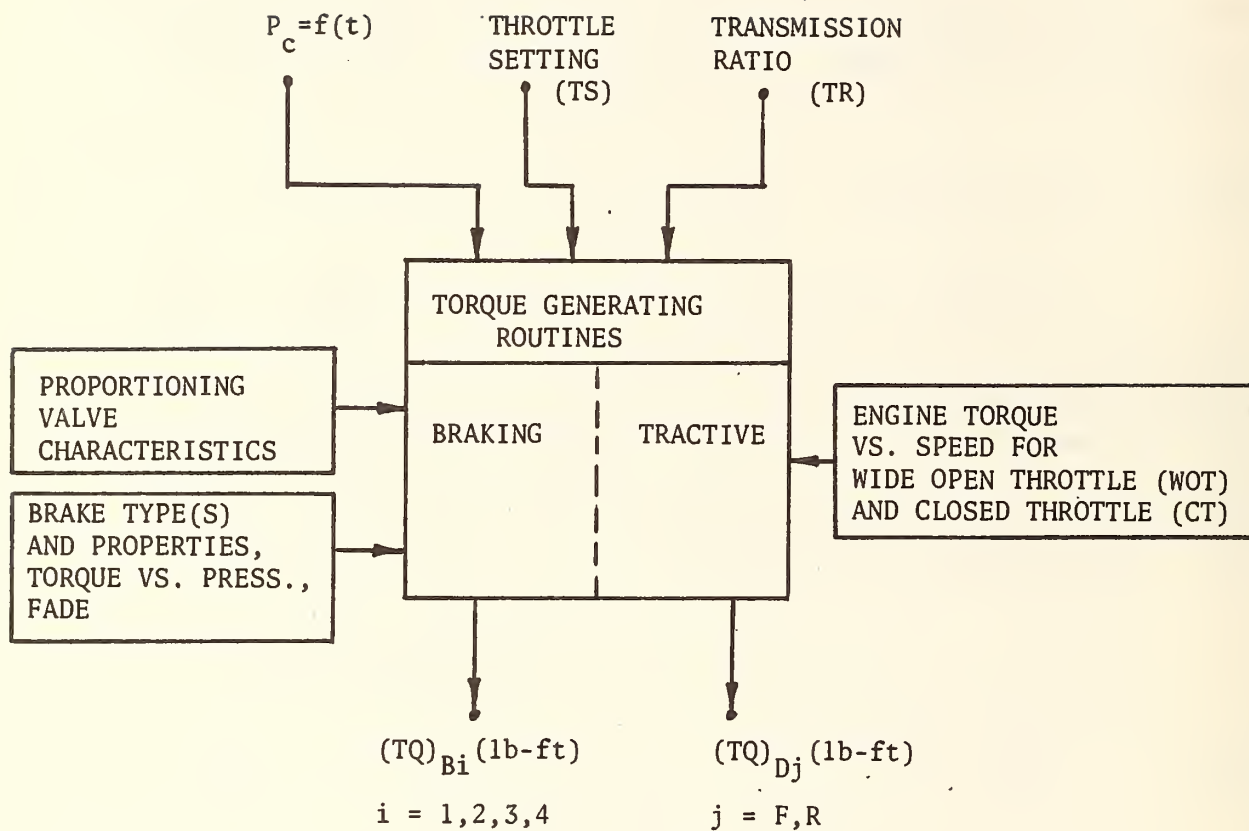


Figure 3.8 GENERATION OF WHEEL TORQUES

t	P_c	(TS)	(TR)
Time Sec	Master Cylinder Pressure, PSIG $0 \leq P_c \leq 1000$	Throttle Setting $0.00 \leq TS \leq 1.00$ 1.00 = WOT 0.00 = CT	Transmission Ratio (For Disengaged Clutch, * Enter $TR = 0.000$) $0.500 \leq TR \leq 5.000$

Examples:

2.57	1st
1.83	2nd
1.00	3rd
0.70	OD

- * For engine RPM < 500 during a brake application the transmission ratio is set to zero. The effect is the same as a disengagement of the clutch. Note that disengagement by the driver at other values of engine RPM (e.g., between gears or while braking) can be simulated by directly entering a value of 0.000 for TR .

Figure 3.9 CONTROL INPUTS FOR SPEED CONTROL

3. Brake torques are calculated from

TYPE 1 BRAKE - Drum Type with Leading and Trailing Shoes

$$(TQ)_{B_i} = \begin{cases} 0 & , \text{ for } (P_j - P_{j_0}) < 0 \\ \frac{1}{12}(P_j - P_{j_0}) G_{1j} G_{2j} G_{3j} (LF)_i \left[\frac{G_{4j} (1 + G_{2j} G_{3j} (LF)_i) + G_{5j} (1 - G_{2j} G_{3j} (LF)_i)}{[1 - G_{2j} G_{3j} (LF)_i]^2} \right] & \text{for } (P_j - P_{j_0}) \geq 0 \quad (LB-FT) \end{cases} \quad (198)$$

TYPE 2 BRAKE - Drum Type with Two Leading Shoes

$$(TQ)_{B_i} = \begin{cases} 0 & , \text{ for } (P_j - P_{j_0}) < 0 \\ \frac{1}{6}(P_j - P_{j_0}) G_{4j} G_{1j} \left[\frac{G_{2j} G_{3j} (LF)_i}{1 - G_{2j} G_{3j} (LF)_i} \right] & , \text{ for } (P_j - P_{j_0}) \geq 0 \quad (LB-FT) \end{cases} \quad (199)$$

TYPE 3 BRAKE - Bendix Duo Servo

$$(TQ)_{B_i} = \begin{cases} 0 & , \text{ for } (P_j - P_{j_0}) < 0 \\ \frac{1}{12}(P_j - P_{j_0}) G_{4j} \left\{ \left[1 + \frac{G_{6j} + G_{7j} \sin \xi}{G_{1j} - G_{6j} - G_{7j} \sin \xi} \right] \left[G_{7j} \sin \xi + \frac{G_{8j} G_{11j} G_{12j} (LF)_i}{G_{9j} G_{10j} 1 - G_{2j} G_{12j} (LF)_i} \right] - \frac{G_{1j} G_{8j} G_{12j} (LF)_i}{G_{9j} G_{10j} 1 - G_{2j} G_{12j} (LF)_i} \right\} & , \text{ for } (P_j - P_{j_0}) \geq 0 \quad (LB-FT) \end{cases} \quad (200)$$

TYPE 4 BRAKE - Caliper Disk

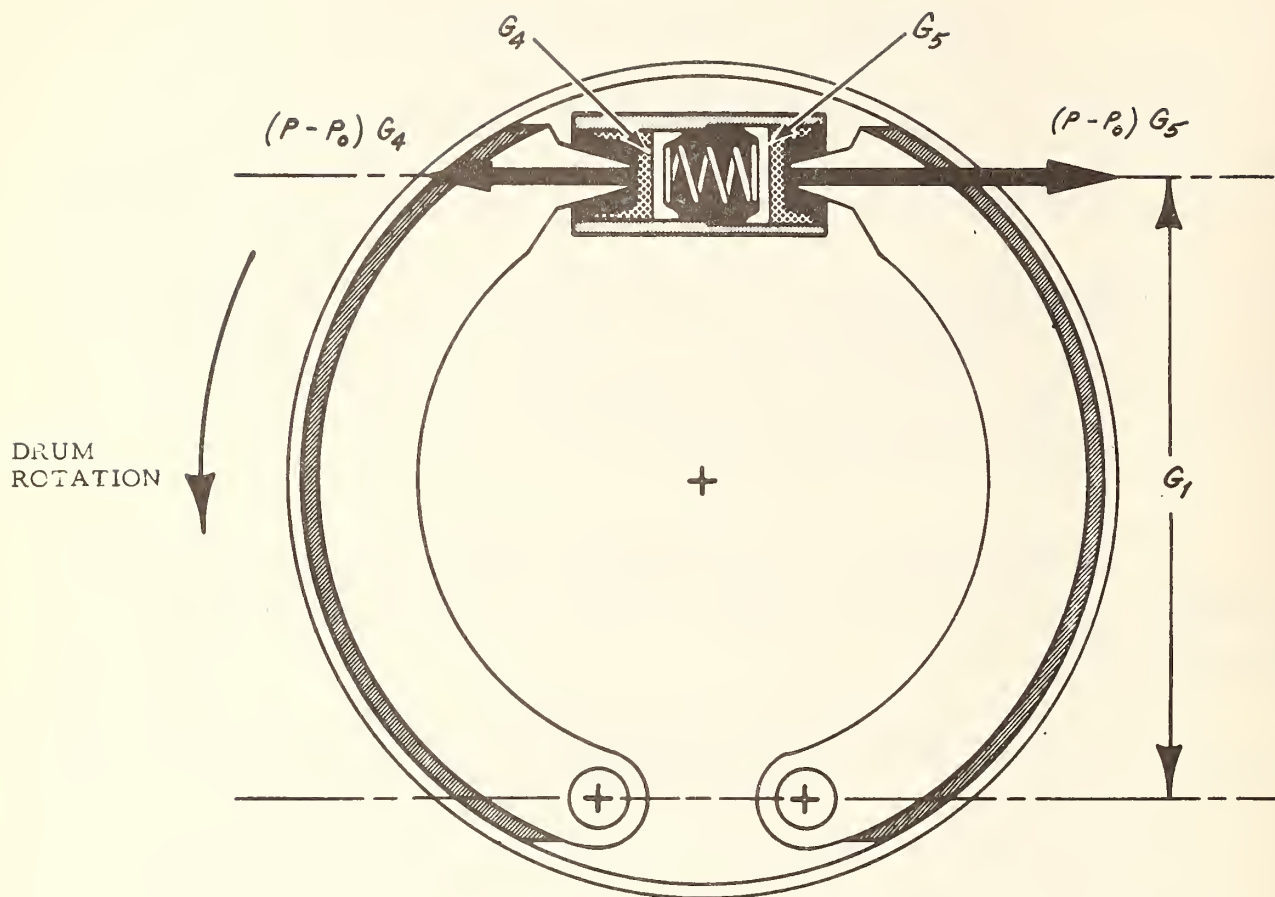
$$(TQ)_{Bi} = \begin{cases} 0 & , \text{ for } (P_j - P_{jo}) < 0 \\ \frac{1}{6} (P_j - P_{jo}) G_{3j} G_{4j} G_{13j} (LF)_i & , \text{ for } (P_j - P_{jo}) \geq 0 \text{ (LB-FI)} \end{cases} \quad (201)$$

Where G_{1j} , G_{2j} , ..., G_{13j} are taken from the input table of brake data (see Figures 3.10 through 3.13, and $(LF)_i$ is interpolated from the brake fade table following calculation of τ_i

Because the brake torques must always oppose wheel rotations, the algebraic signs of the brake torques are set to be opposite those of the wheel rotations:

$$\operatorname{sgn}(TQ)_{Bi} = (-) \operatorname{sgn}(RPS)_i$$

With a digital integration procedure, the simulation of coulomb friction can produce instability at small values of velocity. Since the friction force is held constant during a calculation increment, it can produce an overshoot of zero velocity and, thereby, add energy to the simulated system. To avoid such a problem in the present simulation of braking torques opposing wheel rotations, a sequence of calculation logic has been developed to limit the applied brake torques at small wheel rotational velocities (Figure 3.14). The analytical basis for the logic is presented in the following.



G_1 = Lever arm, inches

G_2 = Actuation constant, assumed to be equal for the two shoes. (Note that $G_2 \approx 1.42$ in Chrysler Products, Ref. 3)

(LF) = Coefficient to permit change of lining friction at elevated temperatures

G_3 = Effective lining-to-drum friction coefficient at design temp.

G_4 = Cylinder area - leading shoe, in.²

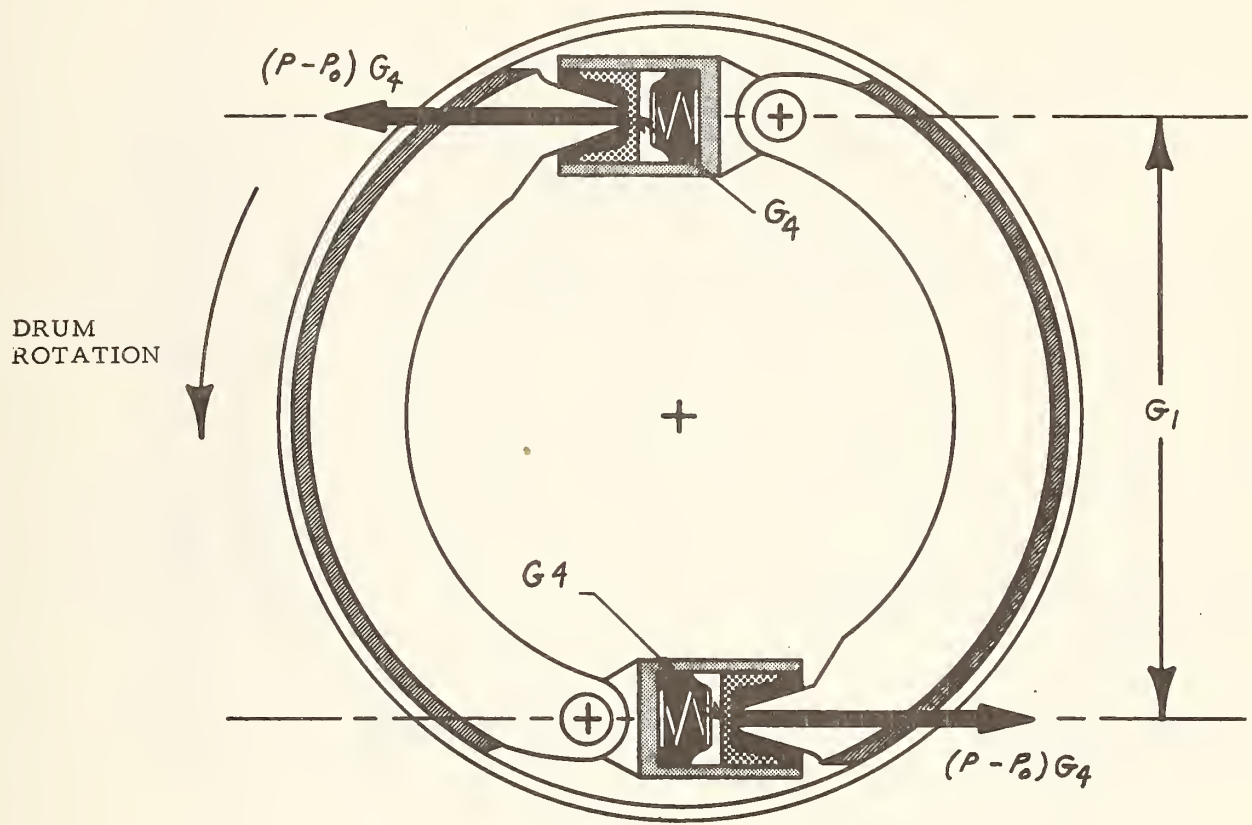
G_5 = Cylinder area - trailing shoe, in.²

P = Hydraulic pressure, psig

P_o = Push-out pressure, psig

$$(TQ)_B = \begin{cases} 0, & \text{for } (P - P_o) \leq 0 \\ \frac{1}{12} (P - P_o) G_1 G_2 G_3 (LF) \left\{ \frac{G_4 [1 + G_2 G_3 (LF)] + G_5 [1 - G_2 G_3 (LF)]}{[1 - G_2 G_3 (LF)]^2} \right\}, & \text{for } 0 < (P - P_o) \end{cases} \quad (\text{LB-FT})$$

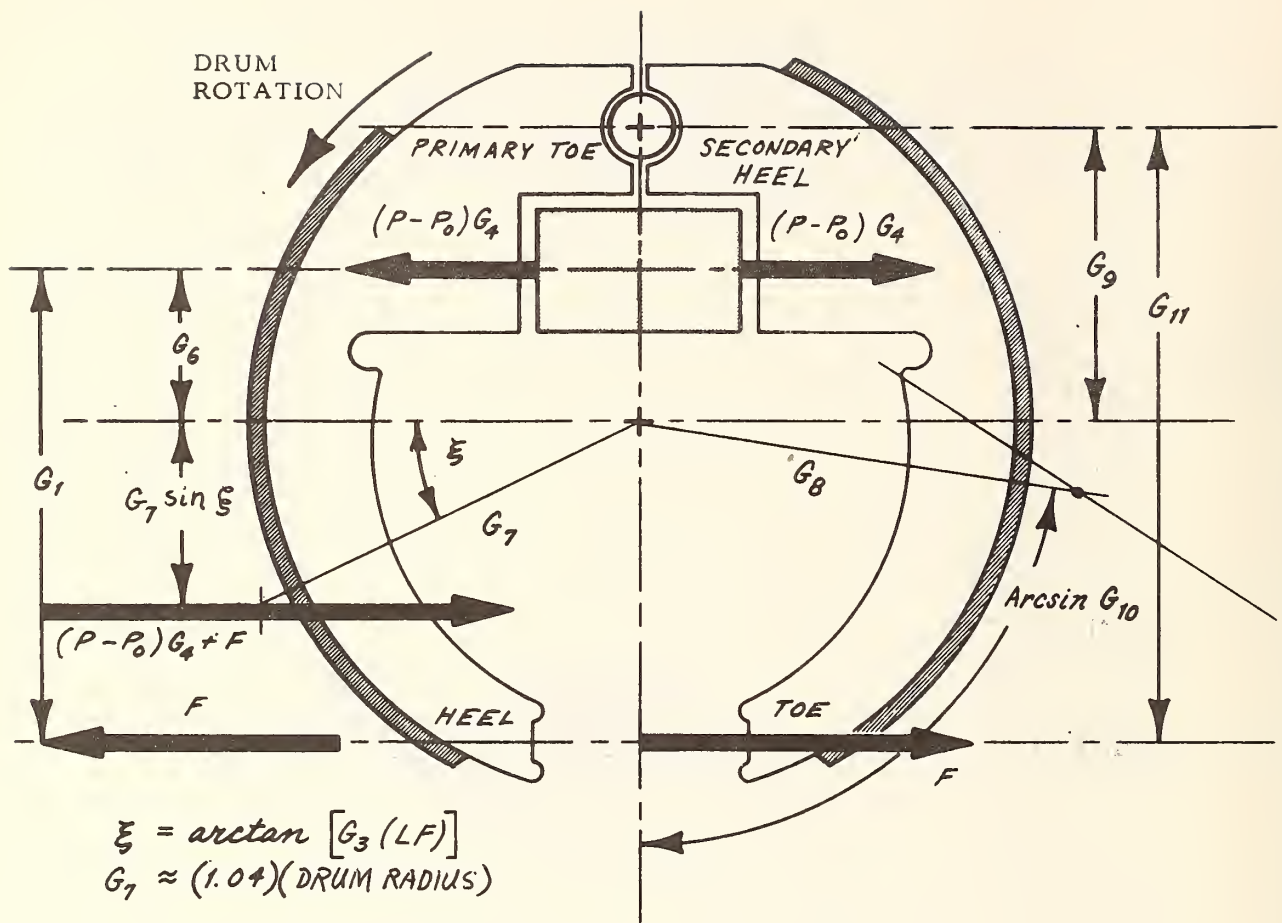
Figure 3.10 TYPE 1 BRAKE - DRUM TYPE WITH LEADING AND TRAILING SHOES, UNIFORM OR STEPPED CYLINDER



G_1	=	Lever arm, inches
G_2	=	Actuation constant
(LF)	=	Coefficient to permit change of lining friction at elevated temperatures
G_3	=	Effective lining-to-drum friction coefficient at design temp.
G_4	=	Cylinder area, in. ²
P	=	Hydraulic pressure, psig
P_o	=	Push-out pressure, psig

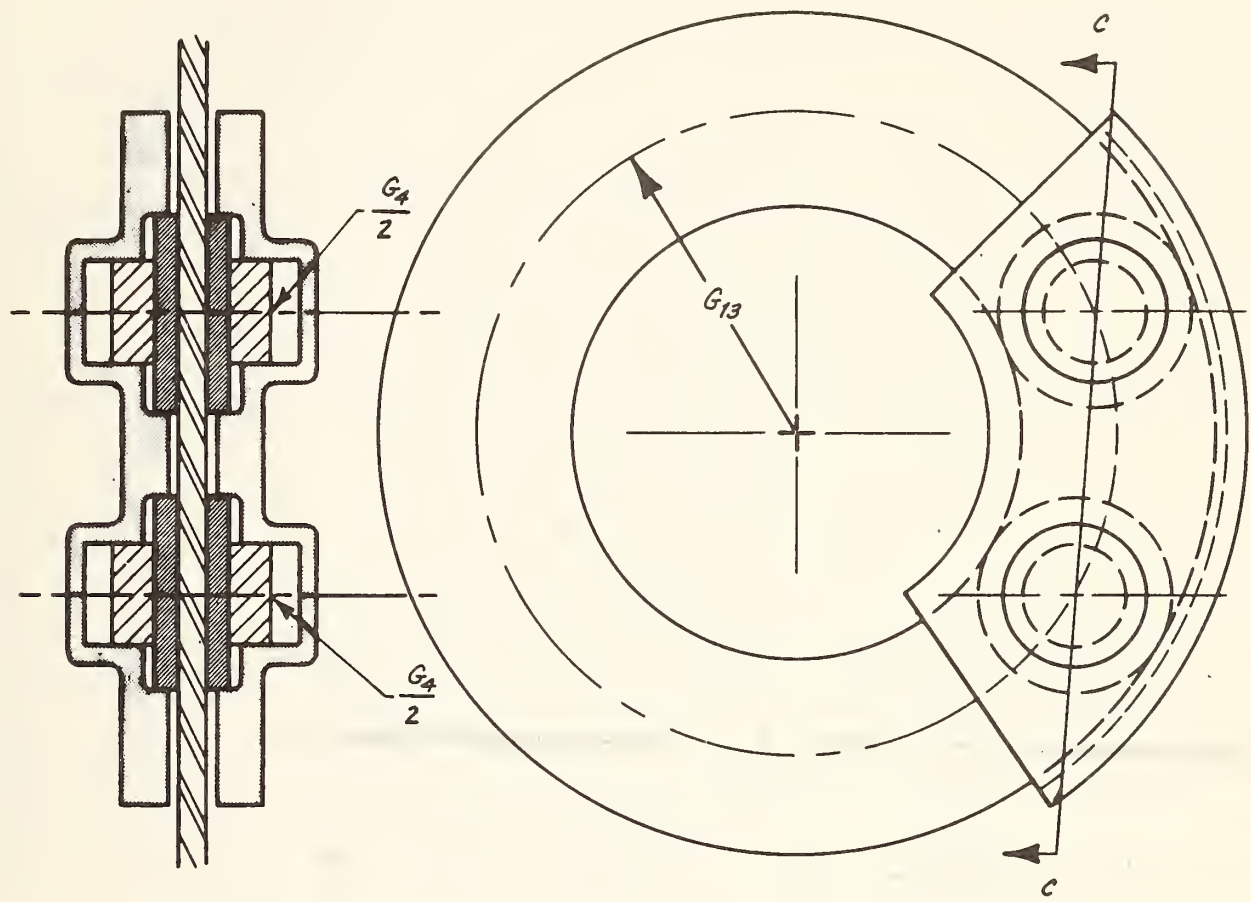
$$(TQ)_B = \begin{cases} 0, & \text{for } (P - P_o) \leq 0 \\ \frac{1}{6} (P - P_o) G_1 G_4 \left[\frac{G_2 G_3 (LF)}{1 - G_2 G_3 (LF)} \right], & \text{for } 0 < (P - P_o) \end{cases} \text{ (LB-FT)}$$

Figure 3.11 TYPE 2 BRAKE - DRUM TYPE WITH TWO LEADING SHOES, TWO CYLINDERS



$$(TQ)_B = \begin{cases} 0, & \text{for } (P - P_0) \leq 0 \\ \frac{1}{12} (P - P_0) G_4 \left\{ \left[1 + \frac{G_6 + G_7 \sin \xi}{G_1 - G_6 - G_7 \sin \xi} \right] \left[G_7 \sin \xi + \frac{G_8 G_{11} G_{12} (LF)}{G_9 G_{10} [1 - G_2 G_{12} (LF)]} \right] - \frac{G_1 G_8 G_{12} (LF)}{G_9 G_{10} [1 - G_2 G_{12} (LF)]} \right\}, & \text{for } 0 < (P - P_0) \end{cases} \quad (\text{LB-FT})$$

Figure 3.12 TYPE 3 BRAKE - BENDIX DUO SERVO



SECT CC

G_4	=	Total cylinder area per side of disc, in. ²
G_{13}	=	Mean lining radius, inches
G_3	=	Effective lining-to-disc friction coefficient
(LF)	=	Coefficient to permit change of lining friction at elevated temperatures
P	=	Hydraulic pressure, psig
P_o	=	Push-out pressure, psig
$(TQ)_B$	=	$\begin{cases} 0, & \text{for } (P - P_o) \leq 0 \\ \frac{1}{6}(P - P_o)G_3 G_4 G_{13} (LF), & \text{for } 0 < (P - P_o) \end{cases}$ (LB-FT)

Figure 3.13 TYPE 4 BRAKE - CALIPER DISC

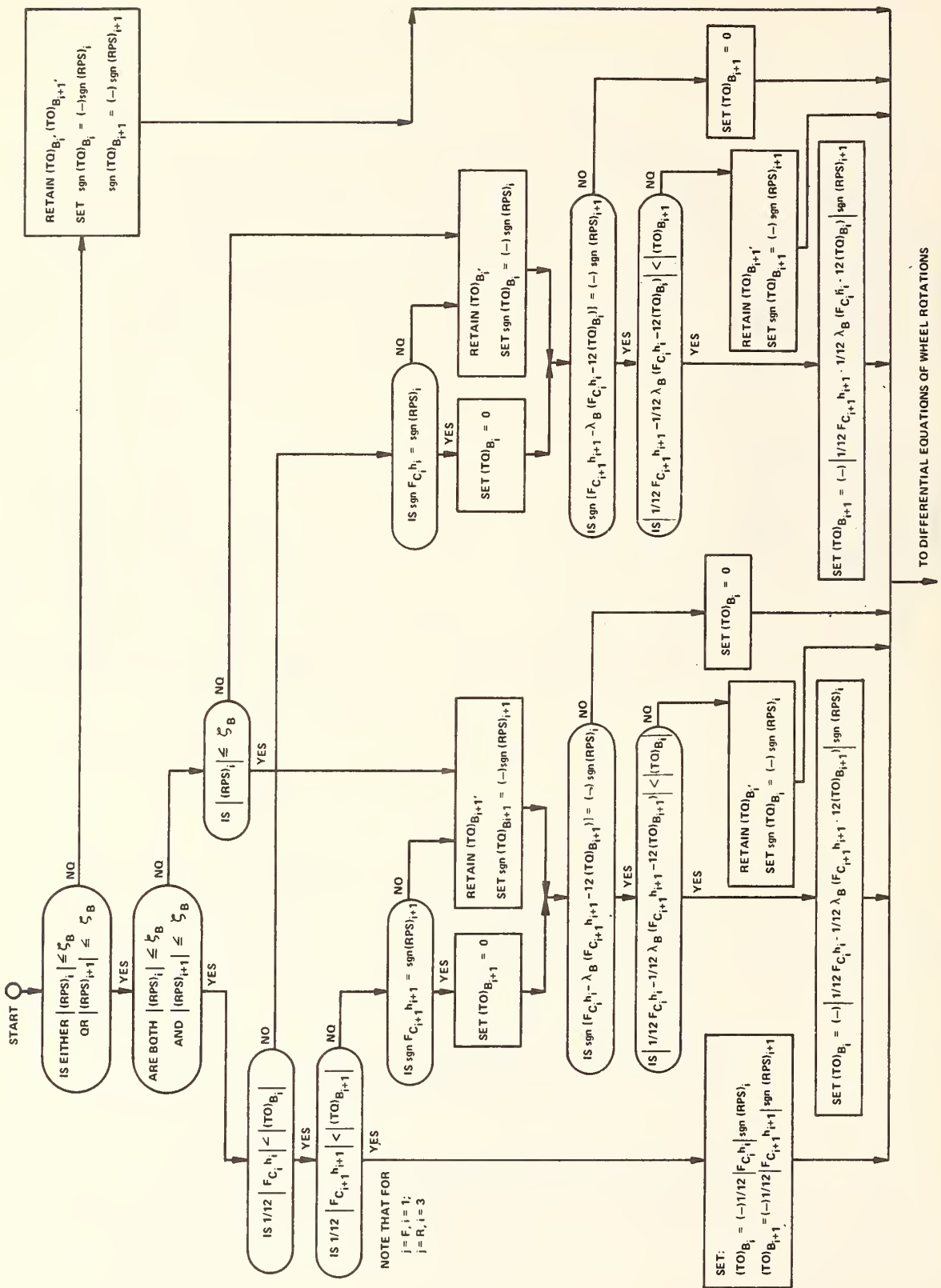


Figure 3.14 ADJUSTMENT OF $(TO)_{B_i}, (TO)_{B_{i+1}}$

Solution of Equations (44) and (45) of Section 3.1.4 for $(RPS)_i$ and $(RPS)_{i+1}$ yields

$$\frac{d}{dt} (RPS)_i = \frac{I_{Wj} \left[-F_{ci} h_i + 12(TQ)_{Bi} + 6(AR)_j (TQ)_{Dj} \right] + \frac{I_{Dj} (AR)_j^2}{4} \left[-F_{ci+1} h_{i+1} - F_{ci} h_i + 12(TQ)_{Bi} - TQ_{Bi+1} \right]}{I_{Wj} \left[I_{Wj} + \frac{I_{Dj} (AR)_j^2}{2} \right]} \quad (202)$$

$$\frac{d}{dt} (RPS)_{i+1} = \frac{I_{Wj} \left[-F_{ci+1} h_{i+1} + 12(TQ)_{Bi+1} + 6(AR)_j (TQ)_{Dj} \right] + \frac{I_{Dj} (AR)_j^2}{4} \left[-F_{ci+1} h_{i+1} + F_{ci} h_i - 12(TQ)_{Bi} - TQ_{Bi+1} \right]}{I_{Wj} \left[I_{Wj} + \frac{I_{Dj} (AR)_j^2}{2} \right]} \quad (203)$$

For very small values of $(RPS)_i$, $(RPS)_{i+1}$ (i.e., smaller than an arbitrarily specified threshold value of λ_B radians/second) it is desired to prevent the applied brake torques from erroneously accelerating the wheels. To accomplish this objective, the values of $(TQ)_{Bi}$, $(TQ)_{Bi+1}$ are limited to those required to make the numerators of Equations (202) and (203) equal to zero (with the exception of the tractive term).

From Equation (202), the limiting value of brake torque is

$$(TQ)_{Bi} = \frac{1}{12} F_{ci} h_i - \frac{1}{12} \lambda_B (F_{ci+1} h_{i+1} - 12 TQ_{Bi+1}) \quad (204)$$

where

$$\lambda_B = \frac{\frac{I_{Dj}}{4} \frac{(AR)_j^2}{4}}{I_{Wj} + \frac{I_{Dj} (AR)_j^2}{4}}$$

Similarly, from Equation (201), the limiting value of brake torque is

$$(TQ)_{Bi+1} = \frac{1}{12} F_{ci+1} h_{i+1} - \frac{1}{12} \lambda_B (F_{ci} h_i - 12 TQ_{Bi}) \quad (205)$$

The value of λ_B distinguishes between the driving and non-driving ends of the vehicle (i.e., for $I_{Dj} = 0$, $\lambda_B = 0$).

The need for the inclusion of inertial coupling with the other wheel of a driving pair is illustrated in Figure 3.19. The traversal of the patch of ice by braked wheel i can reduce the circumferential force, F_{ci} , permitting the brake to rapidly decelerate the wheel to a small rotational velocity. If the inertial coupling term were not included in Equation (202), the value of $(TQ)_{Bi}$ would be set to the low value ($F_{ci} h_i$) when $(RPS)_i$ became smaller than β_B . In this case, however, because of the inertial coupling terms in Equation (202), the large value of F_{ci+1} could then accelerate wheel i in reverse rotation unopposed by the true brake torque applied to wheel i . Therefore, the inclusion of inertial coupling effects in the determination of a limiting value of $(TQ)_{Bi}$ is seen to be a necessity.

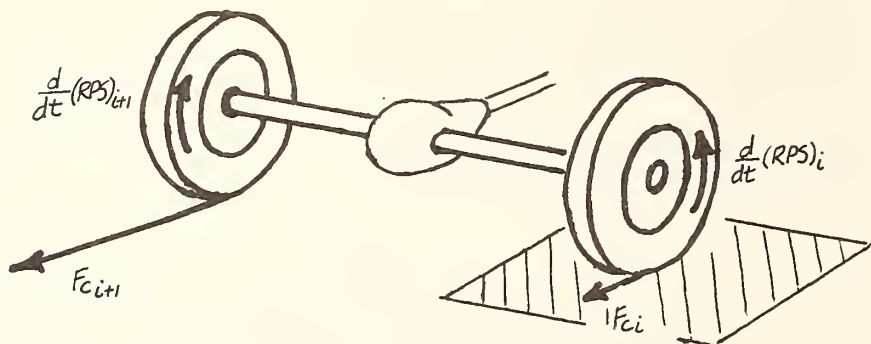


Figure 3.15 EFFECTS OF INERTIAL COUPLING OF DRIVE WHEELS

In the case where both wheels have rotational velocities less than the specified threshold value of ω_B rad/sec, the simultaneous satisfaction of Equations (204) and (205) requires that

$$(TQ)_{B_i} = \frac{1}{12} F_{c_i} h_i , \text{ and} \quad (206)$$

$$(TQ)_{B_{i+1}} = \frac{1}{12} F_{c_{i+1}} h_{i+1}$$

Note that this case is the same as the one in which $I_{Df} = 0$.

If both wheels have rotational velocities greater than ω_B rad/sec, the limitation of brake torques is bypassed.

The effects of brake fade are approximated by means of interpolation of a lining-to-drum fade coefficient, $(LF)_i$, that is entered as a tabular function of brake temperature. The brake temperatures are approximated by the following relationships:

$$\tilde{\tau}_i = \tilde{\tau}_{i_0} + \sum (\Delta \tilde{\tau}_i) , \text{ } ^\circ F \quad (207)$$

where

$$\Delta \tilde{\tau}_i = \frac{\Delta E_i}{G_{15j} G_{16j}} , \text{ } ^\circ F \quad (208)$$

$$\Delta E_i = \frac{(TQ)_{Bi} (RPS)_i}{777.8} - G_{14j} |u_{6i}|^{0.36} (\tilde{\tau}_i - \tilde{\tau}_A) \Delta t , \text{ BTU} \quad (209)$$

$$\begin{aligned} i &= 1, 2 & \text{for } j = F \\ i &= 3, 4 & \text{for } j = R \end{aligned}$$

3.6.2.2 Tractive Torque

The engine torque is interpolated from tabular entries of engine torque vs. engine RPM, for the given throttle setting, as shown in Figure 3.16. (The throttle setting is entered as a tabular function of time.) It is assumed that the engine torque increases linearly with throttle setting between the values entered for closed throttle and for wide open throttle. Thus, the engine torque is obtained from

$$(TQ)_E = (CT) + (TS) (WOT - CT)$$

$$0 \leq TS \leq 1.0 \quad (210)$$

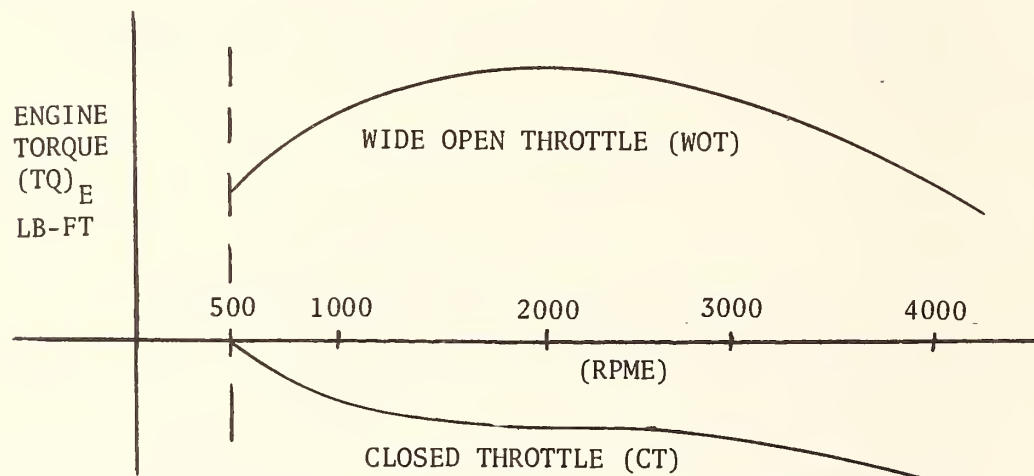


Figure 3.16 INPUTS TO DEFINE ENGINE PROPERTIES

The engine speed in revolutions per minute, $(RPME)$, is calculated from

$$(RPME) = \begin{cases} 500 & , \text{ or} \\ \frac{15(AR)}{\pi} [(RPS)_i + (RPS)_{i+1}] (TR) \end{cases} \quad (211)$$

whichever is larger, for $(RPS)_i$, $(RPS)_{i+1}$ at driving end of vehicle.

To permit the simulation of a standing start, the logic depicted in Figure 3.17 has been incorporated in the program.

3.7 Tire Forces

3.7.1 HVOSM-RD2 Version

The side, braking and traction forces are, of course, related to the tire load normal to the plane of the tire-terrain contact patch, F'_R_i , rather than the radial tire load, F_{Ri} . Therefore it is necessary to find the value of F'_R_i corresponding to the radial load, F_{Ri} , and the side force, F_{Si} . The components of the external applied forces, F'_R_i and F_{Si} , along the line of action of the radial tire force, F_{Ri} , are depicted in Figure 3.18. These force components must be in equilibrium with F_{Ri} , such that

$$F'_R_i \cos \phi_{CG_i} + F_{Si} \sin \phi_{CG_i} = F_{Ri} \quad (212)$$

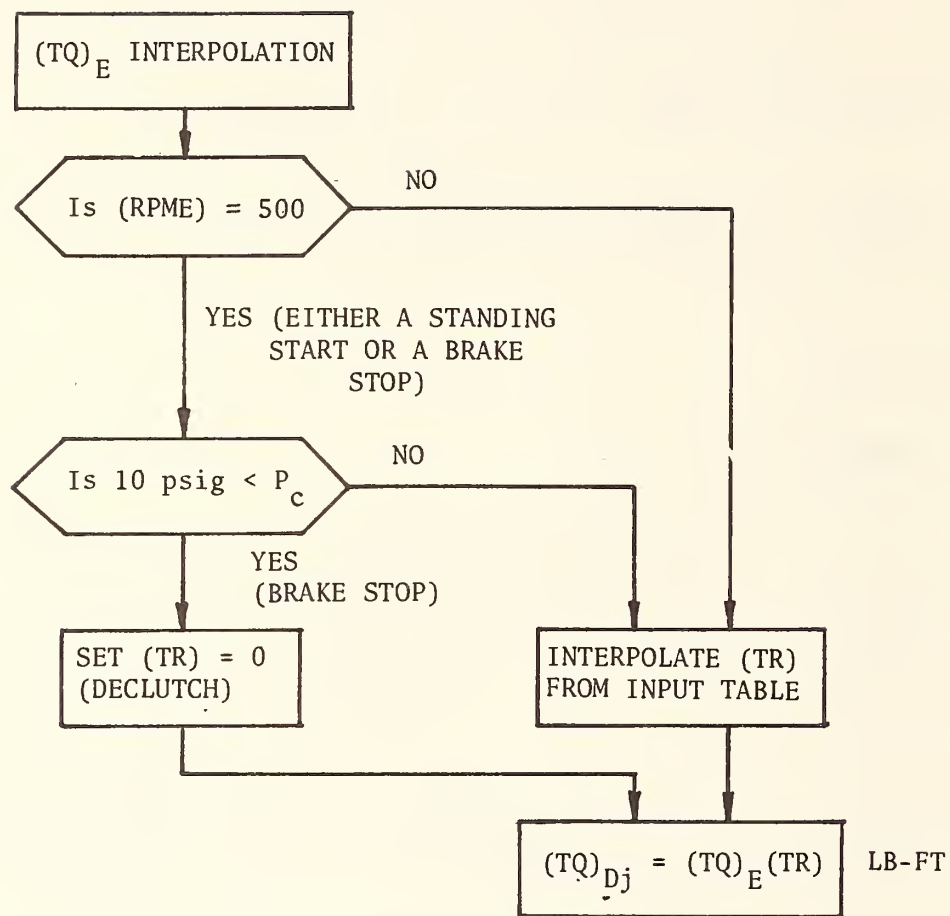
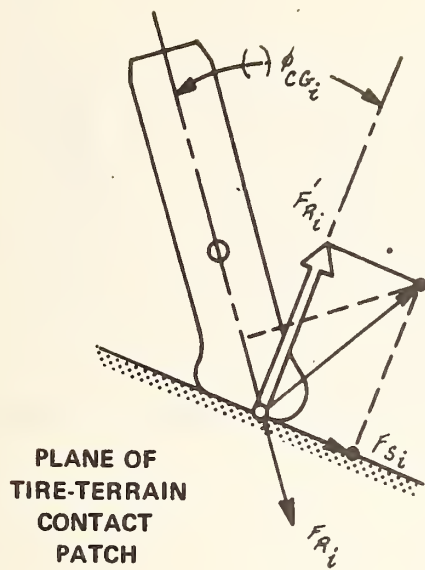


Figure 3.17 LOGIC TO PERMIT A STANDING START



ϕ_{CG_i} = CAMBER ANGLE
RELATIVE TO
TERRAIN (SHOWN
NEGATIVE)

F_{S_i} = SIDE FORCE
PRODUCED BY
COMBINATION OF
SLIP ANGLE AND
CAMBER ANGLE

$i = 1, 2, 3, 4$

Figure 3.18 VECTOR SUMMATION OF FORCES WITH COMPONENTS ALONG THE LINE OF ACTION OF THE RADIAL TIRE FORCE (VIEWED FROM REAR)

Solution of (209) for F'_{Ri} yields

$$F'_{Ri} = F_{Ri} \sec \phi_{CG_i} - F_{S_i} \tan \phi_{CG_i} \quad (213)$$

Since F'_{Ri} is required for the determination of F_{S_i} , an initial approximation of F_{S_i} is obtained by extrapolation from the previous time increment. Following the calculation of F_{S_i} in the current time increment, an iterative procedure is employed to correct both F'_{Ri} and F_{S_i} .

Side Forces

The side force calculations are based on the small angle properties of the tires which are "saturated" at large angles. Variations in the small-angle cornering and camber stiffnesses produced by changes in tire loading are approximated by parabolic curves fitted to experimental data (Figure 3.19). The small-angle cornering stiffness is taken to be the partial derivative of lateral force with respect to slip angle as measured at zero slip angle for various tire loads. The upper plot of Figure 3.19 depicts a parabola fitted to the small-angle cornering stiffness as a function of tire loading, in which the cornering stiffness varies as,

$$C_{so} = A_0 + A_1 F'_{R_i} - \frac{A_1}{A_2} (F'_{R_i})^2 \quad (214)$$

The lower plot of Figure 3.19 depicts a similar fit to small-angle camber stiffness, the partial derivative of lateral force with respect to camber angle as measured at zero camber angle, in which the camber stiffness varies as,

$$C_{co} = A_3 F'_{R_i} - \frac{A_3}{A_4} (F'_{R_i})^2 \quad (215)$$

The fitted parabolic curves are abandoned for tire loading in excess of $\Omega_T A_2$ (see Figure 3.19), where the approximate range of the coefficient is $0.80 < \Omega_T < 1.15$ (Ω_T is an adjustable item of input data). The side force properties are then treated as being independent of tire loading. The use of Ω_T is necessary to avoid artificial reversal of the slip angle forces under conditions of extreme loading (i.e., where $A_2 \ll F'_{R_i}$). Actual properties of tires in this range of loading (i.e., extreme overload) are not known.

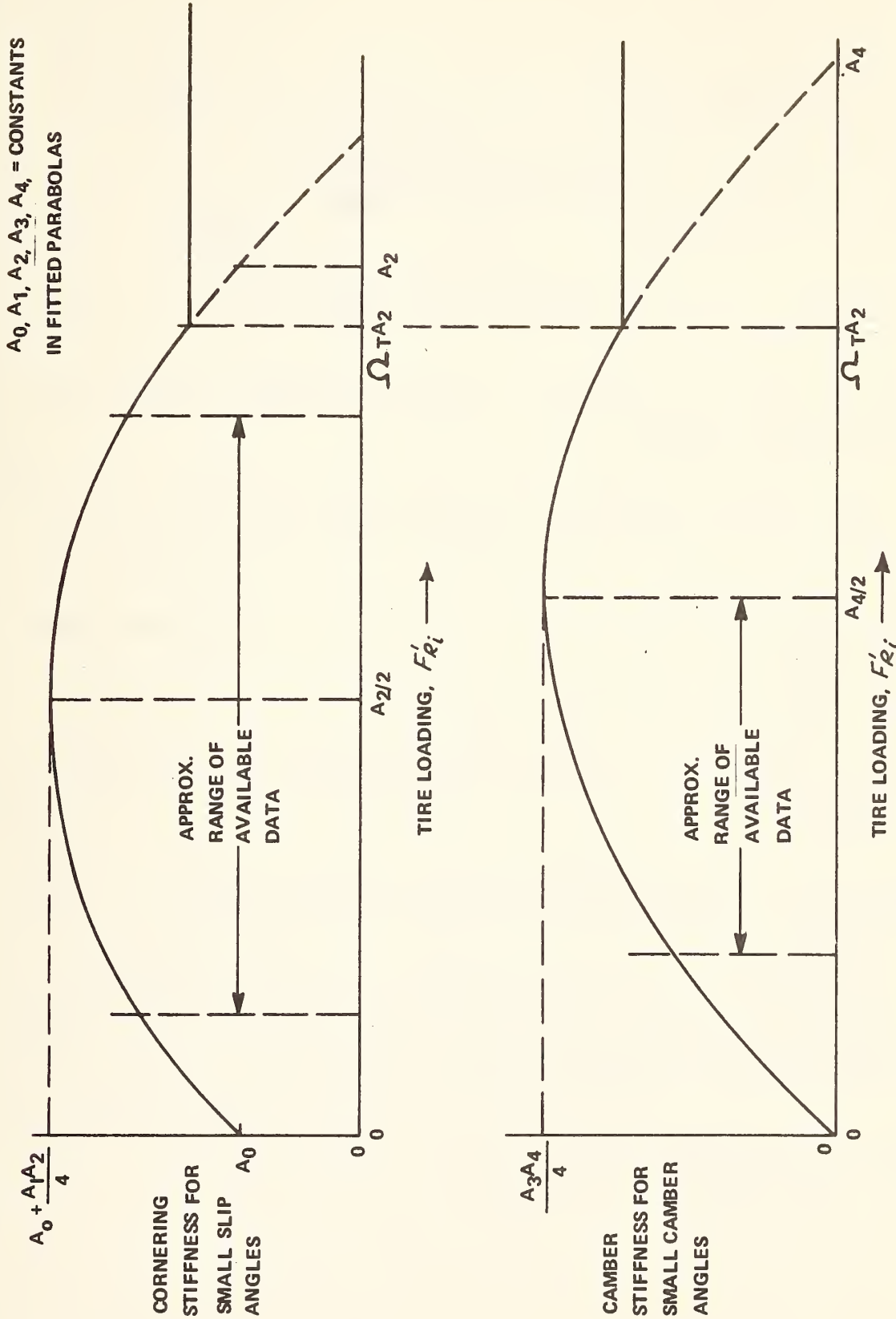


Figure 3.19 SIMULATED VARIATION OF SMALL-ANGLE CORNERING AND CAMBER STIFFNESS WITH LOADING NORMAL TO TIRE-TERRAIN CONTACT PATCH

For the case of zero traction and braking the side forces, for small slip and camber angles, can be expressed from (215) and (214) as

$$(F_{S_i})_{CAMBER} = - \left[\frac{A_3 F'_{R_i} (F'_{R_i} - A_4)}{A_4} \right] \phi_{cG_i} \quad (216)$$

$$(F_{S_i})_{SLIP} = \left[\frac{A_1 F'_{R_i} (F'_{R_i} - A_2) - A_0 A_2}{A_2} \right] \left[\frac{v_{G_i}}{u_{G_i}} - \psi'_i \right] \quad (217)$$

where the sign convention corresponds to the right-hand rule applied to the system depicted in Figure 3.1.

The tire model must handle extremely large camber angles relative to the tire-terrain contact planes. Applicable tire data are not known to be available. Therefore, the assumption has been made that the camber force, for a given normal load, will reach its maximum value of 45 degrees of camber. In accordance with this assumption, a parabolic variation of camber force with camber angle is simulated with the peak occurring at 45 degrees (see Figure 3.20). With the assumed large-angle camber characteristic depicted in Figure 3.20, Equation (216), for the complete range of possible camber angles, becomes

$$(F_{S_i})_{CAMBER} = - \left[\frac{A_3 F'_{R_i} (F'_{R_i} - A_4)}{A_4} \right] \left[\phi_{cG_i} - \frac{2}{\pi} \phi_{cG_i} |\phi_{cG_i}| \right] \quad (218)$$

To permit the use of the nondimensional slip angle concept which "saturates" the side force at large slip angles, an "equivalent" slip angle is defined to approximate camber effects

$$\beta'_i = \left\{ \frac{A_2 A_3 F'_{R_i} (A_4 - F'_{R_i})}{A_4 [A_1 F'_{R_i} (F'_{R_i} - A_2) - A_0 A_2]} \right\} \left[\phi_{cG_i} - \frac{2}{\pi} \phi_{cG_i} |\phi_{cG_i}| \right] \quad (219)$$

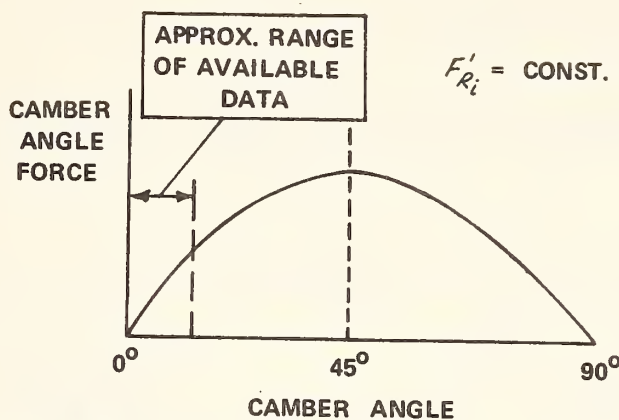


Figure 3.20 ASSUMED VARIATION OF CAMBER FORCE WITH CAMBER ANGLE

Note that the selected analytical treatment of camber angles subjects the camber force to the saturation effects of the slip angle, superimposed on the assumed behavior shown in Figure 3.20. While the assumption depicted in Figure 3.20 may be shown to be in error when appropriate tire data becomes available, it was found to be necessary to reduce the "equivalent" slip angle of large camber angles to avoid an unrealistic predominance of camber effects on steeply inclined terrain obstacles. On the basis of the comparisons of predicted and experimental responses that have been made to date, it must be concluded that the selected analytical representation of large-angle camber effects is at least adequate.

Using definition (219), the resultant side force for small slip angles and the entire range of camber angles can be expressed as

$$F'_{s_i} = \left[\frac{A_1 F'_{R_i} (F'_{R_i} - A_2) - A_o A_2}{A_2} \right] \left[\frac{v_{G_i}}{u_{G_i}} - \psi'_i + \beta'_i \right]. \quad (220)$$

Application of Equation (220) to the nondimensional side force relationship (see Figure 3.21) yields

$$f(\bar{\beta}_i) = \frac{F'_{s_i}}{(F'_{s_i})_{\max}} = \bar{\beta}_i - \frac{1}{3} \bar{\beta}_i |\bar{\beta}_i| + \frac{1}{27} \bar{\beta}_i^3 \quad (221)$$

where \dot{F}_{s_i} = resultant side force for entire range of slip and camber angles, and

$$\bar{\beta}_i = \frac{F'_{s_i}}{(F'_{s_i})_{\max}} \quad (222)$$

Large values of the slip angles, particularly in skidding, make it necessary to use the arctan (v_{G_i}/u_{G_i}) rather than (v_{G_i}/u_{G_i}). Also, in cases where reversal of the vehicle velocity has occurred, it has been found to be necessary to control the algebraic signs of the slip and steer angles. Equation (222) requires that Equation (220) be modified as follows:

$$\bar{\beta}_i = \left[\frac{A_1 F'_{R_i} (F'_{R_i} - A_2) - A_o A_2}{A_2 (F'_{s_i})_{\max}} \right] \left[\arctan \frac{v_{G_i}}{|u_{G_i}|} - (\operatorname{sgn} u_{G_i}) \psi'_i + \beta'_i \right] \quad (223)$$

$$f(\bar{\beta}) = \begin{cases} \bar{\beta} - \frac{1}{3}\bar{\beta}|\bar{\beta}| + \frac{1}{27}\bar{\beta}^3, & \text{for } |\bar{\beta}| < 3 \\ 1, & \text{for } 3 < |\bar{\beta}| \end{cases}$$

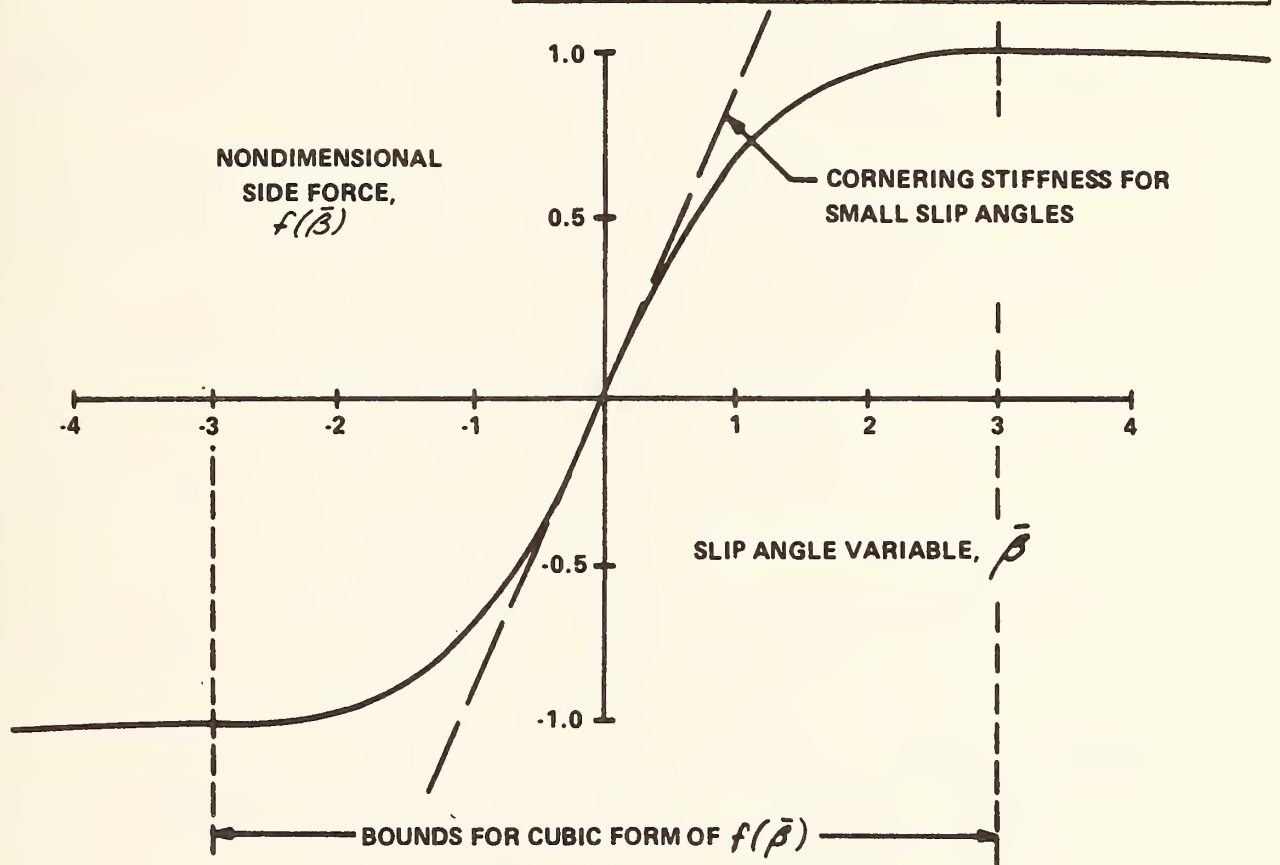


Figure 3-21. Nondimensional tire side-force curve

The "friction circle" concept is based on the assumption that the maximum force that can be generated by the tires in the plane of the tire-terrain contact patch is equal in all directions. With the use of the "friction circle" concept (see Figure 3.22), the maximum side force can be expressed as

$$(F_{S_i})_{max} = \sqrt{\mu_i^2 (F'_{R_i})^2 - F'_{C_i}^2} \quad (224)$$

where F'_{C_i} = circumferential tire force (i.e., traction or braking) at wheel i , in pounds which is determined from interpolation of the input tables of applied torque.

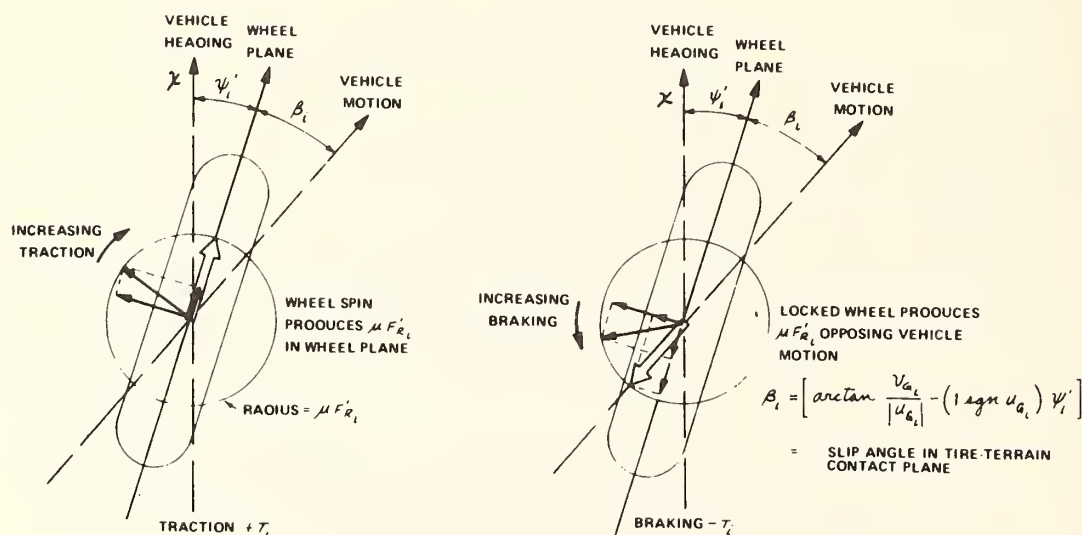


Figure 3.22¹ FRICTION CIRCLE CONCEPT

The detailed calculation procedure is shown below.

The determination of the tire side force, F_{si} , for the current time increment requires the use of F'_{ri} , and a value of F_{si} is, therefore, not available at this point in the calculation. For this reason F_{si} from the previous time increment, is initially used. The subsequently calculated value of F_{si} is then used to recalculate F'_{ri} , where

$$F'_{ri} = F_{ri} \sec \phi_{CGi} - F_{si} \tan \phi_{CGi}$$

The following tests are employed to determine if the tire has lost contact with the ground, or if the force normal to the ground, F'_{ri} , is calculated to be a negative quantity (this condition can be produced by the extrapolated value of F_{si} under conditions in which the side force reverses signs).

If $F_{ri} = 0$, or $(F_{ri} - F_{si} \sin \phi_{CGi}) \leq 0$, bypass calculation of the tire side and circumferential forces, set $F_{si} = F_{ci} = F'_{ri} = 0$.

The circumferential tire forces are calculated from the following relationships:

$$1. \quad T_i = \frac{12(TQ)_F}{h_i}, \text{ for } i = 1, 2 \text{ (front wheels)}$$

$$T_i = \frac{12(TQ)_R}{h_i}, \text{ for } i = 3, 4 \text{ (rear wheels)}$$

2. A. If $T_i = 0$, bypass calculation of F_{ci} , set $F_{ci} = 0$

B. If $0 < T_i$ (Traction)

$$(1) \quad F_{ci} = \begin{cases} T_i, & \text{for } T_i \leq |\mu_i F'_{ri}| \\ \mu_i F'_{ri}, & \text{for } T_i > |\mu_i F'_{ri}| \end{cases} \quad (225)$$

(2) Is any $T_i > |\mu F'_R i|$?

(a) If no, set $F_{ci} = F'_R i$

(b) If yes, compare the corresponding product ($F_{ci} h_i$) for the other wheel of the pair (i.e., the pairs (1, 2) and (3, 4)). Set the values of the products ($F_{ci} h_i$) in the given pair to the smaller of the individual products. For example, say $F_{c2} h_2 < F_{c1} h_1$, then $F_{c2} = F_{c1}$ and $F_{c1} = F_{c2} (h_2/h_1)$. (Effects of differential drive gears.)

C. If $T_L < 0$ (Braking),

(1) For $1.932 \text{ in/sec} \leq |u_{gi}|$,

$$F_{ci} = \begin{cases} T_i (\operatorname{sgn} u_{gi}) , \text{ for } |T_i| \leq \left| \mu F'_R i \cos \left[\arctan \frac{v_{gi}}{|u_{gi}|} - \psi'_i (\operatorname{sgn} u_{gi}) \right] \right| \\ -\mu F'_R i (\operatorname{sgn} u_{gi}) \cos \left[\arctan \frac{v_{gi}}{|u_{gi}|} - \psi'_i (\operatorname{sgn} u_{gi}) \right] , \\ \text{for } \left| \mu F'_R i \cos \left[\arctan \frac{v_{gi}}{|u_{gi}|} - \psi'_i (\operatorname{sgn} u_{gi}) \right] \right| < |T_i| \end{cases} \quad (226)$$

(2) For $|u_{gi}| < 1.932 \text{ in/sec}$

Calculate F_{ci} as above (Equation 226), but multiply it by

$$\frac{|u_{gi}|}{1.932}$$

The calculation of tire side force includes testing as to whether effectively all of the available force (via the friction circle concept) is taken up by braking or tractive forces, and whether the vehicle is in motion.

Thus:

If $|F_{ci}| \geq |\mu_i F'_{ri}| - 1.0$, bypass side force calculation,
set $F_{si} = 0$

If both $|v_{gi}|$ and $|u_{gi}| < 0.5$, bypass side force calculation, set $F_{si} = 0$

If either $|v_{gi}|$ or $|u_{gi}| \geq 0.5$, and $|\bar{\beta}_i| < 3$,

$$F_{si} = \sqrt{\mu_i^2 (F'_{ri})^2 - F_{ci}^2} \left[\bar{\beta}_i - \frac{1}{3} \bar{\beta}_i |\bar{\beta}_i| + \frac{1}{27} \bar{\beta}_i^3 \right] \quad (227)$$

For $3 \leq |\bar{\beta}_i|$,

$$F_{si} = \sqrt{\mu_i^2 (F'_{ri})^2 - F_{ci}^2} \quad \text{where} \quad \operatorname{sgn} F_{si} = \operatorname{sgn} \bar{\beta}_i \quad (228)$$

For conditions of tire loading that are not extreme (i.e.,

$$\begin{aligned} F'_{ri} &\doteq A_{2i} \Omega_{Ti} \\ \bar{\beta}_i &= \left[\frac{A_{1i} F'_{ri} (F'_{ri} - A_{2i}) - A_{0i} A_{2i}}{A_{2i} \sqrt{\mu_i^2 (F'_{ri})^2 - F_{ci}^2}} \right] \arctan \left[\frac{v_{gi}}{|u_{gi}|} + \beta'_i - (\operatorname{sgn} u_{gi}) \psi'_i \right] \end{aligned} \quad (229)$$

and

$$\beta'_i = \left[\frac{A_{2i} A_{3i} (A_{4i} - F'_{ri}) F'_{ri}}{A_{4i} (A_{1i} F'_{ri} (F'_{ri} - A_{2i}) - A_{0i} A_{2i})} \right] \left(\phi_{CGi} - \frac{2}{\pi} \phi_{CGi} |\phi_{CGi}| \right) \quad (230)$$

For conditions of extreme tire overload (i.e., $F'_{ri} > A_2 \Omega_T$),

$$\bar{\beta}_i = \left[\frac{A_{1i} A_{2i} \Omega_{Ti} (\Omega_{Ti} - 1) - A_{0i}}{\sqrt{\mu_i^2 (F'_{ri})^2 - F_{ci}^2}} \right] \arctan \left[\frac{v_{gi}}{|u_{gi}|} + \beta'_i - (\operatorname{sgn} u_{gi}) \psi'_i \right] \quad (231)$$

and

$$\beta'_i = \left[\frac{A_{2i} A_{3i} \Omega_{T_i} (A_{4i} - \Omega_{T_i} A_{2i})}{A_{4i} (A_{1i} A_{2i} \Omega_{T_i} (\Omega_{T_i} - 1) - A_{0i})} \right] \left(\phi_{CGi} - \frac{2}{\pi} \phi_{CGi} |\phi_{CGi}| \right) \quad (232)$$

3.7.2 HVOSM-VD2 Version

The calculation of the tire loading normal to the ground, F_{Ri}' , and the tire side force, F_{Si}' , follows the same assumptions and derivations given in Section 3.7.1. However, the tire model employed in this program version makes use of the "friction ellipse" concept in establishing the relationship between side and circumferential forces. In addition, the inclusion of wheelspin as a degree-of-freedom necessitates the use of longitudinal tire characteristics in determining the instantaneous, circumferential force based on measured tire properties.

The "friction ellipse" is an extension of the widely used "friction circle" concept (e.g., References 5 and 6) that permits a more realistic analytical treatment of interactions between the circumferential force (i.e., tractive or braking) and the side force of a tire. Experimental evidence that the maximum values of tire friction forces are dependent on direction relative to the wheel plane is presented in References 7 and 8. General representation of frictional properties of pneumatic tires requires independent specification of lateral and circumferential friction coefficient and their variation with load and speed. Further, two characteristic coefficients are required to represent the circumferential friction, i.e., the peak (μ_{xp}) and sliding (μ_{xs}) coefficient.

In the "friction ellipse" form of treatment of interactions, the maximum value of the resultant tire friction force in the tire-terrain contact plane is assumed to be bounded by an ellipse with the minor axis equal to $2\mu_{xp} F_R'$ and major axis equal to $2\mu_{xp} F_R'$, where

μ_y = effective tire-terrain friction coefficient for side forces, for the given conditions of vehicle speed and tire loading. Note that, in the absence of circumferential forces, the value $\mu_y F'_R$ constitutes the maximum achievable side force.

μ_{xp} = peak tire terrain friction coefficient for circumferential forces for the given conditions of vehicle speed and tire loading.

= tire loading perpendicular to the tire-terrain contact plane, lbs.

The bounding ellipse is depicted in Figure 3.23. Note that a value of $\mu_{xp} = \mu_y$ will reduce the "friction ellipse" to a "friction circle".

In the calculation procedure of the developed analytical treatment of interactions, the circumferential tire force, F_c , is given first priority in utilization of the available friction. The maximum value of side force, $(F_s)_{\max}$, corresponds to a resultant force that constitutes a radius vector of the bounding ellipse, is then determined for use in the calculation of side forces (see Figure 3.23). Note that this sequence of calculations is identical with those of References 4 and 5 for the "friction circle" concept.

In Figure 3.23, the maximum value of side force, $(F_s)_{\max}$, for a given circumferential force, F_c , is determined in the following manner.

$$\frac{(F_s)_{\max}^2}{\mu_y^2} + \frac{F_c^2}{\mu_{xp}^2} = (F'_R)^2 \quad (233)$$

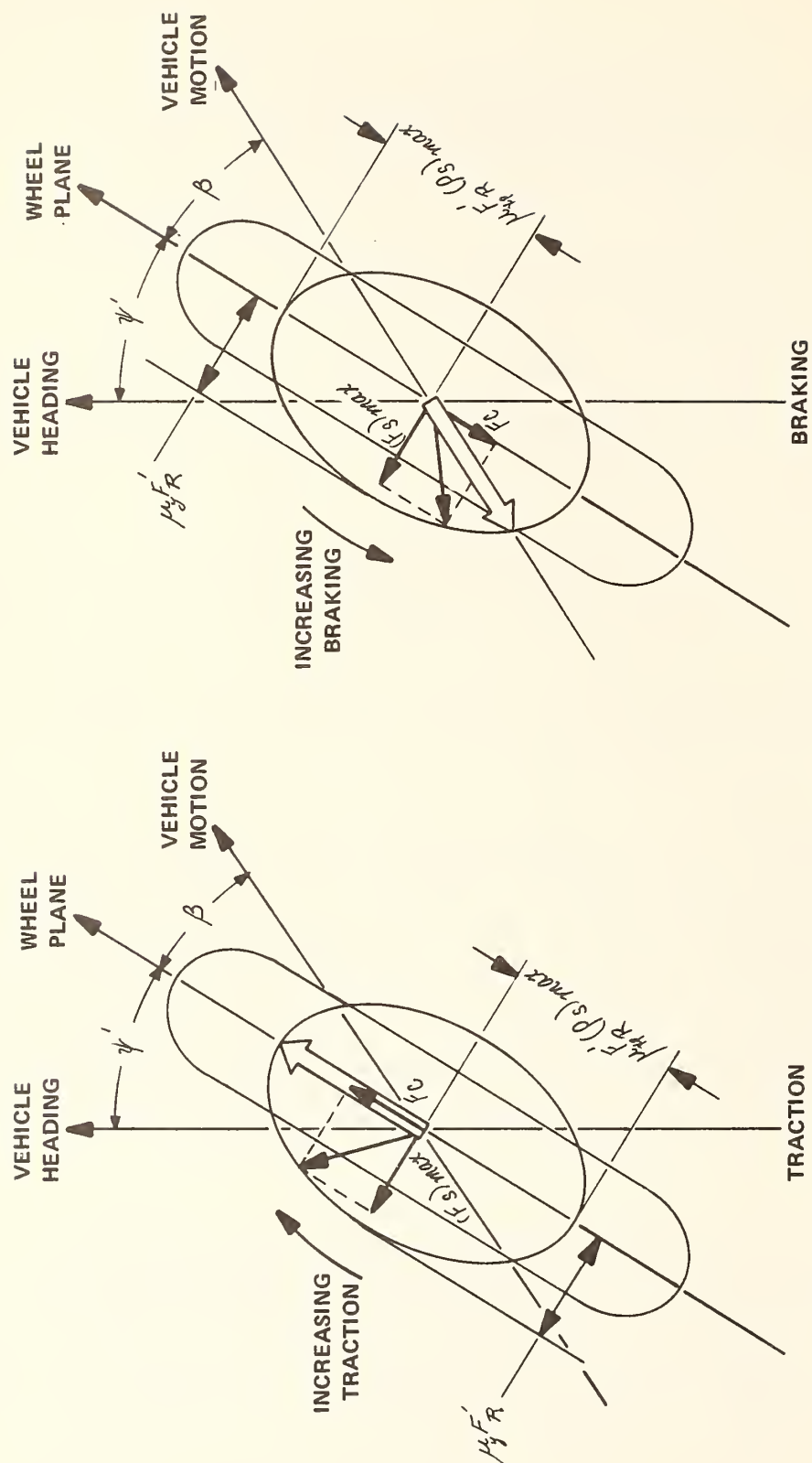


Figure 3.23 FRICTION ELLIPSE CONCEPT

Solution of (233) for $(F_s)_{\max}$ yields

$$(F_s)_{\max} = \sqrt{\mu_y^2(F'_R)^2 - \frac{\mu_y^2 F_c^2}{\mu_x^2}} \quad (234)$$

For the case of traction, the magnitude of the circumferential force is limited only by the bounding ellipse, since the resultant force lies in the wheel plane under the condition of maximum traction. Therefore, F_c is determined directly from

$$F_c = \mu_x F'_R \quad (235)$$

In the case of braking, where the limiting condition on the resultant force is that of opposing the direction of vehicle motion, the maximum circumferential force may be less than $\mu_x F'_R$. Therefore, the circumferential component corresponding to the cited limiting condition on the resultant force is calculated, as follows, for comparison with $\mu_x F'_R$, and the smaller of the two values (i.e., smaller absolute value) is used in Equation (234). From Equation (233) and inspection of Figure 3.23,

$$F_c^2 + (F_s)_{\max}^2 = \mu_y^2(F'_R)^2 + F_c^2 \left[1 - \frac{\mu_y^2}{\mu_x^2} \right] = F_c^2 \sec^2 \beta \quad (236)$$

Solution of (226) for F_c yields

$$F_c = \frac{\mu_x F'_R}{\sqrt{\tan^2 \beta + \frac{\mu_y^2}{\mu_x^2}}} \quad (237)$$

Thus, the calculation of F_c , to treat either traction or braking, is as follows:

$$F_c = \begin{cases} \mu_x F_R' , \text{ or} \\ \frac{\mu_y F_R'}{\sqrt{\tan^2 \beta + \frac{\mu_y^2}{\mu_{xp}^2}}} \end{cases} \quad (238)$$

whichever has the smaller value. Application of the value of F_c obtained from Equation (238) in Equation (234) yields the required value of $(F_s)_{\max}$.

The determination of the actual value of the circumferential friction coefficient μ_x is dependent on the instantaneous value of rotational slip, SLIP_i , and the μ_x vs. SLIP relationship. This relationship, as shown in Figure 3.24, is in turn characterized by four measurable quantities:

C_T = the slope of the μ_x vs. SLIP curve in the small SLIP region

μ_{xp} = the maximum value of the circumferential friction

SLIP_p = the value of SLIP at which μ_{xp} occurs

μ_{xs} = the value of μ_x at 100% SLIP

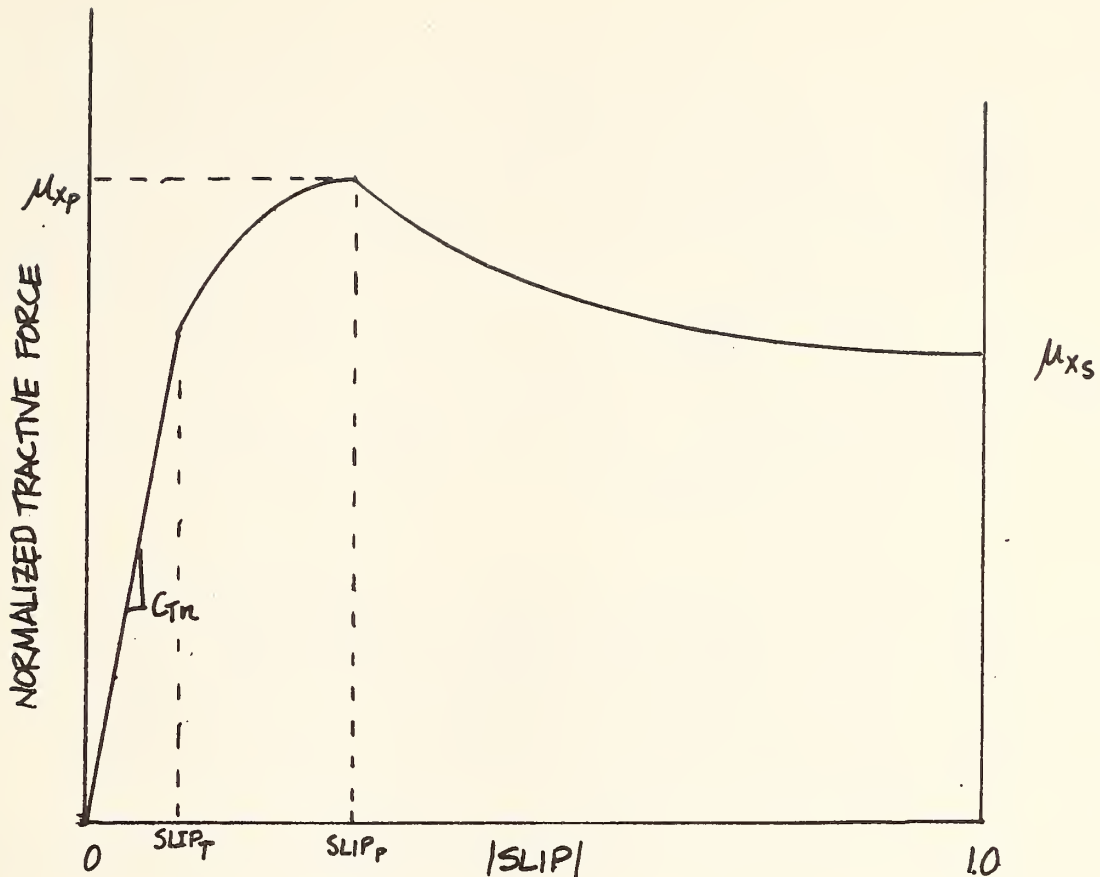


Figure 3.24 Normalized Tractive Force vs. SLIP Model

The relationships employed to define the entire μ_x vs. SLIP characteristic are:

$$\begin{aligned}
 \mu_x &= C_0/|SLIP| && \text{for } 0 \leq |SLIP| \leq SLIP_T \\
 \mu_x &= C_0 + C_1/|SLIP| + C_2/|SLIP|^2 && \text{for } SLIP_T < |SLIP| \leq SLIP_p \\
 \mu_x &= C_3 + C_4/|SLIP| + C_5/|SLIP|^2 && \text{for } SLIP_p < |SLIP| < 1.0 \\
 C_m &= \frac{C_T}{F'_R}
 \end{aligned} \tag{240}$$

where:

$$SLIP_T = \frac{-0.8\mu_{xp}}{C_{Tr}}$$

$$c_2 = \frac{-0.2\mu_{xp}}{(SLIP_P - \frac{0.8\mu_{xp}}{C_{Tr}})^2}$$

$$c_5 = \frac{\mu_{xp} - \mu_{xs}}{(SLIP_P - 1.0)^2}$$

$$c_1 = -2c_2(SLIP_P)$$

$$c_4 = -2c_5$$

$$c_0 = \mu_{xp} + c_2(SLIP_P)^2$$

$$c_3 = \mu_{xs} + c_5$$

The preceding calculation procedure is applied for all values of rotational slip less than that which produces the value μ_{xp} . For rotational slips greater than that corresponding to μ_{xp} , Equations (234) and (238) are modified by the substitution of μ_x to replace μ_{xp} . The effect of this substitution is the prevention of an excessive recovery of side force capability at rotational slips greater than that at which $\mu_x = \mu_{xp}$.

The detailed calculational procedure follows.

The following expression is used for the calculation of tire loading perpendicular to the local terrain:

$$F'_R_i = F_{Ri} \sec \phi_{CGi} - F_{Si} \tan \phi_{CGi} \quad (239)$$

The determination of the tire side force, F_{Si} , for the current time increment requires the use of F'_R_i , and a value of F_{Si} is, therefore, not available at this point in the calculation. For this reason, an approximation of F_{Si} , extrapolated from the previous time increment, is initially used. The subsequently calculated value of F_{Si} is compared with the extrapolated value, and an iterative procedure is then applied to achieve agreement.

The following tests are employed to determine if the tire has lost contact with the ground, or if the force normal to the ground, F_{Ri}' , is calculated to be a negative quantity (this condition can be produced by the extrapolated value of F_{Si} under conditions in which the side force reverses signs).

If $F_{Ri}' = 0$, or $(F_{Ri}' - F_{Sl} \sin \phi_{CGi}) \leq 0$, bypass calculation of the tire side and circumferential forces, set $F_{Si} = F_{Cl} = F_{Ri}' = 0$.

Rotational Slip

$$\text{Let } U_{GWi} = U_{Gi} \cos \psi_i' + V_{Gi} \sin \psi_i'$$

$$\text{Test } U_{GWi}$$

(1) If $|U_{GWi}| < 0.5$ in/sec
test $h_i(RPS)_i$

(a) for $|h_i(RPS)_i| < 0.5$, set $(SLIP)_i = 0$,

(b) for $0.5 \leq |h_i(RPS)_i|$ set $(SLIP)_i = -1.00 \operatorname{sgn}[U_{GWi}(RPS)_i]$.

(2) If $0.5 \leq |U_{GWi}|$

$$(SLIP)_i = 1 - \frac{h_i(RPS)_i}{U_{GWi}} \quad (241)$$

For $1.000 < |(SLIP)_i|$, set $(SLIP)_i = \pm 1.000$, retaining algebraic sign.

Circumferential Force

- (1) For $(P_j - P_{j0}) \leq 0$, where $j = F$ for $i = 1, 2$
 $j = R$ for $i = 3, 4$

$$F_{ci} = -\rho_{si} \mu_i F'_{ri} (\operatorname{sgn} u_{gi}) \quad (242)$$

- (2) For $0 < (P_j - P_{j0})$

$$F_{ci} = \begin{cases} -\rho_{si} \mu_i F'_{ri} (\operatorname{sgn} u_{gi}) & , \text{ or} \\ \frac{-\mu_i F'_{ri} (\operatorname{sgn} u_{gi}) (\operatorname{sgn} \rho_{si})}{\sqrt{\epsilon_{si} + \tan^2 \left[\arctan \frac{v_{gi}}{|u_{gi}|} - \psi'_i (\operatorname{sgn} u_{gi}) \right]}} \end{cases} \quad (245)$$

whichever has the smaller absolute value, where

$$\epsilon_{si} = \begin{cases} \frac{1}{(\rho_{si})_{\max}^2} & , \text{ for } |(\text{SLIP})_i| \leq |(\text{SLIP})_{p_i}| \\ \frac{1}{(\rho_{si})^2} & , \text{ for } |(\text{SLIP})_{p_i}| < |(\text{SLIP})_i| \end{cases} \quad (246)$$

$$(\rho_{si})_{\max} = \mu_{xpi} / \mu_{yi}$$

$$\rho_{si} = \frac{\mu_{xi}}{\mu_{yi}} \operatorname{sgn} (\text{SLIP}_i)$$

Side Force

The calculation of tire side force includes testing as to whether effectively all the available friction force is taken up by braking or tractive forces, and whether the vehicle is in motion.

Thus:

(1) If $\epsilon_{si} F_{ci}^2 \geq (\mu_i^2 F_{ri}'^2 - 1.00)$, bypass side force calculation, set $F_{si} = 0$.

(2) If both $|v_{gi}|$ and $|u_{gi}| < 0.5$, bypass side force calculation, set $F_{si} = 0$.

(3) If either $0.5 \leq |v_{gi}|$ or $0.5 \leq |u_{gi}|$, test $\bar{\beta}_i$:

(a) for $|\bar{\beta}_i| < 3$,

$$F_{si} = \sqrt{\mu_i^2 (F_{ri}')^2 - \epsilon_{si} F_{ci}^2} \left[\bar{\beta}_i - \frac{1}{3} \bar{\beta}_i |\bar{\beta}_i| + \frac{1}{27} \bar{\beta}_i^3 \right] \quad (247)$$

(b) for $3 \leq |\bar{\beta}_i|$,

$$F_{si} = \sqrt{\mu_i^2 (F_{ri}')^2 - \epsilon_{si} F_{ci}^2} , \text{ and } \operatorname{sgn} F_{si} = \operatorname{sgn} \bar{\beta}_i \quad (248)$$

For conditions of tire loading that are not extreme, (i.e., $F_{ri}' \leq A_2 \Omega_T$),

$$\bar{\beta}_i = \left[\frac{A_{ri} F_{ri}' (F_{ri}' - A_{zi}) - A_{zi} A_{ri}'}{A_{zi} \sqrt{\mu_i^2 (F_{ri}')^2 - \epsilon_{si} F_{ci}^2}} \right] \left[\arctan \frac{v_{gi}}{|u_{gi}|} + \beta_i' - (\operatorname{sgn} u_{gi}) \psi_i' \right] \quad (249)$$

and

$$\beta'_i = \left[\frac{A_{2i} A_{3i} (A_{4i} - F_{Ri}') F_{Ri}'}{A_{4i} (A_{1i} F_{Ri}' (F_{Ri}' - A_{2i}) - A_{0i} A_{2i})} \right] \left(\phi_{c\sigma i} - \frac{2}{\pi} \phi_{c\sigma i} |\phi_{c\sigma i}| \right) \quad (250)$$

For conditions of extreme tire overload (i.e., $F_{Ri} > A_2 \Omega_T$),

$$\bar{\beta}_i = \left[\frac{A_{1i} A_{2i} \Omega_{T_i} (\Omega_{T_i} - 1) - A_{0i}}{\sqrt{\mu_i^2 (F_{Ri}')^2 - \epsilon_{si} F_{c_i}^2}} \right] \left[\arctan \frac{v_{gi}}{|u_{gi}|} + \beta'_i - (\text{sgn } u_{gi}) \psi_i' \right] \quad (251)$$

and

$$\beta'_i = \left[\frac{A_{2i} A_{3i} \Omega_{T_i} (A_{4i} - \Omega_{T_i} A_{2i})}{A_{4i} (A_{1i} A_{2i} \Omega_{T_i} (\Omega_{T_i} - 1) - A_{0i})} \right] \left(\phi_{c\sigma i} - \frac{2}{\pi} \phi_{c\sigma i} |\phi_{c\sigma i}| \right) \quad (252)$$

3.7.3 Components of Tire Forces

Finally, resolution of the resulting forces acting on the tire, \vec{F}_{Rui} , into components along the vehicle fixed axis system, is required for application to the differential equations for motions other than the wheel rotations.

$$\begin{vmatrix} F_{Rxui} \\ F_{Ryui} \\ F_{Rzui} \end{vmatrix} = -F_{Ri}' \left\{ \begin{vmatrix} A^T \end{vmatrix} \cdot \begin{vmatrix} \cos \alpha_{GZi}' \\ \cos \beta_{GZi}' \\ \cos \delta_{GZi}' \end{vmatrix} \right\} \quad (253)$$

$$\begin{vmatrix} F_{czui} \\ F_{cyui} \\ F_{cxui} \end{vmatrix} = F_{ci} \left\{ \begin{vmatrix} A^T \end{vmatrix} \cdot \begin{vmatrix} \cos \alpha_{ci} \\ \cos \beta_{ci} \\ \cos \delta_{ci} \end{vmatrix} \right\} \quad (254)$$

where

$$\begin{aligned}\cos \alpha_{ci} &= \frac{D_{1i}}{\sqrt{D_{1i}^2 + D_{2i}^2 + D_{3i}^2}} \\ \cos \beta_{ci} &= \frac{D_{2i}}{\sqrt{D_{1i}^2 + D_{2i}^2 + D_{3i}^2}} \\ \cos \gamma_{ci} &= \frac{D_{3i}}{\sqrt{D_{1i}^2 + D_{2i}^2 + D_{3i}^2}}\end{aligned}\quad (255)$$

are the directional cosines of a line perpendicular to the normals to the ground and wheel planes.

$$\begin{vmatrix} F_{sxui} \\ F_{syui} \\ F_{szui} \end{vmatrix} = F_{ci} \left\{ \begin{vmatrix} A^T \end{vmatrix} \cdot \begin{vmatrix} \cos \alpha_{ci} \\ \cos \beta_{ci} \\ \cos \gamma_{ci} \end{vmatrix} \right\} \quad (256)$$

where

$$\begin{aligned}\cos \alpha_{ci} &= \frac{a_{si}}{\sqrt{a_{si}^2 + b_{si}^2 + c_{si}^2}} \\ \cos \beta_{si} &= \frac{b_{si}}{\sqrt{a_{si}^2 + b_{si}^2 + c_{si}^2}} \\ \cos \gamma_{si} &= \frac{c_{si}}{\sqrt{a_{si}^2 + b_{si}^2 + c_{si}^2}}\end{aligned}\quad (257)$$

are the directional cosines of a line perpendicular to the normal to the ground and F_{ci} (i.e., \parallel to the ground plane).

Further,

$$\begin{aligned}a_{si} &= \begin{vmatrix} \cos \gamma_{ci} & \cos \beta_{ci} \\ \cos \delta_{GZ'_i} & \cos \beta_{GZ'_i} \end{vmatrix} \\ b_{si} &= \begin{vmatrix} \cos \alpha_{ci} & \cos \gamma_{ci} \\ \cos \alpha_{GZ'_i} & \cos \gamma_{GZ'_i} \end{vmatrix}\end{aligned}$$

$$c_{si} = \begin{vmatrix} \cos \beta_{ci} & \cos \alpha_{ci} \\ \cos \beta_{Gz'i} & \cos \alpha_{Gz'i} \end{vmatrix} \quad (258)$$

are the directional components of the above line.

The summation of the tire force components acting along their respective vehicular axes are:

$$F_{xui} = F_{Rxui} + F_{Cxui} + F_{Sxui} \quad (259)$$

$$F_{yui} = F_{Ryu_i} + F_{Cyu_i} + F_{Syui} \quad (260)$$

$$F_{zui} = F_{Rzui} + F_{Czui} + F_{Szui} \quad (261)$$

3.8 Impact Forces

This subroutine, used in the HVOSM-RD2 version, calculates forces applied directly to the sprung mass for simulated collisions of the vehicle with horizontally disposed obstacles having flat, vertical faces typified by beam-type guardrails and median barriers, or walls. Two options for simulating different types of barriers are included: (1) rigid or deformable barrier option, and (2) finite or infinite barrier vertical dimensions option. The barrier is always oriented parallel to the X' space-fixed axis and is also treated as being of infinite length.

For simulated impacts with deformable barriers, inertial effects and curvature of the barrier are not considered. The deflection of the barrier at a given time is determined by incrementing the barrier in small discrete steps ($\Delta y_b'$), from a pseudo-deflected position that results in no vehicle-barrier interference, until a barrier deflection is found for which the force required to produce that deflection is balanced with the force required to crush the vehicle structure in the region of mutual interference.

Rigid-barrier impact forces are computed in a similar manner except that, in this case, the barrier is "incremented" to its original, undeflected position in determining the vehicle crushed volume and, thereby, the forces acting on the sprung mass.

Provision is also made for the calculation of point forces arising from the deformation of structural "hard points" as originally documented by the Texas Transportation Institute in Reference 13. The undeformed location of three hard points together with an omni-directional stiffness are input and forces calculated based on the amount of deformation imposed on these points.

3.8.1 Vehicle to Barrier Interface

In this calculation procedure, the analytic geometry of the vehicle-barrier interface is determined. Like the curb impact subroutine, use of the sprung mass impact subroutine is determined by a series of logical tests. If no sprung mass impact input data are supplied, the subroutine is not activated during the course of the computations. However, if input data are supplied, a test for excessive spin-out is first made since the left rear corner of the vehicle is not simulated.

If $\psi > 135^\circ$ stop calculations.

The corner points of the vehicle are tested for proximity to the barrier:

$$\begin{vmatrix} x'_{cpn} \\ y'_{cpn} \\ z'_{cpn} \end{vmatrix} = \begin{vmatrix} x'_c \\ y'_c \\ z'_c \end{vmatrix} + \|A\| \cdot \begin{vmatrix} x_{cpn} \\ y_{cpn} \\ z_{cpn} \end{vmatrix} \quad (262)$$

where x_{cpn} , y_{cpn} , z_{cpn} are the corner points with respect to the space fixed axes, and

n	x_{cpn}	y_{cpn}	z_{cpn}	VEHICLE CORNER
1	x_{VF}	y_v	0	RIGHT FRONT
2	x_{VR}	y_v	0	RIGHT REAR
3	x_{VF}	$-y_v$	0	LEFT FRONT

are the vehicle corner points in the plane $z = 0$ to be tested.

Using the value of n that corresponds to the largest value of y'_{cpn} , the coordinates of the top and bottom points on that corner are calculated:

$$\begin{vmatrix} x'_{cpt} \\ y'_{cpt} \\ z'_{cpt} \end{vmatrix} = \begin{vmatrix} x'_c \\ y'_c \\ z'_c \end{vmatrix} + \|A\| \cdot \begin{vmatrix} x_{cpn} \\ y_{cpn} \\ z_{vt} \end{vmatrix} \quad (263)$$

$$\begin{vmatrix} x'_{cpb} \\ y'_{cpb} \\ z'_{cpb} \end{vmatrix} = \begin{vmatrix} x'_c \\ y'_c \\ z'_c \end{vmatrix} + \|A\| \cdot \begin{vmatrix} x_{cpn} \\ y_{cpn} \\ z_{vb} \end{vmatrix} \quad (264)$$

and, y'_{cpm} = the larger of y'_{cpt} and y'_{cpb}

If $2(\Delta y'_B) > y'_{cpm} - (y'_B)_{t-1}$

1. bypass remainder of sprung mass impact subroutine for current time increment,

2. set $F_N = \sum F_{xs} = \sum F_{ys} = \sum F_{zs} = 0$

$$\sum N_{\phi s} = \sum N_{\theta s} = \sum N_{\psi s} = 0$$

If $2(\Delta y'_B) < y'_{CPm} - (y'_B)_{t-1}$, continue with calculation of barrier face plane constants and set time increments to Δt_B

The location of the undeformed hardpoints with respect to the initial axis system are:

$$\begin{vmatrix} x'_{STio} \\ y'_{STio} \\ z'_{STio} \end{vmatrix} = \begin{vmatrix} x'_c \\ y'_c \\ z'_c \end{vmatrix} + \|A\| \cdot \begin{vmatrix} x_{STio} \\ y_{STio} \\ z_{STio} \end{vmatrix} \quad (265)$$

The direction cosines of a normal to the barrier face plane in the vehicle-fixed axes are:

$$\begin{vmatrix} \cos \alpha_B \\ \cos \beta_B \\ \cos \gamma_B \end{vmatrix} = \|A^T\| \cdot \begin{vmatrix} 0 \\ 1 \\ 0 \end{vmatrix} \quad (266)$$

And the point of intersection of the y' axis and the barrier face plane is:

$$\begin{vmatrix} x_{B_i} \\ y_{B_i} \\ z_{B_i} \end{vmatrix} = \|A^T\| \cdot \begin{vmatrix} -x'_c \\ (y'_B)_i - y'_c \\ -z'_c \end{vmatrix} \quad (267)$$

where $(y'_B)_i = (y'_B)_{t-1} + n'(\Delta y'_B) - (i-1)(\Delta y'_B)$ (268)

barrier cutting plane, $i = 1, 2, \dots, n', n' + 1$
and

$$n' = \text{the characteristic of } \left[\frac{y'_{CPm} - (y'_B)_{t-1}}{\Delta y'_B} + 1 \right]$$

Knowing the direction cosines of the barrier face plane normal and a point on the barrier face plane, (both with respect to the vehicle axis system) a constant for the barrier face plane is determined:

$$R_{B1} = x_{B1} \cos \alpha_B + y_{B1} \cos \beta_B + z_{B1} \cos \gamma_B \quad (269)$$

The approximate line about which the vehicle rotates is determined by the intersection of the previous time increment barrier-vehicle equilibrium plane, and the present barrier plane with an assumed deflection of $(\delta_B)_{t-1}$. A plane is passed through this line perpendicular to the boundary of compression of the vehicle structure are found.

The coordinates of the axis of rotation at the plane $Z = (Z)_R t - 1$ are:

$$\begin{vmatrix} (\cos \alpha_B)_t & (\cos \beta_B)_t & (\cos \gamma_B)_t \\ (\cos \alpha_B)_{t-1} & (\cos \beta_B)_{t-1} & (\cos \gamma_B)_{t-1} \\ 0 & 0 & 1 \end{vmatrix} \cdot \begin{vmatrix} x_{B1} \\ y_{B1} \\ z_{B1} \end{vmatrix} = \begin{vmatrix} R_{B1} \\ (R_B)_{t-1} \\ (Z_R)_{t-1} \end{vmatrix} \quad (270)$$

where, $R_{B1} = x_{B1} (\cos \alpha_B)_t + y_{B1} (\cos \beta_B)_t + z_{B1} (\cos \gamma_B)_t \quad (271)$

and

$$\begin{vmatrix} x_{B1} \\ y_{B1} \\ z_{B1} \end{vmatrix} = \| A^T \| \cdot \begin{vmatrix} -x_c' \\ (y'_B)_{t-1} - y_c' \\ -z_c' \end{vmatrix} \quad (272)$$

A constant for the plane perpendicular to the present barrier face plane and containing the axis of rotation is:

$$R_{B1} = x_{B1} \cos \alpha_{B1} + y_{B1} \cos \beta_{B1} + z_{B1} \cos \gamma_{B1}$$

and the directional cosines of a normal to the plane are

$$\begin{aligned}\cos \alpha_{B1} &= \frac{a'''}{d'''} \\ \cos \beta_{B1} &= \frac{b'''}{d'''} \\ \cos \gamma_{B1} &= \frac{c'''}{d'''}\end{aligned}\tag{273}$$

where

$$\begin{aligned}a''' &= b''(\cos \gamma_B)_t - c''(\cos \beta_B)_t \\ b''' &= +c''(\cos \alpha_B)_t - a''(\cos \gamma_B)_t \\ c''' &= +a''(\cos \beta_B)_t - b''(\cos \alpha_B)_t \\ d''' &= \sqrt{(a''')^2 + (b''')^2 + (c''')^2}\end{aligned}\tag{274}$$

and

$$\begin{aligned}a'' &= \begin{vmatrix} (\cos \beta_B)_t & (\cos \gamma_B)_t \\ (\cos \beta_B)_{t-1} & (\cos \gamma_B)_{t-1} \end{vmatrix} \\ b'' &= \begin{vmatrix} (\cos \gamma_B)_t & (\cos \alpha_B)_t \\ (\cos \gamma_B)_{t-1} & (\cos \alpha_B)_{t-1} \end{vmatrix} \\ c'' &= \begin{vmatrix} (\cos \alpha_B)_t & (\cos \beta_B)_t \\ (\cos \alpha_B)_{t-1} & (\cos \beta_B)_{t-1} \end{vmatrix}\end{aligned}\tag{275}$$

Possible intercepts of the cutting plane, \mathcal{L} , on the vehicle periphery are then given as:

$$\begin{vmatrix} \cos \alpha_B & \cos \beta_B & \cos \gamma_B \\ A_1 & B_1 & C_1 \\ A_2 & B_2 & C_2 \end{vmatrix} \cdot \begin{vmatrix} x_n \\ y_n \\ z_n \end{vmatrix} = \begin{vmatrix} R_{B1} \\ R_1 \\ R_2 \end{vmatrix}\tag{276}$$

where $n = 1, 2, 3, \dots, 17$. See Table 3-1 for definitions of $A_1, B_1, C_1, R_1, A_2, B_2, C_2, R_2$ corresponding to n .

The following tests are employed to prevent Equation (276) from becoming indeterminate. Note that this condition exists when the barrier and one or more of the lines or planes describing the vehicle boundaries are parallel.

```

if   cosαB = 0, omit points 4, 5, 10, 11
if   cosβB = 0, omit points 1, 2, 7, 8
if   cosγB = 0, omit points 3, 6, 9
if   cosαB1cosβB = cosβB1cosαB, omit points 12, 13
if   cosβB1cosγB = cosγB1cosβB, omit points 14, 15
if   cosγB1cosαB = cosαB1cosγB, omit points 16, 17

```

Note that points to be omitted refer to points in Table 3.1.

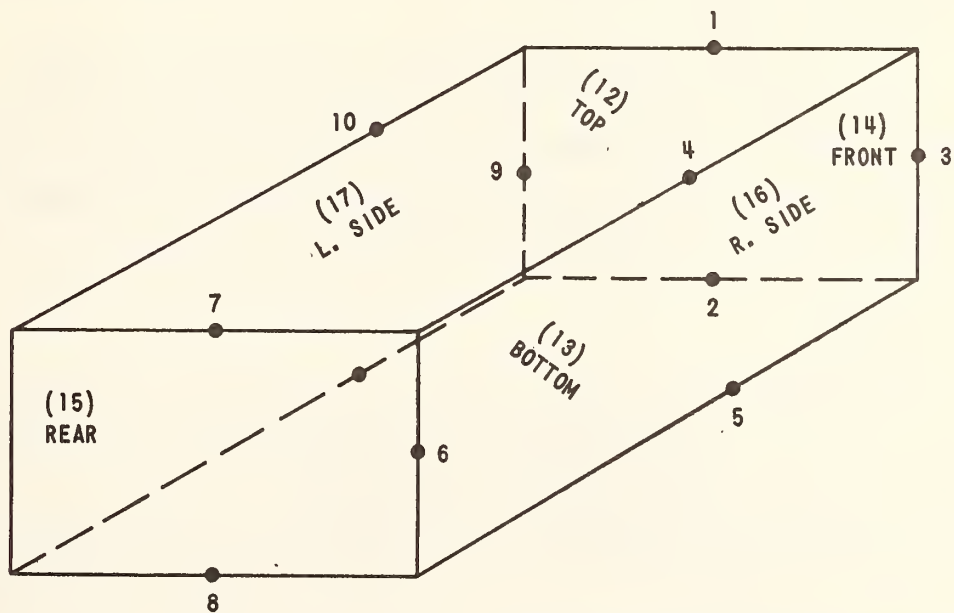
Each point that exceeds the following ranges is rejected as being outside the vehicle periphery:

$$\begin{aligned} x_{VR} &\leq x_n \leq x_{VF} \\ -y_v &\leq y_n \leq y_v \\ z_{VT} &\leq z_n \leq z_{VB} \end{aligned}$$

To avoid retention of improper points for subsequent calculation of vehicle crush forces, the following logic is employed. The plane perpendicular to the barrier face plane and containing the axis of rotation (the R_{B1} plane) is a compression boundary when the axis of rotation is located within the bounds of the vehicle. The axis of rotation is inside the vehicle if

Table 3-1
DEFINITION OF ELEMENTS IN MATRIX EQUATION (276)

ITEM	1	2	3	4	5	6	7	8	9	10	11	12*	13	14	15	16	17
A ₁	1	1	1	0	0	0	1	1	1	0	0	0	0	1	1	0	0
B ₁	0	0	0	1	1	1	0	0	0	1	1	0	0	0	0	1	1
C ₁	0	0	0	0	0	0	0	0	0	0	0	1	1	0	0	0	0
R ₁	X _{VF}	X _{VF}	X _{VF}	Y _V	Y _V	Y _V	X _{VR}	X _{VR}	X _{VF}	-Y _V	-Y _V	Z _{VT}	Z _{VB}	X _{VF}	X _{VR}	Y _V	-Y _V
A ₂	0	0	0	0	0	1	0	0	0	0	0	(cos α_{B1})	—	—	—	—	→
B ₂	0	0	1	0	0	0	0	0	1	0	0	(cos β_{B1})	—	—	—	—	→
C ₂	1	1	0	1	1	0	1	1	0	1	1	(cos γ_{B1})	—	—	—	—	→
R ₂	Z _{VT}	Z _{VB}	Y _V	Z _{VT}	Z _{VB}	X _{VR}	Z _{VT}	Z _{VB}	-Y _V	Z _{VT}	Z _{VB}	(R _{B1})	—	—	—	—	→



*OMIT PTS 12-17 AT INITIAL CONTACT

$$x_{VR} < x_{B1} < x_{VF}$$

$$-y_v < y_{B1} < y_B$$

$$z_{VT} < z_{B1} < z_{VB}$$

The intersection of the R_{B1} , x_{VF} , and $z = 0$ planes is

$$Y_{B1VF} = \frac{R_{B1} - x_{VF} \cos \alpha_{B1}}{\cos \beta_{B1}}$$

1. If the axis of rotation is outside the vehicle, omit points 12, 13, 14, 15, 16, 17.
2. If the axis of rotation is inside the vehicle and $Y_{B1VF} > y_v$, reject all points if one of them is not a point 12, 13, 14, 15, 16 or 17.

If less than three points are retained, let $i = i + 1$ and return to calculation of the point of intersection of the y' axis and the barrier face plane (Equation 267).

If option 2, finite vertical barrier dimensions, is desired the preceding calculations are carried out, and it is necessary to obtain the equations of the top and bottom barrier planes with respect to the vehicle axis system in the same manner as for the barrier face plane.

Thus:

$$\begin{vmatrix} \cos \alpha_{BT} \\ \cos \beta_{BT} \\ \cos \gamma_{BT} \end{vmatrix} = \begin{vmatrix} A^T \end{vmatrix} \cdot \begin{vmatrix} 0 \\ 0 \\ 1 \end{vmatrix} \quad (277)$$

are the direction cosines of the normal to the barrier top and bottom planes with respect to the vehicle axis system, and a point on the barrier top plane is:

$$\begin{vmatrix} x_{BT} \\ y_{BT} \\ z_{BT} \end{vmatrix} = \|A^T\| \cdot \begin{vmatrix} -x'_c \\ -y'_c \\ z'_{BT} - z'_c \end{vmatrix} \quad (278)$$

A point on the barrier bottom plane is:

$$\begin{vmatrix} x_{BB} \\ y_{BB} \\ z_{BB} \end{vmatrix} = \|A^T\| \cdot \begin{vmatrix} -x'_c \\ -y'_c \\ z'_{BB} - z'_c \end{vmatrix} \quad (279)$$

Hence, the constants for the barrier top and bottom planes are:

$$R_{BT} = x_{BT} \cos \alpha_{BT} + y_{BT} \cos \beta_{BT} + z_{BT} \cos \gamma_{BT} \quad (280)$$

$$R_{BB} = x_{BB} \cos \alpha_{BT} + y_{BB} \cos \beta_{BT} + z_{BB} \cos \gamma_{BT} \quad (281)$$

Determination of points 1, 2, 4, 5, 7, 8, 10, 11, 12, 13, 14, 15, 16, 17 is repeated using definitions given in Table 3-2 except as follows:

If $\psi < 0$, omit points 1, 2..

If any of the points 12-17 have not been retained from Table 3-1, omit the corresponding point in Table 3-2.

If both points 1 and 2 from Table 3-1 have been retained, omit point 14.

If both points 7 and 8 from Table 3-1 have been retained, omit point 15.

If both points 4 and 5 from Table 3-1 have been retained, omit point 16.

If both points 10 and 11 from Table 3-1 have been retained, omit point 17.

If point 1 from Table 3-1 has been retained, use $R_2 = R_{BB}$ for point 14.

If point 8 from Table 3-1 has been retained, use $R_2 = R_{BT}$ for point 15.

If point 4 from Table 3-1 has been retained, use $R_2 = R_{BB}$ for point 16.

If point 11 from Table 3-1 has been retained, use $R_2 = R_{BT}$ for point 17.

Table 3-2
DEFINITION OF ELEMENTS IN MATRIX EQUATION (276)

ITEM	1	2	4	5	7	8	10	11	12	13	14	15	16	17
A ₁	1	1	0	0	1	1	0	0	$\cos \alpha_{B1}$					
B ₁	0	0	1	1	0	0	1	1	$\cos \beta_{B1}$					
C ₁	0	0	0	0	0	0	0	0	$\cos \gamma_{B1}$					
R ₁	x_{VF}	x_{VF}	y_V	y_V	x_{VR}	x_{VR}	$-y_V$	$-y_V$	R_{B1}					
A ₂	$\cos \alpha_{BT}$													
B ₂	$\cos \beta_{BT}$													
C ₂	$\cos \gamma_{BT}$													
R ₂	R_{BT}	R_{BB}	R_{BT}	R_{BB}	R_{BT}	R_{BB}	R_{BT}	R_{BB}	R_{BT}	R_{BB}	R_{BT}	R_{BB}	R_{BT}	R_{BB}

The following tests are also employed for use with Table 3-2 to prevent the solution to Equation (276) from becoming indeterminate with the above points:

$$\text{if } \cos\alpha_B \cos\gamma_{BT} = \cos\gamma_B \cos\alpha_{BT} \quad , \text{ omit points 4, 5, 10, 11.}$$

$$\text{if } \cos\gamma_B \cos\beta_{BT} = \cos\beta_B \cos\gamma_{BT} \quad , \text{ omit points 1, 2, 7, 8.}$$

$$\begin{aligned} \text{if } & \cos\alpha_B [\cos\beta_{B1} \cos\gamma_{BT} - \cos\beta_{BT} \cos\gamma_{B1}] + \cos\alpha_{BT} [\cos\beta_B \cos\gamma_{B1} - \cos\beta_{B1} \cos\gamma_B] \\ & = \cos\alpha_{B1} [\cos\beta_B \cos\gamma_{BT} - \cos\beta_{BT} \cos\gamma_B] \quad , \text{ omit points 12, 13, 14, 15,} \\ & 16, 17. \end{aligned}$$

Again reject points with values outside the ranges:

$$x_{VR} \leq x_n \leq x_{VF}$$

$$-y_V \leq y_n \leq y_V$$

$$z_{VT} \leq z_n \leq z_{VB}$$

Compare values of $|z_n|$ in both sets of points retained, and where two exist for a given n , reject the point with the larger value of $|z_n|$

If less than three points are retained, let $i = i + 1$ and return to the calculation of the point of intersection of the y' axis and the barrier face plane.

For each point retained, calculate its velocity components:

$$\begin{vmatrix} u'_n \\ v'_n \\ w'_n \end{vmatrix} = \|A\| \cdot \begin{vmatrix} u - y_n R + z_n Q \\ v + x_n R - z_n P \\ w + y_n P - x_n Q \end{vmatrix} \quad (282)$$

Of the remaining points, retain only the four points with the larger values of v_n' . (Note that points 3, 6 and 9 are counted as two points in this selection.)

If a rigid barrier impact is desired and the values of v_n' for the four points retained are negative, bypass the remainder of the sprung mass impact routine for the current time increment,

$$\text{Set } F_N = \sum F_{zs} = \sum F_{ys} = \sum F_{\dot{z}s} = 0$$

$$\sum N_{\phi s} = \sum N_{\theta s} = \sum N_{\nu s} = 0$$

3.8.2 Area Calculation

In this calculation, the contact area of the interface between the vehicle and the individual barrier cutting planes, i , will be determined, as illustrated in Figure 3.25.

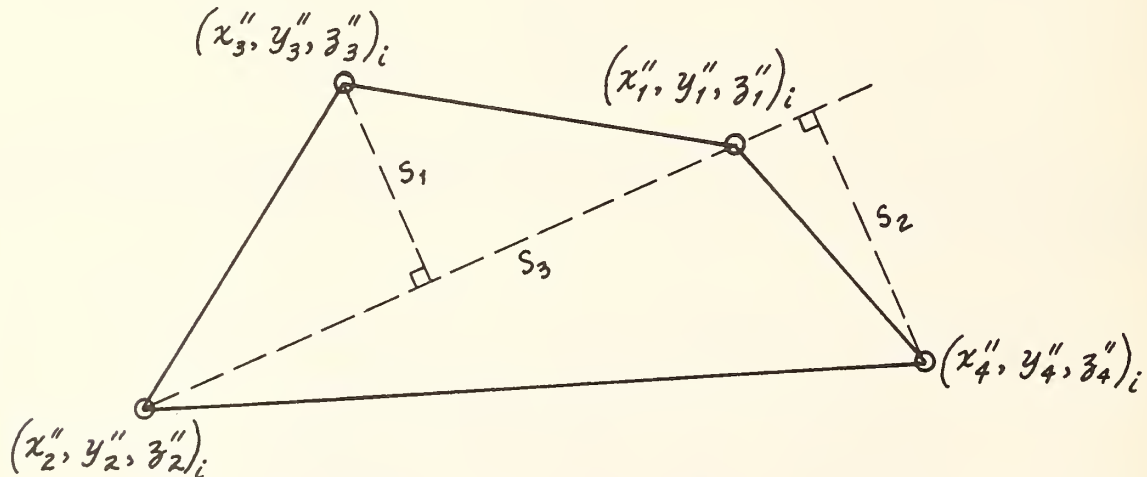


Figure 3.25 INTERSECTION AREA

Given the three, or four, points that define the intersection area, $(x''_j, y''_j, z''_j)_i$, where $j = 1, 2, 3, (4)$, make the following selections: (Note that i identifies the cutting plane.)

Of the two larger values of x''_j , select the point with the larger value of z''_j . Let this point be designated, within the subroutine, as (x''_1, y''_1, z''_1) . For the case of equal values of x''_j , scan all points for the larger value of z''_j . If 2 values of z''_j are equal, select either one.

Of the two smaller values of x''_j , select the point with the smaller value of z''_j . Let this point be designated, within this subroutine, as (x''_2, y''_2, z''_2) . For the case of equal values of x''_j , scan all points for smaller value of z''_j . If 2 values of z''_j are equal, select either one.

Let one of the remaining points be designated, within this subroutine, as (x''_3, y''_3, z''_3) .

If four points, identify the remaining point, within this subroutine, as (x''_4, y''_4, z''_4) .

Direction components of lines in the cutting plane, i , \perp to the line between (x''_1, y''_1, z''_1) and (x''_2, y''_2, z''_2) are:

$$a'_i = \begin{vmatrix} (y''_1 - y''_2)_i & (z''_1 - z''_2)_i \\ \cos \beta_B & \cos \delta_B \end{vmatrix}$$

$$b'_i = \begin{vmatrix} (z''_1 - z''_2)_i & (x''_1 - x''_2)_i \\ \cos \delta_B & \cos \alpha_B \end{vmatrix}$$

$$c'_i = \begin{vmatrix} (x''_1 - x''_2)_i & (y''_1 - y''_2)_i \\ \cos \alpha_B & \cos \beta_B \end{vmatrix}$$

(283)

The length of line S_1 as shown in Figure 3.25 is:

$$(S_1)_i = \frac{|a'_i(x''_3 - x''_2)_i + b'_i(y''_3 - y''_2)_i + c'_i(z''_3 - z''_2)_i|}{\sqrt{(a'_i)^2 + (b'_i)^2 + (c'_i)^2}} \quad (284)$$

The length of S_3 as shown in Figure 3.25 is:

$$(S_3)_i = \sqrt{(x''_1 - x''_2)_i^2 + (y''_1 - y''_2)_i^2 + (z''_1 - z''_2)_i^2} \quad (285)$$

If three points were retained, set $(S_2)_i = 0$.

If four points were retained, the length of S_2 as shown in Figure 3.26 is:

$$(S_2)_i = \frac{|a'_i(x''_4 - x''_2)_i + b'_i(y''_4 - y''_2)_i + c'_i(z''_4 - z''_2)_i|}{\sqrt{(a'_i)^2 + (b'_i)^2 + (c'_i)^2}} \quad (286)$$

The total intersection area is then:

$$(A_{INT})_i = \left(\frac{S_1 + S_2}{2} \right)_i (S_3)_i \quad (287)$$

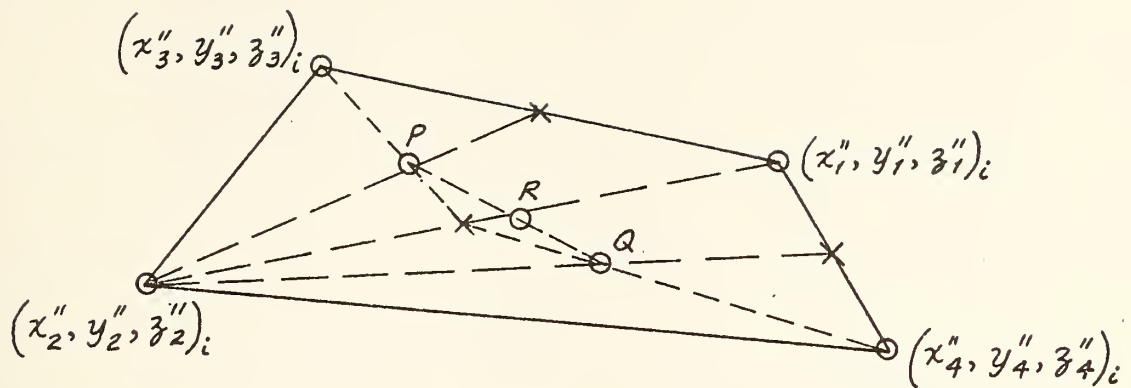


Figure 3.26 CENTROID OF INTERSECTION AREA

Centroid Calculation

In this calculation, coordinates will be determined for the intercept, in the actual vehicle-barrier interface plane, of a normal through the centroid of an individual intersection area.

Calculate the following: (Subletter *i* omitted for convenience)

$$\begin{aligned}
 a_{c1} &= \frac{x''_1 + x''_2}{2} - x''_3, & a'_{c1} &= b_{c1} \cos \delta_B - c_{c1} \cos \beta_B \\
 b_{c1} &= \frac{y''_1 + y''_2}{2} - y''_3, & b'_{c1} &= c_{c1} \cos \alpha_B - a_{c1} \cos \delta_B \\
 c_{c1} &= \frac{z''_1 + z''_2}{2} - z''_3, & c'_{c1} &= a_{c1} \cos \beta_B - b_{c1} \cos \alpha_B \\
 G_1 &= a'_{c1} x''_3 + b'_{c1} y''_3 + c'_{c1} z''_3 & (288)
 \end{aligned}$$

$$\begin{aligned}
a_{c2} &= \frac{x_1'' + x_3''}{2} - x_2'', \quad a'_{c2} = b_{c2} \cos \gamma_B - c_{c2} \cos \beta_B \\
b_{c2} &= \frac{y_1'' + y_3''}{2} - y_2'', \quad b'_{c2} = c_{c2} \cos \alpha_B - a_{c2} \cos \gamma_B \\
c_{c2} &= \frac{z_1'' + z_3''}{2} - z_2'', \quad c'_{c2} = a_{c2} \cos \beta_B - b_{c2} \cos \alpha_B \\
G_2 &= a'_{c2} x_2'' + b'_{c2} y_2'' + c'_{c2} z_2'' \tag{289}
\end{aligned}$$

Find the centroid of the upper triangle in Figure 3.26 (i.e., point P) by solving the following:

$$\begin{vmatrix} \cos \alpha_B & \cos \beta_B & \cos \gamma_B \\ a'_{c1} & b'_{c1} & c'_{c1} \\ a'_{c2} & b'_{c2} & c'_{c2} \end{vmatrix} \cdot \begin{vmatrix} x_p \\ y_p \\ z_p \end{vmatrix} = \begin{vmatrix} (R_B)_{t-1} \\ G_1 \\ G_2 \end{vmatrix} \tag{290}$$

(Note that $(R_B)_{t-1}$ corresponds to the actual equilibrium interface plane from the previous time increment.)

If 3 points only, set

$$\begin{aligned}
(x_R)_i &= (x_p)_i \\
(y_R)_i &= (y_p)_i \\
(z_R)_i &= (z_p)_i
\end{aligned}$$

If 4 points, calculate the following:

$$\begin{aligned}
a_{c3} &= \frac{x_1'' + x_2''}{2} - x_4'', \quad a'_{c3} = b_{c3} \cos \gamma_B - c_{c3} \cos \beta_B \\
b_{c3} &= \frac{y_1'' + y_2''}{2} - y_4'', \quad b'_{c3} = c_{c3} \cos \alpha_B - a_{c3} \cos \gamma_B \\
c_{c3} &= \frac{z_1'' + z_2''}{2} - z_4'', \quad c'_{c3} = a_{c3} \cos \beta_B - b_{c3} \cos \alpha_B \\
G_3 &= a'_{c3} x_4'' + b'_{c3} y_4'' + c'_{c3} z_4'' \tag{291}
\end{aligned}$$

$$\begin{aligned}
a_{c4} &= \frac{x_1'' + x_4''}{2} - x_2'', \quad a'_{c4} = b_{c4} \cos \alpha_B - c_{c4} \cos \beta_B \\
b_{c4} &= \frac{y_1'' + y_4''}{2} - y_2'', \quad b'_{c4} = c_{c4} \cos \alpha_B - a_{c4} \cos \beta_B \\
c_{c4} &= \frac{z_1'' + z_4''}{2} - z_2'', \quad c'_{c4} = a_{c4} \cos \beta_B - b_{c4} \cos \alpha_B \\
G_4 &= a'_{c4} x_2'' + b'_{c4} y_2'' + c'_{c4} z_2'' \tag{292}
\end{aligned}$$

Find the centroid of the lower triangle in Figure 3.26 (i.e., point Q) by solving the following:

$$\begin{vmatrix} \cos \alpha_B & \cos \beta_B & \cos \gamma_B \\ a'_{c3} & b'_{c3} & c'_{c3} \\ a'_{c4} & b'_{c4} & c'_{c4} \end{vmatrix} \cdot \begin{vmatrix} x_g \\ y_g \\ z_g \end{vmatrix} = \begin{vmatrix} (R_B)_{t-1} \\ G_3 \\ G_4 \end{vmatrix} \tag{293}$$

(Note that $(R_B)_{t-1}$ corresponds to the actual equilibrium interface plane from the previous time increment.)

The centroid of the entire area is obtained from the following relationships:

$$\begin{aligned}
(x_R)_i &= (x_p)_i + \left(\frac{s_2}{s_1 + s_2}_i \right) (x_g - x_p)_i \\
(y_R)_i &= (y_p)_i + \left(\frac{s_2}{s_1 + s_2}_i \right) (y_g - y_p)_i \\
(z_R)_i &= (z_p)_i + \left(\frac{s_2}{s_1 + s_2}_i \right) (z_g - z_p)_i \tag{294}
\end{aligned}$$

In this calculation, the total force normal to the barrier will be calculated and the coordinates of the application point for an equivalent concentrated load will be determined.

The point of application may be obtained from:

$$(\sum x_R)_t = \frac{\sum_{i=1}^{n+1} \left\{ \left[\frac{(A_{INT})_i + (A_{INT})_{i-1}}{2} \right] \left[\frac{x_{R_i} + x_{R_{i-1}}}{2} \right] \right\}}{\sum_{i=1}^{n+1} \left[\frac{(A_{INT})_i + (A_{INT})_{i-1}}{2} \right]} \quad (295)$$

$$(\sum y_R)_t = \frac{\sum_{i=1}^{n+1} \left\{ \left[\frac{(A_{INT})_i + (A_{INT})_{i-1}}{2} \right] \left[\frac{y_{R_i} + y_{R_{i-1}}}{2} \right] \right\}}{\sum_{i=1}^{n+1} \left[\frac{(A_{INT})_i + (A_{INT})_{i-1}}{2} \right]} \quad (296)$$

$$(\sum z_R)_t = \frac{\sum_{i=1}^{n+1} \left\{ \left[\frac{(A_{INT})_i + (A_{INT})_{i-1}}{2} \right] \left[\frac{z_{R_i} + z_{R_{i-1}}}{2} \right] \right\}}{\sum_{i=1}^{n+1} \left[\frac{(A_{INT})_i + (A_{INT})_{i-1}}{2} \right]} \quad (297)$$

The total force normal to the barrier due to vehicle crush is given by:

$$(F_N)_t = K_V (\Delta y'_B) \sum_{i=1}^{n+1} \left[\frac{(A_{INT})_i + (A_{INT})_{i-1}}{2} \right] \quad (298)$$

The force normal to the barrier due to deformation of the hard points is assumed to be zero if the lateral position of the undeformed hard point becomes less than that of the barrier or if the lateral velocity of the hard point becomes less than zero. That is

$$F_{NST,i} = 0 \text{ if } y'_{ST,i} < y'_B \text{ or } v'_{ST,i} < 0$$

where:

$$\begin{vmatrix} u'_{STi} \\ v'_{STi} \\ w'_{STi} \end{vmatrix} = \|A\| \cdot \begin{vmatrix} u - Ry_{STi} + Qz_{STi} \\ v + Rx_{STi} - Pz_{STi} \\ w + Py_{STi} - Qx_{STi} \end{vmatrix} \quad (299)$$

However, if $v'_{STi} \geq 0$ and $y'_{STi} > y'_B$

$$F_{NSTi} = K_{STi} (y'_{STi} - y'_B) \quad (300)$$

Note that the position of the deformed hard point in the vehicle system is:

$$\begin{vmatrix} x_{STi} \\ y_{STi} \\ z_{STi} \end{vmatrix} = \|A^T\| \cdot \begin{vmatrix} x'_{STi} - x'_C \\ y'_B - y'_C \\ z'_{STi} - z'_C \end{vmatrix} \quad (301)$$

And the total vehicle force is $F_N = (F_N)_t + \sum_{i=1}^3 F_{NSTi}$ (302)

If the barrier is rigid, let $i = i + 1$ and return to the calculation of the point of intersection of the y' axis and the barrier face plane until $(y'_B)_t = (y'_B)_o$. Then proceed to the calculation of sprung mass resultant forces and moments (Section 3.8.4).

If the barrier is deformable,

1. let the assumed deflection of the barrier be

$$\delta_B = (y'_B)_i - (y'_B)_o - \epsilon_n$$

where ϵ_n is the permanent set of the barrier (initially zero),

2. calculate the barrier force, F_B , as described in the next section (Section 3.8.3)

If the vehicle normal force and the barrier normal force are not in balance (within limit. ϵ_B), i.e.,

$$\epsilon_B < (F_B - F_N)$$

let $i = i + 1$, and return to the calculation of the point of intersection of the y' axis and the barrier face plane.

If $\epsilon_B > (F_B - F_N)$, proceed to the calculation of sprung mass resultant forces and moments (Section 3.8.4).

3.8.3 Simulation of Deformable Barrier Load-Deflection Characteristics

A previously developed general subroutine for handling non-linear load-deflection characteristics (Reference 12) has been adapted for calculating barrier forces for simulation of sprung mass impacts with deformable barriers. Use of the subroutine requires that the load-deflection characteristics of the simulated barrier be known.

The load-deflection relationship for increasing load is represented by a general polynomial function of deflection and the velocity of deflection. (Velocity terms, included in the original application for which this subroutine was developed, have been retained. However, since simulated barrier deflections occur in discrete steps of $\Delta y'_B$, the coefficients of the velocity terms in the polynomial for the load-deflection relationship should be entered as zero for the present application to barriers.) For decreasing

load, the load-deflection relationship is represented by a parabolic function of the deflection that is determined from specified (input data) ratios of: (1) conserved energy to total absorbed energy, and (2) residual deflection to maximum deflection (see Figure 3.27).

When recurrent loading takes place, the residual deformation for each cycle is incorporated, in the form of initial surface displacement, for subsequent cycles.. If the unloading between cycles is incomplete, a value of residual deformation is determined such that the new loading curve will pass through the final point on the preceding unloading curve (see Figure 3.28).

The general procedure followed in the nonlinear load-deflection subroutine is described briefly in the following paragraphs.

1. The deflection and the velocity of deflection are determined from analytic geometry and applied in the appropriate functional relationship to determine the corresponding load.
2. The change in area under the force deflection curve, $(F_t - F_{t-1})(\delta_t - \delta_{t-1})/2$ is calculated and stored for each time increment.
3. When a maximum load point is reached (as indicated by an initial negative value for the velocity of deflection), the total area under the loading curve (total absorbed energy) is calculated, and the coefficients for a parabolic unloading curve are determined from input specifications for (1) the ratio of conserved energy to total absorbed energy, and (2) the ratio of residual deflection to maximum deflection.

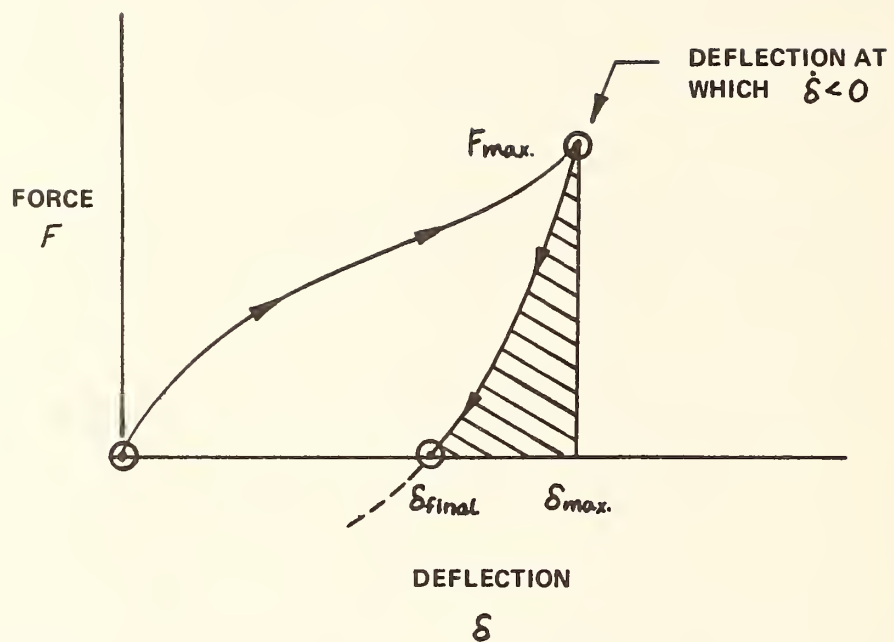


Figure 3.27 GENERAL FORM OF BARRIER LOAD-DEFLECTION CHARACTERISTICS

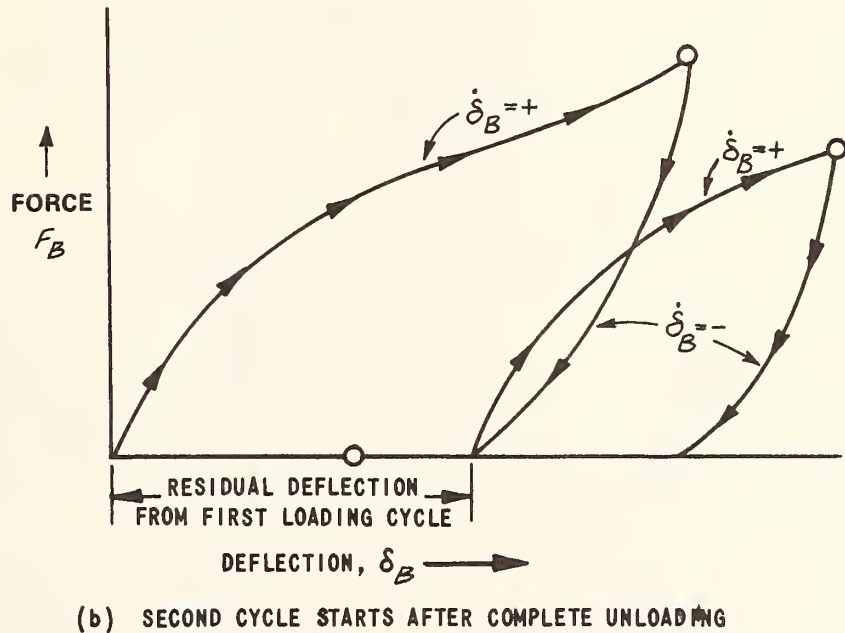
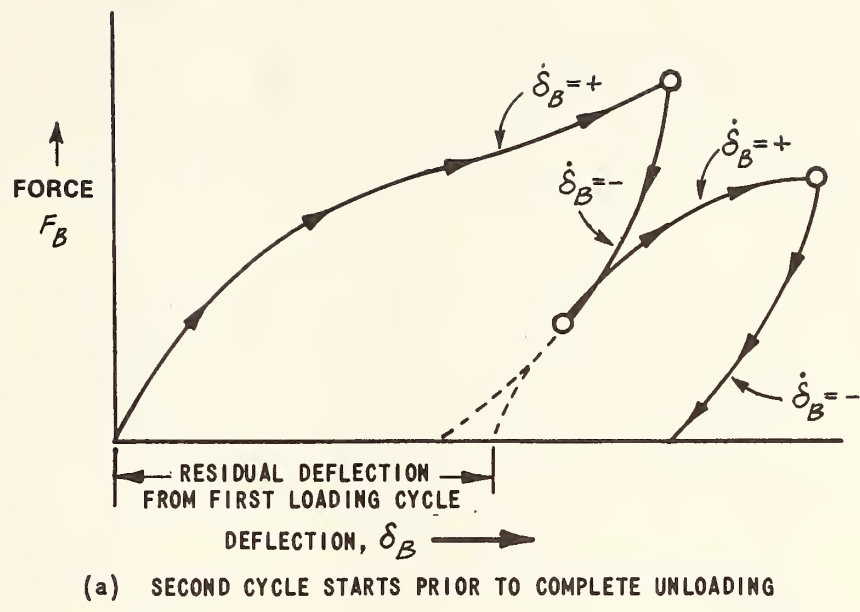


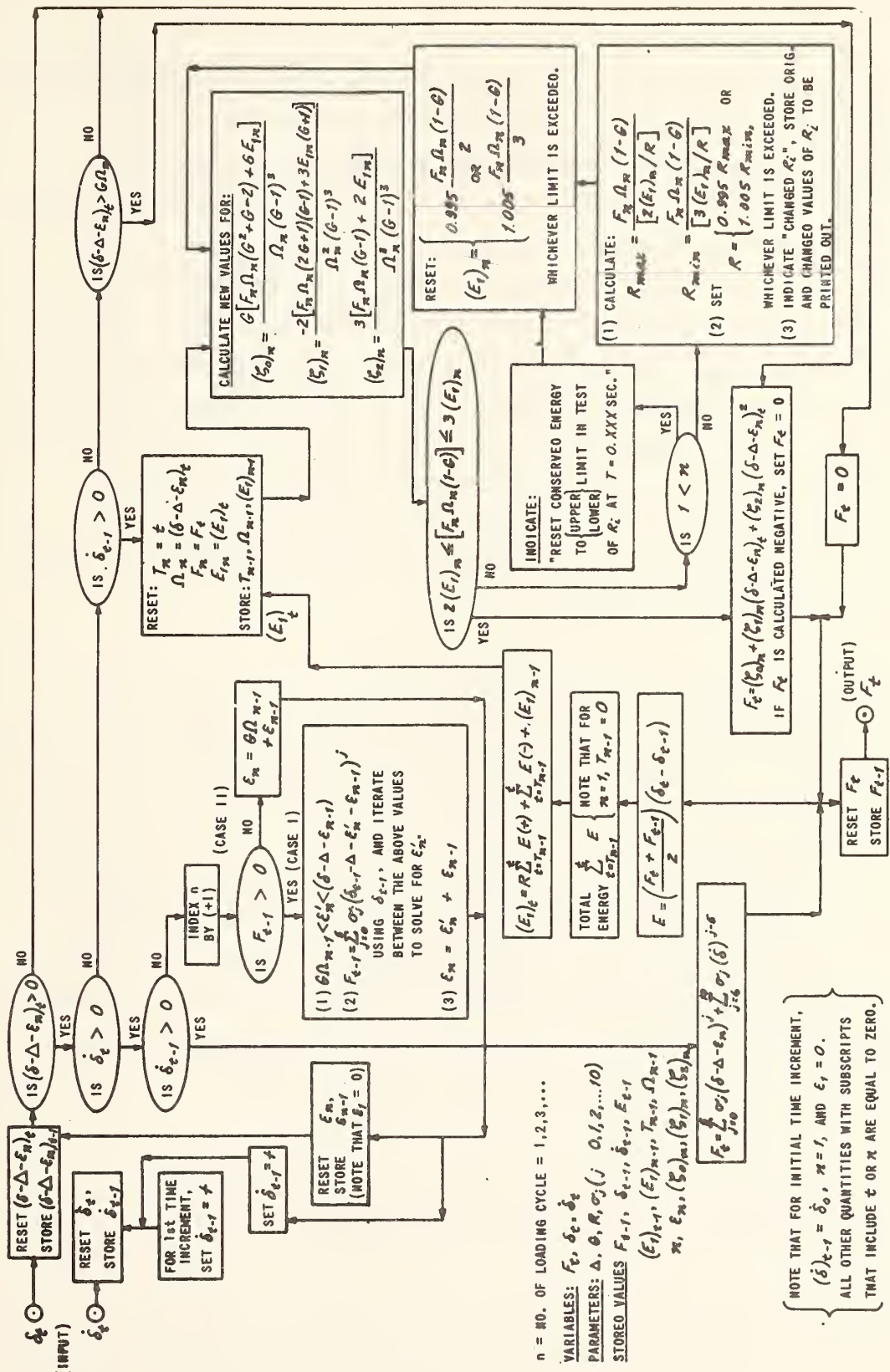
Figure 3.28 ASSUMED FORM OF LOAD-DEFLECTION FOR RECURRENT LOADING

4. When the deflection, during the unloading, becomes equal to or less than the specified residual deflection (from the calculated maximum deflection and the specified ratio of residual to maximum deflection), the force is set equal to zero.

The logic and calculation steps for the general nonlinear load-deflection subroutine are presented in Figure 3.29. Note that the correspondence between the symbols used in Figure 3.29 and those defined in this report for application to deformable barriers is given in the following table.

Symbol in Figure 3.29	Symbol for Application to Barriers
F	F_B
δ	δ_B
Δ	O
$\dot{\delta}$	$\frac{(y'_B)_t - (y'_B)_{t-1}}{\Delta t_B}$
G	\overline{SET}
R	\overline{CONS}
σ_j	$\sigma_R \quad (R=0,1,2,3,\dots,10)$

Figure 3.29 GENERAL SUBROUTINE FOR NONLINEAR LOAD-DEFLECTION



In the logic depicted in Figure 3.29, the criteria for a "proper" range of combinations of the input parameters that control unloading characteristics (i.e., SET and CONS) are based on an adopted requirement that unloading curves (i.e., load vs. deflection for decreasing deflection) should be concave upward, with the linear case as an upper limit and zero minimum slope as a lower limit. During the original development of the general nonlinear load-deflection subroutines, it was found that a dynamic load-deflection characteristic for increasing deflection that was initially quasi-linear but then yielded at a constant force level required exploratory variation of the input parameters that control unloading characteristics, since the "proper" range of combinations was dependent upon the maximum deflection. Further difficulty was encountered in the case of multiple loading cycles, in which the range of maximum deflections for the individual loading cycles are generally different.

In order to avoid the above difficulties while still retaining control of unloading curve characteristics, the depicted program logic automatically adjusts the input values of CONS, as required in initial loading cycles. Any adjustments made in the input values of CONS are, of course, indicated in the program output. In addition, whenever a sequence of loading cycles leads to an "improper" unloading curve, either through the mechanism of different ranges of maximum deflections or through the accumulation of "carry-over" energy from previous loading cycles with incomplete unloading, the revised program logic resets the conserved energy to a value corresponding to the exceeded limiting case of unloading curve characteristics. Again, the program output indicates any adjustments that are made.

3.8.4 Resultant Forces and Moments

The velocity components of the points of application of the sprung mass forces are:

$$\begin{vmatrix} U'_Ri \\ V'_Ri \\ W'_Ri \end{vmatrix} = \|A\| \cdot \begin{vmatrix} u - y_i R + z_i Q \\ v + x_i R - z_i P \\ w - y_i P - x_i Q \end{vmatrix} \quad (303)$$

where:

$$x_i = \sum x_R$$

$$y_i = \sum y_R$$

$$z_i = \sum z_R$$

and

$$\begin{vmatrix} x_i \\ y_i \\ z_i \end{vmatrix} = \begin{vmatrix} x_{STi-1} \\ y_{STi-1} \\ z_{STi-1} \end{vmatrix} \quad \text{for } i = 2, 3, 4 \quad (304)$$

And its velocity tangential to the barrier is:

$$VTAN_i = \left[\sqrt{(u'_R)^2 + (w'_R)^2} \right] (\operatorname{sgn} u'_R) \quad (305)$$

The friction force acting on the vehicle due to contact with the barrier is:

$$\overline{FRICT}_i = \begin{cases} 0, & \text{for } |VTAN_i| \leq \varepsilon_v \\ \mu_B \overline{F_{SHi}} \operatorname{sgn}(VTAN_i), & \text{for } \varepsilon_v < |VTAN_i| \end{cases} \quad (306)$$

The resultant force components along the vehicle fixed axes acting on the sprung mass are:

$$\begin{vmatrix} F_{xsi} \\ F_{ysi} \\ F_{zsi} \end{vmatrix} = \|A^T\| \cdot \begin{vmatrix} -\mu_B F_{SNi} \cos \theta_{Bi} \\ -F_{SNi} \\ -\mu_B F_{SNi} \sin \theta_{Bi} \end{vmatrix} \quad (307)$$

where,

$$\theta_{Bi} = \arctan \left(\frac{w_{Ri}}{u_{Ri}} \right)$$

and

$$F_{SNi} = (F_N)_t$$

$$F_{SNi} = F_{STi} \quad \text{for } i = 2, 3, 4.$$

The moments acting on the vehicle sprung mass are, therefore,

$$\sum N_{\phi s} = \sum [y_i F_{zsi} - z_i F_{ysi}] \quad (308)$$

$$\sum N_{\theta s} = \sum [z_i F_{xsi} - x_i F_{zsi}] \quad (309)$$

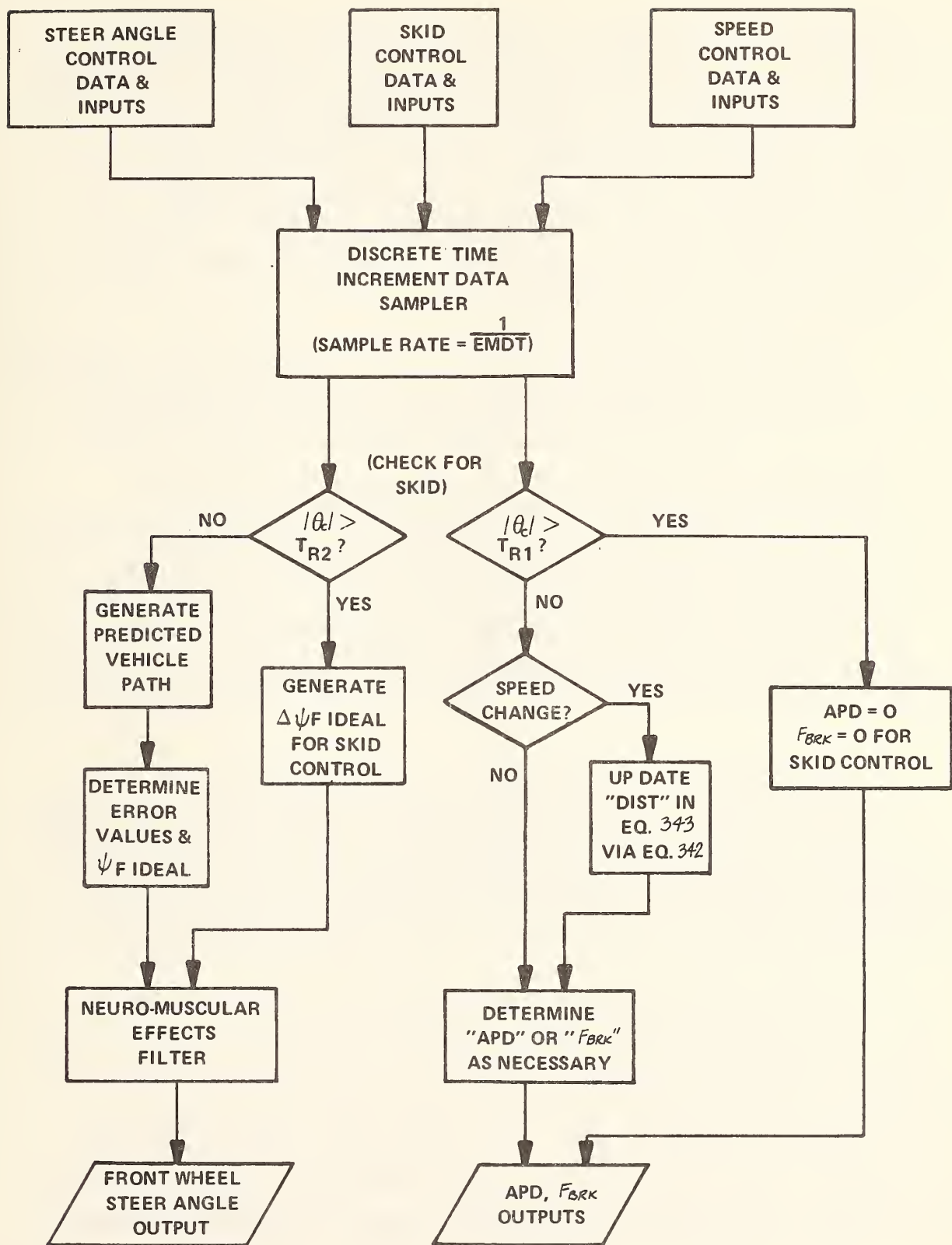
$$\sum N_{\psi s} = \sum [x_i F_{ysi} - y_i F_{xsi}] \quad (310)$$

3.9

Preview-Predictor Driver Model

The driver model includes several modes of operation: path-following, speed maintenance, speed change and skid recovery modes (Figure 3.30). The normal steering mode is path-following. The path-following mechanism predicts the future vehicle path based on the instantaneous velocity and an estimated lateral acceleration due to the instantaneous front wheel steer angle. In the calculation of the projected path, the model assumes that the vehicle will maintain its present velocity except for the continuous effect of the lateral acceleration. The estimated lateral acceleration is a function of the forward velocity, the front wheel steer angle and the stability and control characteristics of the vehicle. Error estimates are made between the predicted path and the desired path at evently spaced

Figure 3.30 MODEL OUTLINE



points along the predicted path. These error estimates are weighted to account for the reduction in lateral acceleration required to null errors at further distances ahead of the vehicle. The error estimates are also weighted to emphasize the importance of errors at particular locations along the desired path. The change in the front wheel steer angle is proportional to the average of the weighted error estimates. This steer command is filtered to reflect human dynamic capabilities, specifically neuro-muscular dynamic characteristics.

Operating simultaneously with the path-following mode is either the speed change mode or the speed maintenance mode. The speed change mode uses input data values of the desired speeds, their initiation times and attainment distances to determine the required brake pedal forces and accelerator pedal deflections. In calculating the brake and throttle control commands, the model assumes linear relationships between deceleration and brake pedal force and acceleration and throttle position. Initialization of the path-following mode requires that the initial vehicle position and heading be consistent with the desired path. To initialize the speed control mode the initial vehicle speed is set equal to the first desired speed.

If, because of terrain features or cornering forces, the vehicle should gain or lose speed such that the difference between the desired speed and the actual speed exceeds the threshold values, the model will activate the speed maintenance mode and attempt to return the vehicle to its most recent desired speed. These threshold values are variable model inputs.

The skid recovery mode is activated if the vehicle slip angle, θ_c , the angle between the vehicle heading and its velocity vector, exceeds a pre-selected threshold value, T_{R1} . The degree of severity of the skid is determined from comparison of the vehicle slip angle with a second (higher) threshold, T_{R2} . For skids of low severity the brake pedal force (F_{BRK}) and accelerator pedal deflection (APD) are set to zero; however, the steering control remains under the path-following mode.

If the skid is of high severity, in which the higher vehicle slip angle threshold is exceeded, the steering commands are determined by the skid recovery routine. Thus, for more severe skids, brake pedal force and accelerator pedal deflection are set to zero, path-following is discontinued and steer commands are generated strictly to recover the directional control of the vehicle. Under the skid recovery mode, the steer angle change is proportional to the average front wheel slip angle, ψ_F , and the sign of the steer correlation is in the direction of reducing the average front wheel slip angle. Repetitive steer angle correlations are made until the wheel slip angle is equal to zero. Steer commands are filtered, as in the path-following mode, before being applied to the vehicle.

The data sampling scheme is virtually identical to the one investigated by Kriefeld (Reference 14). All of the model functions operate on their appropriate inputs at discrete time increments, as determined by the input value of EMDT, the time between driver samples in seconds. Significant changes in model output can be produced by this mechanism, including improved correlation with recorded nonlinear responses of human operators.

It should be noted that the thresholds or indifference levels mentioned above are designed to be single parameters representing the minimum detection level for that particular control input or, if the driver chooses not to act until a higher value is reached, the minimum indifference level for that control input.

3.9.1 Path-Following Mode

3.9.1.1 Specification of Desired Path

The center line of the desired path is entered into the program by a series of continuous straight line segments, i.e., first order polynomials.

3.9.1.2 Determination of Predicted Path

The predicted path (i.e., driver prediction) is obtained by integration, from the present vehicle position, of the instantaneous velocity and estimated lateral acceleration. The estimated lateral acceleration due to the front wheel steer angle, $\psi_{F,ideal}$, can be calculated by

$$a_y = \frac{u_T^2 \psi_{F,ideal}}{(a+b)(1+K_d u_T^2)} \quad (311)$$

where a and b are the distances along the vehicle-fixed x axis from the sprung mass center of gravity to the center lines of the front and rear wheels, respectively, inches, u_T = magnitude of the vehicle velocity and K_d is a performance parameter characterizing the understeer-oversteer properties of the vehicle. Rewriting the lateral acceleration in the inertial reference system yields

$$\begin{vmatrix} a'_x \\ a'_y \\ a'_z \end{vmatrix} = \begin{vmatrix} A \end{vmatrix} \cdot \begin{vmatrix} 0 \\ a_y \\ 0 \end{vmatrix}$$

where $\|A\|$ is the transformation matrix from the vehicle fixed reference system to the space fixed system. The coordinates (x'_{VP_i} , y'_{VP_i}) at evenly spaced points a distance ΔS apart along the predicted path can be found by

$$x'_{VP_i} = x'_c + \left(\frac{\Delta S}{u_T} \cdot i \right) u' + \frac{1}{2} \left(\frac{\Delta S}{u_T} \cdot i \right)^2 a'_x \quad (312)$$

$$y'_{VP_i} = y'_c + \left(\frac{\Delta S}{u_T} \cdot i \right) v' + \frac{1}{2} \left(\frac{\Delta S}{u_T} \cdot i \right)^2 a'_y \quad (313)$$

where

u_T = magnitude of the vehicle velocity vector

and

$$\frac{\Delta S}{u_T} \cdot i = t - t_i, \text{ an incremental time into the future.}$$

The error, e_i , between the predicted path and the desired path is measured at EN different points, each one ΔS times i ($i = 1, \dots, EN$) inches along the predicted path ahead of the vehicle. The measured errors are individually weighted and the results are averaged to yield E_T

3.9.1.3 Error Determination

The manner of error calculation is outlined below.

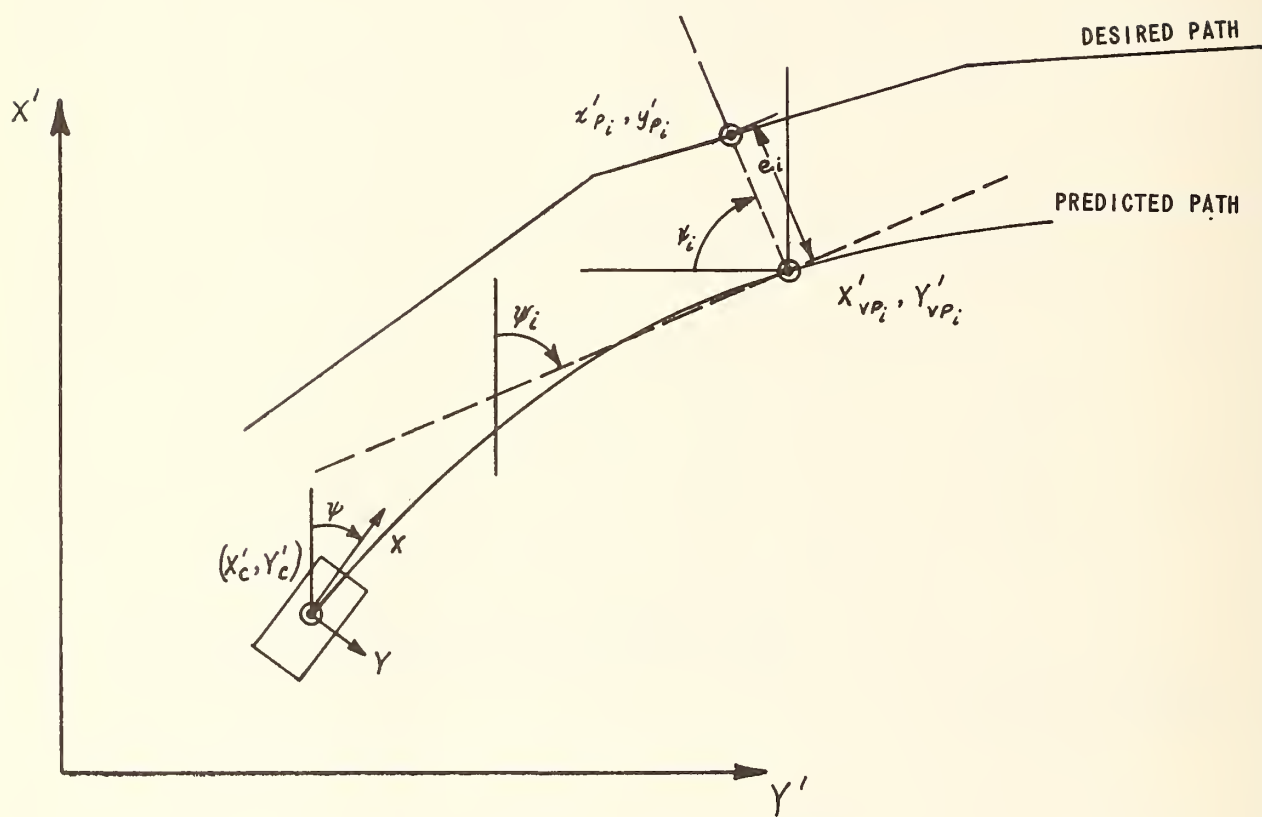


Figure 3.31 ERROR CALCULATION

It can be seen in Figure 3.31 that

$$\frac{x'_{P_i} - x'_{vP_i}}{Y'_{vP_i} - y'_{P_i}} = \tan \psi_i \quad (314)$$

Since ϵ_i is measured normal to the projected path at point (x'_{vP_i}, y'_{vP_i}) , the slope along which ϵ_i is measured, relative to the y' axis, can be determined from

$$\frac{df(y)}{dy} = \tan \psi_i \quad (315)$$

In the present case the indicated derivative is equal to the ratio of the x velocity at point (x'_{vP_i}, y'_{vP_i}) to the y velocity.

$$\frac{df(y)}{dy} = \frac{u' + \left(\frac{\Delta S}{u_T} \cdot i\right) a'_x}{v' + \left(\frac{\Delta S}{u_T} \cdot i\right) a'_y} \quad (316)$$

Combining Equations (314), (315) and (316), one obtains

$$\frac{x'_{P_i} - x'_{vP_i}}{Y'_{vP_i} - y'_{P_i}} = \frac{u' + \left(\frac{\Delta S}{u_T} \cdot i\right) a'_x}{v' + \left(\frac{\Delta S}{u_T} \cdot i\right) a'_y} \quad (317)$$

From the desired path input

$$x'_{P_i} = SP_n + SP_{n+1} y'_{P_i} \quad (318)$$

where

$$\begin{aligned} n &= 1 \text{ for } y'_{P_i} \leq Y'_{P_1} \\ n &= 3 \text{ for } Y'_{P_1} < y'_{P_i} \leq Y'_{P_2} \\ n &= 5 \text{ for } Y'_{P_2} < y'_{P_i} \leq Y'_{P_3} \\ n &= 7 \text{ for } Y'_{P_3} < y'_{P_i} \leq Y'_{P_4} \\ n &= 9 \text{ for } Y'_{P_4} < y'_{P_i} \end{aligned}$$

Equation (317) can now be written as

$$\frac{(SP_n + SP_{n+1}, y'_{P_i}) - x'_{vP_i}}{y'_{vP_i} - y'_{P_i}} = \frac{u' + \left(\frac{\Delta s}{u_T} \cdot i\right) a'_x}{v' + \left(\frac{\Delta s}{u_T} \cdot i\right) a'_y} \quad (319)$$

Solution of Equation (319) allows determination of the error via

$$|e_i| = \left[(x'_{P_i} - x'_{vP_i})^2 + (y'_{P_i} - y'_{vP_i})^2 \right]^{1/2} \quad (320)$$

The algebraic sign of e is determined by the sign of y'_P in the normal-tangential reference system at each point i

$$y'_{P_i} = (x'_{P_i} - x'_{vP_i}) \sin \psi_i + (y'_{P_i} - y'_{vP_i}) \cos \psi_i \quad (321)$$

$$SGN(e_i) = SGN(y'_{P_i}) \quad (322)$$

The i th error e_i would, therefore, be

$$e_i = |e_i| SGN(e_i) \quad (323)$$

The lateral acceleration required to displace the path of the vehicle by e at a distance d ahead of the vehicle is

$$a_y = 2 \frac{e u_T^2}{d^2} \quad (324)$$

From Equations (311) and (324), it can be seen that the steer angle change required to null an error e at a distance d ahead of the vehicle on its projected path is

$$\Delta \psi_f = \frac{2(a+b)(1+K_d u_T^2)}{d^2} e \quad (325)$$

Because the driver model samples the error between the desired path and the projected path at EN evenly spaced points ΔS apart, the steer angle change required to null the error e_i of the i th point a distance from the vehicle is

$$\Delta \psi_{f_i} = \frac{2(a+b)(1+K_d u_T^2)}{(\Delta S \cdot i)^2} e_i \quad (326)$$

3.9.1.4 Importance Weighting Function

If the importance weighting of error e_i is WI_i , then the resultant steer angle change is the weighted average of the steer angle changes computed for individual sample points.

$$\Delta \psi_{f_i} = \frac{1}{EN} \sum_{i=1}^{EN} \frac{2(a+b)(1+K_d u_T^2)}{(\Delta S \cdot i)^2} WI_i e_i \quad (327)$$

or

$$\Delta \psi_{f_i} = K_p \sum_{i=1}^{EN} WE_i WI_i e_i \quad (328)$$

where

$$WE_i = \frac{1}{i^2} \quad \text{is the error weighting function.}$$

WI_i is the importance weighting function.

$K_p = \frac{2(a+b)(1+K_d u_T^2)}{EN \Delta S^2}$ is the control gain. The driver's estimate of the vehicle handling parameter $(1 + K_d u_T^2)$ is probably a constant. Therefore, for the preview-predictor driver model K_p should be determined for the normal velocity and then held constant.

3.9.1.5 Filter Structure

A simplified model of the physiological operator is assumed which incorporates a time delay τ , a possible lead τ_L and a lag τ_I .

This filter structure corresponds to the first order effects of the neurological and muscular systems of a human driver (Reference 17). The parameters τ_I and τ_L determine the exact shape of the output curve $\Delta\psi_{F_j}(t)$, and τ sets the time delay before onset of the smoothed output (Figure 3.32).

All of these parameters are variable inputs of the model and, therefore, readily permit alterations in the exact shape of the filter output in order to match a particular set of driver characteristics.

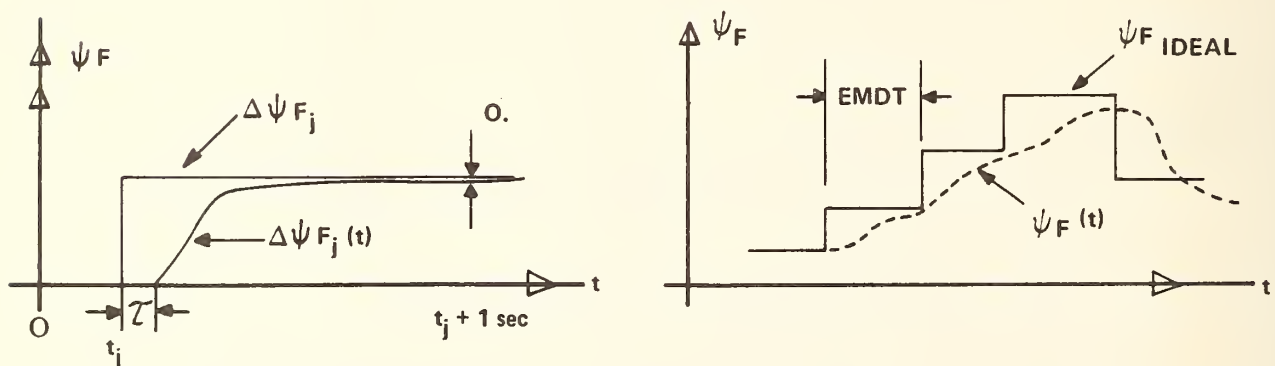


Figure 3.32 NEURO - MUSCULAR FILTER CHARACTERISTICS

Mathematically, the j th desired steer change from time t_j yields an actual steer change at time t of

$$\Delta \psi_{f_j}(t) = \Delta \psi_{f_j} \left\{ 1 - \frac{\tau_I - \tau_L}{\tau_I} e^{-\frac{1}{\tau_I}(t-t_j-r)} \right\} \mu(t-t_j-r) \quad (329)$$

To account for the time delay

$$\mu(t-t_j-r) = \begin{cases} 0 & \text{for } (t-t_j-r) < 0 \\ 1 & \text{for } (t-t_j-r) \geq 0 \end{cases} \quad (330)$$

and since the transients are assumed to have disappeared after one second, the steady state response becomes:

$$\Delta \psi_{f_j}(t) = \Delta \psi_{f_j} \quad \text{for } (t-t_j-r) \geq 1 \quad (331)$$

The time functional form of the actual steer angle would then be the sum of the j th independent inputs

$$\psi_f(t) = \sum_{j=1}^{t/EMDT} \Delta \psi_{f_j}(t) \quad (332)$$

and the ideal steer angle would be

$$\psi_{f_{ideal}} = \sum_{j=1}^{t/EMDT} \Delta \psi_{f_j} \quad (333)$$

where $EMDT$ is the time interval between driver samples (Figure 3.32).

If $|\psi_F(t)| > \Omega_\psi$, where Ω_ψ is the maximum steer angle, then (334)

$$\psi_F(t) = \Omega_\psi \operatorname{sgn}(\psi_{F,IDEAL})$$

and (335)

$$\psi_{F,IDEAL} = \Omega_\psi \operatorname{sgn}(\psi_{F,IDEAL})$$

3.9.2 Skid Control Mode

To effect the control of a vehicle skid it is first necessary to detect the skid. This is usually done by the "feel" of the brake, steering and/or accelerator systems along with visual and inertial cues. No attempt has yet been made to simulate the detection mechanism per se, except for a comparison of the vehicle slip angle with threshold values.

Three types of vehicle skids are considered: braking skids, acceleration skids and cornering skids. In all cases, the first attempt to control the skid, in the model, is through a nulling of all wheel torques. For a pure rear wheel acceleration skid, torque nulling should be a sufficient action to return control of the vehicle to the driver, providing that the yaw velocity has not attained an excessive value. If a skid is of such severity that the nulling of the wheel torques will not reduce the vehicle slip angle below the threshold value, steer angle commands are generated in an attempt to regain control. In such a case, instead of following the desired path through steer angle inputs, the driver model attempts to orient the vehicle, through steering commands, so that its heading corresponds to the direction of its velocity vector.

From Figure 3.33 it can be seen that

$$\theta_C = \arctan\left(\frac{v_r}{u}\right) \quad (336)$$

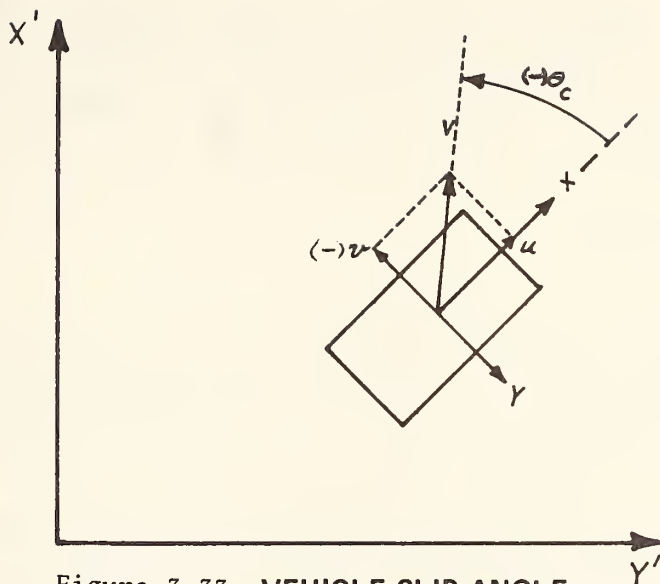


Figure 3.33 VEHICLE SLIP ANGLE

where θ_c is the vehicle slip angle. The skid is detected when the vehicle slip angle, θ_c , exceeds the lower skid threshold T_{R_1} . The brake and throttle controls are set to zero until the condition represented by Equation (337) is no longer met, following which the model returns to the speed control mode.

$$\text{If } |\theta_c| > T_{R_1}, \quad (337)$$

$$\text{then } APD = F_{BRK} = 0 \quad (338)$$

For cases of extreme skidding where the vehicle slip angle exceeds the higher skid threshold T_{R_2} ($T_{R_2} > T_{R_1}$), path following is discontinued, and the steer angle commands are made proportional to the front wheel slip angle.

$$\text{If } |\theta_c| > T_{R_2} \quad (339)$$

$$\text{then } \Delta \psi_{sj} = K_s (-\psi_f + \theta_c) \quad (340)$$

If the vehicle has not rotated more than ninety degrees during a skid correction maneuver, the driver will return to his path-following behavior. However, if the vehicle orientation has changed more than ninety degrees, the driver model will bring the vehicle to rest.

3.9.3 Speed Control Mode

The speed control section of the driver model is much less complex than the path-following mechanism. The model determines the difference between the desired and the actual forward speed of the vehicle, ΔV , and then attempts to null the difference within a specified distance. It will be possible in the future to have the driver model include a calculation of the desired nulling distance. However, for the sake of initial simplicity, the nulling distance is prespecified as a tabular input for each speed change required. For speed maintenance, on the other hand, the acceleration is specified as a function of ΔV . The speed control outputs are in terms of inches of accelerator pedal deflection or pounds of brake pedal effort. The modeled driver "assumes" that a vehicle deceleration of 0.1 g will result for each ten pounds of applied brake pedal force and also that there is a linear relationship between change in throttle position and change in the magnitude of the vehicle acceleration.

The order of calculation for the speed control section of the driver model is as follows. The velocity error is calculated as

$$\Delta V = DS - U_T \quad (341)$$

A set of threshold/indifference levels T_{S1} and T_{S2} are applied for positive and negative ΔV , respectively. A desired acceleration D_{ax} is calculated using the desired nulling distance, $DIST$

$$D_{ax} = \frac{\Delta V U_T}{DIST} \quad (342)$$

For a change of speed task the new desired speed, DS_k ; the time of the change, t_{ck} ; and the desired distance to null ΔV , $DISTIk$, are among the data read into the program. $DIST$ is set equal to $DISTIk$ at t_k . At each time increment after t_k , $DIST$ is reduced by the distance traveled by the vehicle,

$$DIST = DIST - u_T EMDT \quad (344)$$

until $DIST \leq 0$ when it is reset equal to $DISTIk$ and the speed maintenance mode is resumed.

The speed maintenance mode consists of exactly the same equations as the speed change mode except no periodic update of $DIST$ at each calculation time is done, i.e., the desired acceleration is proportional to the vehicle velocity and the magnitude of the error times a gain, $\frac{1}{DIST}$. For $Dax > 0$, an accelerator pedal deflection APD is the model output.

$$APD = APD + Ks_2 Dax \quad (345)$$

The initial value of APD is found by solving the net horsepower versus speed function at DS_1 for constant velocity. The vehicle, therefore, starts all computer runs in equilibrium at the first desired speed. Since APD can never exceed $APDMAX$, nor be less than zero, for cases of Equation (345) where this happens, APD is set to $APDMAX$ or zero at the exceeded limit.

For $Dax > Tb$, the braking indifference level, the applied brake pedal force, F_{BRK} , is

$$F_{BRK} = Ks_1 Dax \quad (346)$$

where Ks_1 is the assumed response of the brake system.

3.9.4 Driver Vehicle Interface

3.9.4.1 Braking

The output from the driver model is a force acting on the brake pedal. This force is converted to a master cylinder hydraulic pressure which is subsequently used to determine brake torques as described in Section 3.6.2 by the following equation

$$P = B_{PF_1}(F_{BRK}) + B_{PF_2}(F_{BRK})^2 \quad (347)$$

3.9.4.2 Engine Torque

Engine output is controlled by the accelerator pedal deflection (APD) and the engine speed. The accelerator pedal deflection is normalized with respect to the maximum ($APDMAX$) to produce a throttle setting as defined in Section 3.6.2.2

$$TS = \frac{APD}{APDMAX} \quad (348)$$

The throttle setting and engine speed are then used to interpolate between the input engine torque values. The engine speed is determined from the average drive rotational velocity of the drive wheels, the rear axle ratio and the transmission ratio:

$$RPME = \frac{15}{\pi} (AR_j)(TR)(RPS_i + RPS_{i+1}) \quad (349)$$

A simplified representation of an automatic transmission is used with the driver model to determine the transmission ratio which allows transmission upshifts and downshifts at input engine speeds. The instantaneous transmission ratio is determined by calculating the engine speed using Equation (349) with each input gear ratio and comparing the calculated engine speed with the input engine speed shift points. Note that down shifts are assumed to occur only if the previous value of engine torque is negative.

Letting IG represent the gear number at the previous time increment, then the gear ratio is $GEAR_{IG}$ and the upshift engine speed is $VGRU_{IG, IG+1}$

If $RPME > VGRU_{IG, IG+1}$, an upshift occurs, i.e.

$$TR = GEAR_{IG+1}$$

Similarly, for downshifts ($TQE < 0$)

If $RPME < VGRD_{IG, IG-1}$, a downshift occurs, i.e.

$$TR = GEAR_{IG-1}$$

3.10 Aerodynamic and Rolling Resistances (HVOSM Vehicle Dynamics Version)

The effects of aerodynamic and rolling resistances are grossly approximated by means of a force, ΣF_{xs} , acting along the X axis of the sprung mass. The magnitude of the force is determined from an empirical relationship which relates the driving force that is required to overcome the cited resistances to the component of linear velocity along the vehicle X axis. For simplicity, it is assumed that ΣF_{xs} acts through the sprung mass center of gravity. The primary objective of this simplified analytical treatment is to approximate the effects of aerodynamic resistance on stopping distances.

A number of empirical-analytical relationships can be found in the literature. The following, representative relationship is taken from Reference 9:

$$F_R = 0.001128 AV^2 + W(0.0001395 V + 0.01676) \quad (350)$$

where

F_R = force required to overcome aero-dynamic and rolling resistances, lbs.

A = front area, square feet.

V = vehicle speed, miles per hour.

W = total vehicle weight, lbs.

Converting Equation (350) to a general format that is suitable for the present simulation program, the following expression is obtained:

$$\sum F_{xs} = \begin{cases} 0 & , \text{ for } |u| < 1 \text{ in/sec} \\ -C_1 u/|u| - C_2 u - C_3 \operatorname{sgn} u & , \text{ for } |u| \geq 1 \text{ in/sec} \end{cases} \quad (351)$$

where

u = scalar component of linear velocity along the X axis, in/sec.

C_1, C_2, C_3 = coefficients to approximate the total force required to overcome aero-dynamic resistance.

In applications where measured resistance data are available, the coefficients C_1 , C_2 , C_3 can be directly selected to achieve an empirical fit. In the absence of such measured data, Equation (350) can provide a basis for approximating C_1 , C_2 and C_3 , by means of the following conversions:

$$C_1 = (3.6415 \times 10^{-6})A$$

$$C_2 = (7.926 \times 10^{-6})W$$

$$C_3 = 0.01676W$$

where

A = frontal area, square feet, and

W = total vehicle weight, lbs.

For $A \approx 26.4$ square feet and $W \approx 3600$ pounds, the following, representative values are obtained for the coefficients:

$$C_1 = 9.6136 \times 10^{-5}$$

$$C_2 = 0.02853$$

$$C_3 = 60.336$$

A rolling resistance torque is approximated by a linear function of tire normal load and is applied directly to the appropriate wheel spin equation of motion:

$$R_{RMi} = -C_{RRM_i} F_{Ri}' \operatorname{sgn}(RPS_i) \quad (352)$$

3.11 Resultant Forces and Moments

The resultant forces on the vehicle that act on the unsprung masses in the x and y directions are determined from the following relationships:

$$\sum F_{xu} = \sum_{i=1}^4 (F_{rxui} + F_{cxui} + F_{sxui}) \quad (353)$$

$$\sum F_{yu} = \sum_{i=1}^4 (F_{ryui} + F_{cyui} + F_{syui}) \quad (354)$$

Forces acting on the unsprung masses in the $\not\equiv$ direction must be treated individually in view of the unsprung mass degrees of freedom:

$$F_{zu_i} = F_{rzui} + F_{czui} + F_{szui} \quad (355)$$

The resultant force that is transmitted through the suspensions in the $\not\equiv$ direction is obtained from

$$\sum F_{z1} = S_1 + S_2 + S_3 + S_4 \quad (356)$$

The resultant moments acting on the sprung and unsprung masses arising from tire and suspension forces are given below for the three suspension options.

Independent Front/Solid Axle Rear Suspension

$$\begin{aligned} \sum N_{\phi u} &= -F_{yu_1}(z_F + \delta_1 + h_1 \cos \gamma_{n_1}) - F_{yu_2}(z_F + \delta_2 + h_2 \cos \gamma_{n_2}) \\ &\quad - (F_{yu_3} + F_{yu_4})(z_R + \delta_3) + S_2(T_F/2 + \Delta T_{HF2}) \\ &\quad - S_1(T_F/2 + \Delta T_{HF1}) + (S_4 - S_3)T_S/2 \end{aligned} \quad (357)$$

$$\begin{aligned} \sum N_{\theta u} &= (S_1 + S_2)a - (S_3 + S_4)b - F_{xu_1}(z_F + \delta_1 + h_1 \cos \gamma_{n_1}) \\ &\quad + F_{xu_2}(z_F + \delta_2 + \cos \gamma_{n_2}) + F_{xu_3}(z_R + \delta_3 + p + T_R \phi_R/2 + h_3 \cos \gamma_{n_3}) \\ &\quad + F_{xu_4}(z_R + \delta_3 + p - T_R \phi_R/2 + h_4 \cos \gamma_{n_4}) \end{aligned} \quad (358)$$

$$\begin{aligned} \sum N_{\psi u} &= F_{yu_1}(a + h_1 \cos \alpha_{n_1}) + F_{yu_2}(a + h_2 \cos \alpha_{n_2}) \\ &\quad - F_{yu_3}(b - h_3 \cos \alpha_{n_3}) - F_{yu_4}(b - h_4 \cos \alpha_{n_4}) \\ &\quad + F_{xu_2}(T_F/2 + \Delta T_{HF2} - h_2 \cos \beta_{n_2}) - F_{xu_1}(T_F/2 + \Delta T_{HF1} + h_1 \cos \beta_{n_1}) \\ &\quad + F_{xu_4}(T_R/2 + p \phi_R - h_4 \cos \beta_{n_4}) - F_{xu_3}(T_R/2 - p \phi_R + h_3 \cos \beta_{n_3}) \end{aligned} \quad (359)$$

$$\begin{aligned}
\Sigma N_{\phi_R} = & F_{zu3}(T_R/2 - \rho\phi_R + h_3 \cos\beta_{n3}) - F_{zu4}(T_R/2 + \rho\phi_R - h_4 \cos\beta_{n4}) \\
& - F_{yu3}(\rho + T_R\phi_R/2 + h_3 \cos\gamma_{n3}) - F_{yu4}(\rho - T_R\phi_R/2 + h_4 \cos\gamma_{n4}) \\
& + (S_3 - S_4)T_S/2
\end{aligned} \tag{360}$$

Independent Front and Rear Suspension

$$\begin{aligned}
\Sigma N_{\phi_U} = & S_2(T_F/2 + \Delta T_{HF2}) - S_1(T_F/2 + \Delta T_{HF1}) + S_4(T_R/2 + \Delta T_{HR4}) - S_3(T_R/2 + \Delta T_{HR3}) \\
& - F_{yu1}(z_F + \delta_1 + h_1 \cos\gamma_{n1}) - F_{yu2}(z_F + \delta_2 + h_2 \cos\gamma_{n2}) \\
& - F_{yu3}(z_R + \delta_3 + h_3 \cos\gamma_{n3}) - F_{yu4}(z_R + \delta_4 + h_4 \cos\gamma_{n4})
\end{aligned} \tag{361}$$

$$\begin{aligned}
\Sigma N_{\theta_U} = & (S_1 + S_2)a - (S_3 + S_4)b + F_{xu1}(z_F + \delta_1 + h_1 \cos\gamma_{n1}) \\
& + F_{xu2}(z_F + \delta_2 + h_2 \cos\gamma_{n2}) + F_{xu3}(z_F + \delta_3 + h_3 \cos\gamma_{n3}) \\
& + F_{xu4}(z_R + \delta_4 + h_4 \cos\gamma_{n4})
\end{aligned} \tag{362}$$

$$\begin{aligned}
\Sigma N_{\psi_U} = & F_{yu1}(a + h_1 \cos\alpha_{n1}) + F_{yu2}(a + h_2 \cos\alpha_{n2}) \\
& - F_{yu3}(b - h_3 \cos\alpha_{n3}) - F_{yu4}(b - h_4 \cos\alpha_{n4}) \\
& + F_{xu2}(T_F/2 + \Delta T_{HF2} - h_2 \cos\beta_{n2}) - F_{xu1}(T_F/2 + \Delta T_{HF1} + h_1 \cos\beta_{n1}) \\
& + F_{xu4}(T_R/2 + \Delta T_{HR4} - h_4 \cos\beta_{n4}) - F_{xu3}(T_R/2 + \Delta T_{HR3} + h_3 \cos\beta_{n3})
\end{aligned} \tag{363}$$

Solid Front and Rear Axles

$$\begin{aligned}
\Sigma N_{\phi_U} = & -(F_{yu1} + F_{yu2})(z_F + \delta_1) - (F_{yu3} + F_{yu4})(z_R + \delta_3) \\
& + (S_2 - S_1)\bar{T}_{SF}/2 + (S_4 - S_3)\bar{T}_S/2
\end{aligned} \tag{364}$$

$$\begin{aligned}
\sum N_{\theta u} = & (S_1 + S_2)a - (S_3 + S_4)b + F_{xu1}(z_F + \delta_1 + \rho_F + T_F \phi_F/2 + h_1 \cos \gamma_{h1}) \\
& + F_{xu2}(z_F + \delta_1 + \rho_F - T_F \phi_F/2 + h_2 \cos \gamma_{h2}) + F_{xu3}(z_R + \delta_3 + \rho + T_R \phi_R/2 + h_3 \cos \gamma_{h3}) \\
& + F_{xu4}(z_R + \delta_3 + \rho - T_R \phi_R/2 + h_4 \cos \gamma_{h4})
\end{aligned} \tag{365}$$

$$\begin{aligned}
\sum N_{\psi u} = & F_{yu1}(a + h_1 \cos \alpha_{h1}) + F_{yu2}(a + h_1 \cos \alpha_{h1}) - F_{yu3}(b - h_3 \cos \alpha_{h3}) \\
& - F_{yu4}(b - h_4 \cos \alpha_{h4}) - F_{xu1}(T_F/2 - \rho_F \phi_F + h_1 \cos \beta_{h1}) \\
& + F_{xu2}(T_F/2 + \rho_F \phi_F - h_2 \cos \beta_{h2}) - F_{xu3}(T_R/2 - \rho \phi_R + h_3 \cos \beta_{h3}) \\
& + F_{xu4}(T_R/2 + \rho \phi_R - h_4 \cos \beta_{h4})
\end{aligned} \tag{366}$$

$$\begin{aligned}
\sum N_{\phi_F} = & F_{zu1}(T_F/2 - \rho_F \phi_F + h_1 \cos \beta_{h1}) - F_{zu2}(T_F/2 + \rho_F \phi_F - h_2 \cos \beta_{h2}) \\
& - F_{yu1}(\rho_F + T_F \phi_F/2 + h_1 \cos \gamma_{h1}) - F_{yu2}(\rho_F - T_F \phi_F/2 + h_2 \cos \gamma_{h2}) \\
& + (S_1 - S_2) T_{SF}/2
\end{aligned} \tag{367}$$

$$\begin{aligned}
\sum N_{\phi_R} = & F_{zu3}(T_R/2 - \rho \phi_R + h_3 \cos \beta_{h3}) - F_{zu4}(T_R/2 + \rho \phi_R - h_4 \cos \beta_{h4}) \\
& - F_{yu3}(\rho + T_R \phi_R/2 + h_3 \cos \gamma_{h3}) - F_{yu4}(\rho - T_R \phi_R/2 + h_4 \cos \gamma_{h4}) \\
& + (S_3 - S_4) T_S/2
\end{aligned} \tag{370}$$

Note that driveline torque reactions are included in the roll moments acting on the sprung and unsprung masses in the HVOSM-VD2 version if the drive axle is solid. For the case of a solid rear axle, with rear drive, the following terms are added to the equations for sprung mass roll moment and rear axle roll moment:

$$\sum N_{\phi_u} = \dots + 12(TQ)_{DR}$$

$$\sum N_{\phi_R} = \dots - 12(TQ)_{DR}$$

For the case of a solid front axle with front drive the following terms are added to the equations for sprung mass roll moment and front axle roll moment:

$$\sum N_{\phi u} = \dots +12(TQ)_{DF}$$

$$\sum N_{\phi F} = \dots -12(TQ)_{DF}$$

4. REFERENCES

1. Etkin, Bernard, "Dynamics of Flight," John Wiley and Sons, 1959, Chapter 4.
2. Kruse, D. F., Edwards, R. C., "Automobile Suspension Bumpers - A Correlation of Parameters Affecting Impact Response and a Technique for Achieving Effective Design," SAE Paper No. 680471, Detroit, May 20-24, 1968.
3. "Automotive Brakes," Chrysler Institute of Engineering, Graduate School Lecture Notes, January 1952.
4. McHenry, Raymond R., "Analysis of the Dynamics of Automobile Braking," Calspan Report No. VJ-2195-V-1, May 1966.
5. McHenry, R. R., DeLeys, N. J., "Vehicle Dynamics in Single Vehicle Accidents - Validation and Extensions of a Computer Simulation," Calspan Report No. VJ-2251-V-3, December 1968.
6. Radt, H. S., Milliken, W. F., "Motions of Skidding Automobiles," SAE Paper No. 205A, June 1960.
7. Krempel, G., "Research on Automobile Tires," Automobiltechnische Zeitschrift 69 (1967) 8.
8. Gengenbach, Werner, "The Effect of Wet Pavement on the Performance of Automobile Tires," Universitat Karlsruhe, Karlsruhe, Deutschland, July 1967.
9. "Car Performance," Chrysler Institute of Engineering, Graduate School Lecture Notes, November 1953.
10. "Automobile Accidents Related to Railroad Grade Crossings - A Study of the Effects of Topography and a Computer-Graphics Display of Traffic Flow," Calspan Report No. VJ-2251-V-4, March 1969.
11. McHenry, R. R. and DeLeys, N. J., "Automobile Dynamics - A Computer Simulation of Three-Dimensional Motions for Use in Studies of Braking Systems and the Driving Task," Calspan Report No. VJ-2251-V-7, August 1970.
12. Segal, David J. and McHenry, Raymond R., "Computer Simulation of the Automobile Crash Victim - Revision No. 1," Calspan Corporation Report No. VJ-2492-V-1, March 1968.

REFERENCES (Contd.)

13. Young, R. D., et al, "Simulation of Vehicle Impact with the Texas Concrete Median Barrier - Volume 1: Test Comparisons and Parameter Study," Texas Transportation Institute Report No. 140-5, June 1972.
14. Kriefeld, J. G., "A Sampled-Data Pursuit Tracking Model," IEEE Transactions on Human Factors in Electronics, September 1965.
15. Kroll, C. V. and Roland, R. D., "A Preview-Predictor Model of Driver Behavior in Emergency Situations," Calspan Report No. VJ-2251-V-6, October 1970.
16. Weaver, G. D., et al, "Effect of Curb Geometry and Location on Vehicle Behavior," NHCRRP Project 20-7, Texas Transportation Report No. RF845, October 1972.
17. Webb, P. W., "Bioastronautics Data Book," NASA Report SP-3006, 1964.







00055289

